

**UNDERSTANDING INTERPARTICLE INTERACTIONS IN
DRY POWDER INHALATION: GLASS BEADS AS AN
INNOVATIVE MODEL CARRIER SYSTEM**



DOCTORAL THESIS
SUBMITTED IN FULFILLMENT OF THE REQUIREMENTS
FOR THE DEGREE OF
DOCTOR IN NATURAL SCIENCES
AT KIEL UNIVERSITY, GERMANY

by

Niklas Ludwig Renner

Kiel 2017

Referee: Prof. Dr. Regina Scherließ

Co-Referee: Prof. Dr. Thomas Kunze

Date of Exam: 13.10.2017

Accepted for publication: 13.10.2017

Prof. Dr. Natascha Oppelt

(Dean)

Published research articles contributing to the present thesis:

Renner, N.; Steckel, H.; Urbanetz, N.A.; Scherließ, R.
Tailoring the surface topography of a model carrier to alter dry powder inhaler performance
Dalby, R.N. (Ed.), RDD Europe 2017 2 (2017), 195-200

Renner, N.; Steckel, H.; Urbanetz, N.A.; Scherließ, R.
Nano- and microstructured model carrier surfaces to alter dry powder inhaler performance
International Journal of Pharmaceutics 518 (2017), 20-28

Conference contributions:

Renner, N.; Steckel, H.; Urbanetz, N.A.; Scherließ, R.
Tailoring the surface topography of a model carrier to alter dry powder inhaler performance
Respiratory Drug Delivery, Nice, France (2017)

Renner, N.; Steckel, H.; Urbanetz, N.A.; Scherließ, R.
A deeper insight into the impact of chemical surface properties on inhalation performance
Drug Delivery to the Lungs 27, Edinburgh, Scotland (2016)

Renner, N.; Scherließ, R.; Steckel, H.
Glass beads as model carriers in dry powder inhalers: the influence of chemical surface properties on inhalation performance
International Congress on Particle Technology, Nurnberg, Germany (2016)

Renner, N.; Scherließ, R.; Steckel, H.
Investigating the influence of carrier surface roughness on drug delivery in DPIs
10th World Meeting on Pharmaceutics, Biopharmaceutics and Pharmaceutical Technology, Glasgow, Scotland (2016)

Renner, N.; Kutelova, Z.; Scherließ, R.; Steckel, H.
Modified glass beads as model carriers to understand the performance of interactive powder blends
Drug Delivery to the Lungs 26, Edinburgh, Scotland (2015)

“If we knew what we were doing it would not be called research, would it?”

Albert Einstein

Meinen Eltern gewidmet

Lack of specific mark or a reference to a trademark or a patent does not imply that this work or part of it can be used or copied without copyright permission.

Table of Contents

1	Introduction and Objectives.....	1
1.1	Introduction.....	1
1.2	Objectives.....	2
2	Theoretical Background.....	4
2.1	The Human Respiratory Tract.....	4
2.2	Pulmonary Drug Delivery	5
2.2.1	General Considerations for Inhalation Products.....	5
2.2.2	Drug Application Devices.....	7
2.2.2.1	Nebulisers	7
2.2.2.2	Pressurised Metered-Dose Inhalers	8
2.2.2.3	Soft Mist Inhalers	8
2.2.2.4	Dry Powder Inhalers	8
2.3	Formulation Strategies for Dry Powder Inhalation	9
2.3.1	Manufacturing of Drug Particles for Inhalation	9
2.3.2	Carriers in Pulmonary Drug Delivery.....	10
2.3.2.1	α -Lactose Monohydrate	11
2.3.2.2	Other Organic Carriers.....	11
2.3.2.3	Model Carrier System: Glass Beads.....	11
2.3.3	Interparticle Interactions.....	12
2.3.3.1	General Considerations for DPI Formulations	12
2.3.3.2	Impact of Particle Properties on Interparticle Interactions	15
2.3.4	The Inhalation Device	17
3	Materials and Methods	19
3.1	Materials	19
3.1.1	Model Drugs	19
3.1.1.1	Budesonide	19
3.1.1.2	Formoterol Fumarate	20

II

3.1.1.3 Ipratropium Bromide	21
3.1.1.4 Tiotropium Bromide.....	21
3.1.2 Glass Beads	22
3.1.3 Tungsten Carbide	23
3.1.4 Hydrofluoric Acid.....	23
3.1.5 Capsules.....	23
3.1.6 Inhalation Devices	24
3.1.6.1 Cyclohaler	24
3.1.6.2 Unihaler/Modular Inhaler.....	24
3.2 Statistical Methods	26
3.2.1 Design of Experiments.....	26
3.2.2 General Statistical Considerations	28
3.3 Preparative Methods.....	29
3.3.1 Spray Drying of Model Drugs.....	29
3.3.1.1 Budesonide	30
3.3.1.2 Formoterol Fumarate	31
3.3.1.3 Tiotropium Bromide.....	31
3.3.1.4 Ipratropium Bromide	31
3.3.2 Modification of Glass Beads.....	31
3.3.2.1 Chemical Surface Modification	32
3.3.2.2 Alteration of Surface Topography	32
3.3.3 Working Under Controlled Ambient Conditions	34
3.3.4 Calculation of Carrier Surface Coverage-Theoretical Considerations.....	34
3.3.5 Preparation of Interactive Mixtures.....	36
3.4 Analytical Methods	38
3.4.1 API and Carrier Characterisation	38
3.4.1.1 Laser Diffraction	38
3.4.1.2 Dynamic Image Analysis.....	38
3.4.1.3 Scanning Electron Microscopy.....	39
3.4.1.4 Contact Angle Measurements.....	40

3.4.1.5 Atomic Force Microscopy.....	40
3.4.1.6 Density Measurements	43
3.4.1.7 Dynamic Vapour Sorption	43
3.4.1.8 X-Ray Powder Diffraction.....	44
3.4.1.9 Inverse Gas Chromatography.....	44
3.4.1.10 Powder Rheometry	45
3.4.2 Characterisation of Interactive Mixtures and <i>in vitro</i> Deposition	47
3.4.2.1 Evaluation of Drug Content.....	47
3.4.2.2 Determination of Content Uniformity.....	47
3.4.2.3 Impaction Analysis	48
3.4.2.4 Determination of Specific Device Resistance	50
3.4.2.5 Calculation of True Surface Coverage.....	51
4 Results and Discussion	53
4.1 Spray Drying of Different APIs.....	53
4.1.1 Budesonide.....	54
4.1.2 Formoterol Fumarate	55
4.1.3 Tiotropium Bromide	58
4.1.4 Characterisation of the Final Products	59
4.1.4.1 Particle Size	59
4.1.4.2 Particle Shape and Morphology.....	60
4.1.4.3 Stability and the Impact of Ambient Conditions	62
4.1.4.4 Dispersive Surface Energy	64
4.2 Chemical Modification of Glass Beads	66
4.2.1 Characterisation of Glass Beads.....	66
4.2.1.1 Contact Angle.....	66
4.2.1.2 Surface Energy	68
4.2.1.3 Particle Size and Shape.....	71
4.2.1.4 Flow Properties	72
4.2.2 Influence on True Surface Coverage	73
4.2.3 Impaction Analysis.....	77

IV

4.3	Alteration of Carrier Surface Topography	86
4.3.1	Characterisation of Glass Beads.....	86
4.3.1.1	Particle Size and Shape.....	90
4.3.1.2	Powder Rheometry	91
4.3.2	Influence on True Surface Coverage	92
4.3.3	Impaction Analysis.....	96
4.3.4	Adhesion Forces.....	102
4.4	The Importance of Inhaler Geometry	104
4.4.1	Design of Experiments.....	105
4.4.2	Influence on Aerodynamic Performance	106
4.4.3	Influence on Device Retention	109
4.4.4	Influence on Specific Device Resistance	112
4.5	The Importance of API Properties	114
4.5.1	Micronised versus Spray Dried Budesonide.....	114
4.5.2	Budesonide versus Ipratropium Bromide Micronised	119
5	Overall Conclusion and Future Perspectives	122
6	Summary	124
7	Summary (German)	126
8	Appendix	129
8.1	HPLC Methods	129
8.1.1	Budesonide.....	129
8.1.2	Formoterol Fumarate	129
8.1.3	Ipratropium Bromide	130
8.1.4	Tiotropium Bromide	131
8.2	Materials	132
8.3	Abbreviations	134
8.4	Formula Symbols.....	137
8.5	Overview of Experimental Designs	139

8.5.1	Spray Drying of Budesonide (section 4.1.1).....	139
8.5.2	Spray Drying of Formoterol Fumarate (section 4.1.2)	140
8.5.3	Spray Drying of Tiotropium Bromide (section 4.1.3).....	141
8.5.4	The Importance of Inhaler Geometry (section 4.4.1)	142
9	References	143

1 Introduction and Objectives

1.1 Introduction

Diseases of the human respiratory tract such as asthma bronchiale, chronic obstructive pulmonary disease (COPD) or local infections are preferentially treated with medicines administered via the pulmonary route. By doing so, the application of comparatively low doses is possible and an adequate drug distribution to its site of action is reached [1,2]. At the same time, a reduced potential for adverse effects is observed compared to an oral or intravenous administration due to minimised systemic exposure of these drugs [3–5]. Besides the treatment of diseases which are locally limited to the airways, pulmonary drug delivery is also explored as an alternative to effectively administer small molecules or peptides to treat systemic diseases such as diabetes or osteoporosis [6,7]. This is reasoned by a large surface area of the lungs, comparatively low local metabolic activity and the possibility to avoid first-pass metabolism [8]. In addition, the drug is rapidly distributed due to an extended blood flow [9].

A considerable percentage of asthma bronchiale and COPD medication is formulated as dry powders intended for inhalation. In order to reach the lower airways, the drug needs to have an aerodynamic particle size between 1 and 5 μm [10,11]. Furthermore, an adequate flowability of the powder is mandatory to ensure processability and accurate dose-metering. These two requirements stand in direct contradiction to each other. For this particular size range, cohesive forces are predominant in relation to gravitational forces due to relatively low weight and large surface area of the particles [12]. To counteract poor flowability and secure dose uniformity as well as processability of the powder, two main formulation strategies have been developed, namely carrier-free and carrier-based systems. The latter approach comprises coarse and desirably inert particles in the size range of 50 – 200 μm with adequate flowability. During a blending step, drug agglomerates are broken up while these particles get attached to the carrier surface. As drug particles interact with the carrier via adhesive forces, these blends are also referred to as interactive mixtures.

During inhalation, the drug needs to be detached again from the carrier to allow delivery to the target site. The detachment is triggered by the patient's inspiration. But at the same time, it is widely governed by interparticle interactions between carrier and

active pharmaceutical ingredient (API). The extent to which these forces occur is highly dependent on physico-chemical properties of carrier and API [13]. Therefore, an in-depth understanding of the impact of material characteristics on the aerodynamic performance is needed to overcome the challenges in the development of dry powder inhaler (DPI) formulations, e.g. insufficient drug detachment from the carrier during inhalation. Besides the formulation and patient's inspiratory flow, the inhalation device plays a key role for this process. Its conception and dimensioning of the different parts have to be evaluated carefully [14]. These determine the dispersion mechanism and trigger the occurrence of turbulences, centrifugal forces and thus, particle-particle and particle-wall collisions which are key to induce drug detachment.

1.2 Objectives

This thesis aims at the investigation of aspects concerning the formulation and the device in dry powder inhalation. Although much research has been performed on the factors influencing drug delivery, the complex mechanisms that govern drug detachment and deagglomeration of carrier-based formulations still remain unclear. To get a more comprehensive understanding of these processes, interparticle interactions between carrier and API are systemically examined using glass beads (GBs) as a model carrier platform. In addition, a detailed investigation on the importance of the inhalation device is conducted with a modular inhaler system. The project has been part of the priority program SPP 1486: particles in contact (PiKo) and was funded by the German Research Foundation (DFG).

To examine a broad range of chemical properties, APIs with largely differing hydrophilicity/hydrophobicity are chosen. Spray drying is used to manufacture API particles with uniform characteristics in terms of particle size ($< 5 \mu\text{m}$), size distribution (narrow) and overall shape (spherical). A uniform spherical shape is mandatory since it secures the independence of contact area between carrier and API from particle orientation.

The main part of this thesis focuses on interparticle interactions between carrier and API and how they are influenced. This shall also elucidate their impact on the behaviour of the formulation. To do so, glass beads were utilised as a model carrier system for carrier-based formulations. These present the advantage to achieve a modification of one specific material property such as surface chemistry or topography without

hardly any change of another. This allows a systematic approach to identify relevant parameters and examine their impact on aerodynamic performance. Initially, suitable techniques to modify the carrier surface in terms of chemistry and topography and consequently interparticle interactions are explored and presented. Resulting material and bulk properties are characterised using various methods. Suitable blending protocols are applied to manufacture blends consisting of GBs and drug with sufficient content uniformity and also to ensure integrity of the drug.

It is further investigated how material properties and thus, API-carrier interactions affect drug load and aerodynamic performance. These findings shall contribute to a successful design of new and the optimisation of current DPI formulations.

In addition, the influence of the inhalation device, or more precisely its dimensioning, for an optimal drug delivery is examined. The comparison of the results to a previous study which utilised lactose as carrier shall emphasise practical differences and similarities when using a conventional carrier or the model carrier system. In addition, impact of API properties on its deposition is examined. These include size, shape, crystallinity and chemical structure and expand the factors under investigation from device and carrier to the API.

2 Theoretical Background

2.1 The Human Respiratory Tract

The human body relies on a continuous supply of oxygen to maintain physiological functions. This is ensured by the respiratory system which facilitates the uptake of oxygen and the release of waste carbon dioxide.

It consists of two major parts. The first one (upper part) comprises airways from mouth and nose to the pharynx and larynx. These are followed by the lower respiratory tract consisting of trachea, bronchi, bronchioles and the alveolar ducts (Figure 2-1). These are lined with around 300 million blood vessel-covered alveoli where gas exchange actually takes place. By that, a 23-fold branching with a steady increase in total cross section is reached [15]. This leads to a very high surface area of 80 – 90 m² [16]. Alveolar cells form a very thin epithelium (~ 0.1 μm) which ensures, in combination with a lung perfusion, the fast uptake of oxygen. This leads to a rapid distribution of drugs.

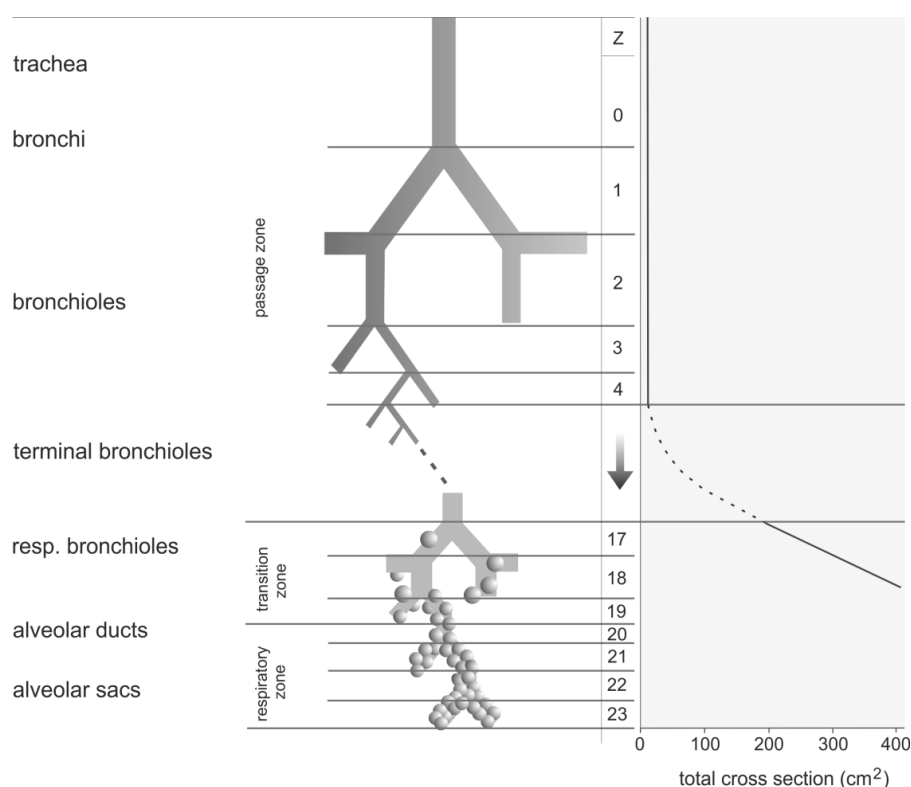


Figure 2-1 Schematic structure of the lower respiratory system (left) with the resulting total cross sectional area (right); adapted from Thews et al. [17]

2.2 Pulmonary Drug Delivery

Inhalation therapy is the most common approach to treat respiratory diseases such as asthma bronchiale or COPD. This allows a lower dose and a better side-effect profile compared to systemic administration of these drugs. In addition a rapid onset of action is maintained. This is especially important in case of an acute asthma attack. Medication to locally treat asthma comprises substance classes with extensively differing mechanisms of action including long- and short-acting β_2 -agonists, inhaled corticosteroids and muscarinic antagonists [18].

In recent years, the pulmonary route has been explored to deliver systemically active drugs currently only available to a parenteral administration. These include peptides and proteins such as insulin or growth hormones which are unstable upon oral administration. Moreover, the lungs provide a large number of immunocompetent cells present on the mucosa. This opens up the opportunity for a vaccination against many diseases, e.g. pneumonia through pulmonary administration [19].

The importance and the recognised potential of pulmonary drug delivery demand a deep understanding of parameters which govern the aerodynamic performance of these formulations. This knowledge will contribute to an optimisation of currently marketed medicines and also provides the basis for the development of new products.

2.2.1 General Considerations for Inhalation Products

The aerodynamic diameter (d_{ae}) is the most suitable parameter to characterise particles intended for inhalation. It is defined as the diameter of a sphere of unit density (1000 kg/m^3) which would have the same terminal velocity as the particle under investigation [20]. It is calculated according to equation 1. d_{geo} is the geometric diameter of the sphere, ρ_p and ρ_0 are the particle and unit density, respectively. χ is defined as the so-called shape factor. It is defined as the ratio of the drag force experienced by the respective particle to that of a perfect sphere with the same volume [21].

$$d_{ae} = \sqrt{\frac{\rho_p}{\rho_0 * \chi}} * d_{geo} \quad \text{equation 1}$$

Relating this to an example of practical relevance it means: the size of a large porous particle with a density of 100 kg/m³ [20] can be increased up to 25 µm and would still present the same d_{ae} as a drug particle of 2.5 µm with a density of 1000 kg/m³. By that, premature impaction in the upper airways can be avoided.

Drug depositing during inhalation is governed by three mechanisms, namely inertial impaction, sedimentation and diffusion (Figure 2-2).

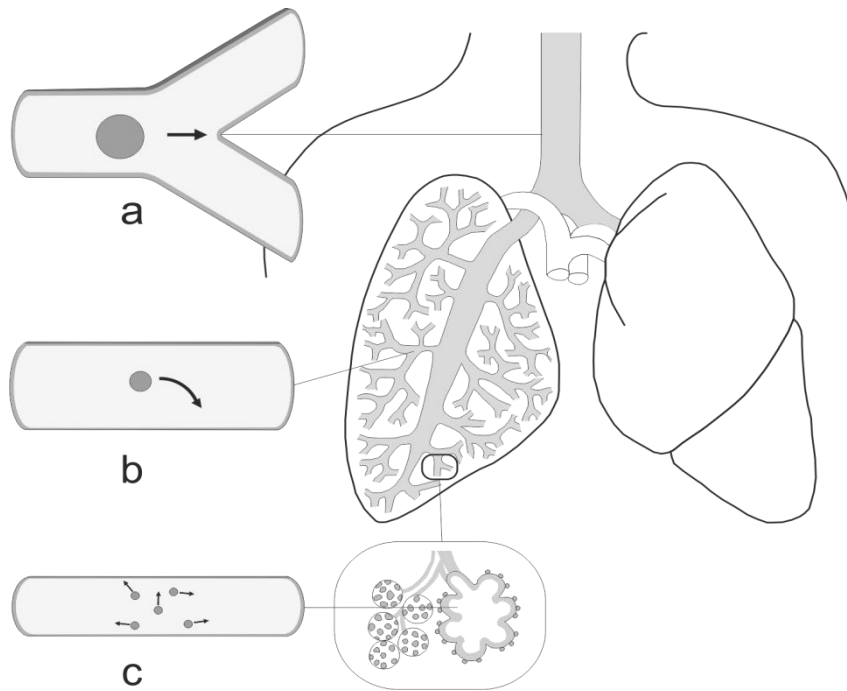


Figure 2-2 Deposition mechanisms of inhaled particles: a) impaction, b) sedimentation and c) diffusion

Airborne particles with a diameter > 6 µm impact on the upper airways. This is due to an inertial separation at bifurcations of the airways since these particles are unable to follow the directional changes of the airstream [22]. The probability of particle impaction can be described by the dimensionless Stokes number (Stk). As seen in equation 2, it is influenced by ρ_p , particle diameter (d), air velocity (V), viscosity of air (η) and airway radius (r). Extended deposition triggered by inertial impaction is a major challenge which needs to be overcome. This could be the result of an insufficiently optimised formulation inducing agglomeration or a persisting attachment of drug to the carrier.

$$Stk = \frac{\rho_p * d^2 * V}{18 * \eta * r} \quad \text{equation 2}$$

Secondly, sedimentation occurs for particles with 2 – 6 μm in diameter that enter the lower airways, where a low airflow velocity prevails. This is a time-dependent process and particles are deposited according to gravitational forces [23]. For particles in the respective size range, it can be described by the Stokes-Cunningham equation to calculate the terminal settling velocity V_{ts} (equation 3). Here, $\Delta\rho$ is the density difference of disperse and dispersed phase, r is the particle radius and g is the acceleration of gravity. In addition, A is a dimensionless factor and λ is defined as median free path length of gas molecules.

$$V_{ts} = \frac{2 \cdot \Delta\rho \cdot r^2 \cdot g}{9 \cdot \eta} * \left(1 + A * \frac{\lambda}{r} \right) \quad \text{equation 3}$$

The third mechanism applies to small particles ($\leq 2 \mu\text{m}$) which have not impacted due to the two prior processes. Diffusion is observed for small particles reaching the terminal bronchioles and the alveolar region, where airflow is negligible [24]. Here, Brownian motion is the dominant force for these particles and can be described by equation 4. D is defined as the diffusion coefficient, k and T are the Boltzmann constant and temperature, respectively.

$$D = \frac{k \cdot T}{3 \cdot \pi \cdot \eta \cdot d} \quad \text{equation 4}$$

2.2.2 Drug Application Devices

Four main groups of inhalation devices are used in inhalation therapy. These include nebulisers, pressurised metered-dose inhalers (pMDIs) as well as soft mist inhalers. These three are presented briefly, while focus is put on dry DPIs in the following section.

2.2.2.1 Nebulisers

Nebulisers convert a solution or nano-suspension into an aerosol. This is done by different mechanisms such as vibration, ultrasound and pressurised air. They are oftentimes prescribed to children and the elderly, as they are easy to use and minimal patient training is needed [25]. In addition, dose modification and the application of more than one drug are possible [26]. One main reported disadvantage is a varying droplet size and consequently a reduced aerosolisation which is triggered by different

temperatures [27]. Moreover, most nebulisers are not portable and they are only intended for a stationary use.

2.2.2.2 Pressurised Metered-Dose Inhalers

Since the launch of the Medihaler[®] in 1956, pMDIs have been widely used to deliver drugs to the lungs [28]. For these inhalers, the API is either dissolved or suspended with an additive propellant, nowadays a hydrofluoroalkane. Portability and the high chemical stability of suspension-based pMDIs are two main advantages [29]. But the occurrence of physical instabilities, e.g. flocculation or sedimentation oftentimes makes the use of further additives such as surfactants and cosolvents necessary.

But the mandatory precise coordination between inspiration and actuation of the device has proven to be difficult [30]. In addition, a generally low respirable fraction is reached if used incorrectly due to an extensive acceleration of the aerosol. This leads to an impaction in the upper part of the airways. These issues can be overcome by the use of spacers [31].

2.2.2.3 Soft Mist Inhalers

The only soft mist inhaler is the Respimat[®] introduced by Boehringer-Ingelheim. It produces a long lasting aerosol cloud with an overall decelerated velocity compared to pMDIs [32]. This triggers a more efficient drug delivery [33]. The independence of the emitted dose from the inspiratory flow and simple handling can also be considered beneficial. However, production of the device is quite cost-intensive and application is limited to an aqueous solution of drugs to this date.

2.2.2.4 Dry Powder Inhalers

After the launch of the first DPI in 1971 (Spinhaler[®]), this device class became increasingly important 17 years later upon the entry into force of the Montreal protocol limiting the use of substances harming the ozone layer. This made the exploration of alternatives to chlorofluorocarbon-containing pMDI formulations necessary. Due to the lack of any liquid components, the physical stability of the API is generally secured. Nevertheless a certain sensitivity to environmental conditions inducing moisture uptake or tribo-charging has been reported [34,35].

DPIs are available as single-dose, multiple unit-dose or multi-dose (reservoir) devices [36]. In general, a single-dose device delivers the medication from a blister (Elpenhaler[®]) or a capsule (e.g. Handihaler[®] and Cyclohaler[®]) which are placed inside the inhaler. Multiple unit-dose devices contain a certain amount of capsules or blisters such as FlowCaps[®] and Diskhaler[®]. In Multi-dose inhalers, the API is dispensed from a reservoir, for example Turbuhaler[®] and Novolizer[®]. Dispersion of the formulation is triggered by the patient's inhalation which precludes the need to coordinate device actuation with inspiration. By that, handling is facilitated.

DPIs were used throughout the present work including the Cyclohaler and a Modular Inhaler system which is presented in section 3.1.6.2.

2.3 Formulation Strategies for Dry Powder Inhalation

The effectiveness of drug delivery to the lungs is highly dependent on correct inspiration by the patient and the used inhalation device. Furthermore, the DPI formulation plays a key role in this process. Over the years two main strategies have been presented for a successful formulation design: carrier-free and carrier-based. The former, more recent approach firstly focuses on targeted particle engineering to meet the requirements for successful drug delivery, e.g. by employing large porous particles [37,38]. Secondly, a controlled agglomeration of spheronised drug particles (softpellets) can be utilised to improve flowability [39]. This also secures a sufficient aerosolisation upon inhalation if the suitable inhalation device is used. The latter approach uses an inert coarse carrier with sufficient flowability to form a so-called interactive mixture with the API.

Formulation design is critical, as many factors concerning its components have to be taken into account which will be discussed in this chapter. Ambient conditions potentially influence forces prevailing within the formulation as well.

2.3.1 Manufacturing of Drug Particles for Inhalation

In order to obtain API particles in the suitable size range, different techniques have been introduced over the years. These can mainly be classified into two categories, namely top-down and bottom-up processes [40]. Micronisation via milling is a typical example for a top-down process where a high energy input is needed to reduce the

size of larger crystals [41]. One main disadvantage is a possible post-micronisation relaxation which causes a change in size and surface area over time [42]. Bottom-up processing includes the formation of particles from, for example, a solution. Here, precipitation has been used with a major advantage to manufacture particles consisting of more than one drug [43]. This method can also be applied to poorly (water-) soluble drugs using an aerosol solvent extraction system and supercritical carbon dioxide [44].

Another example for a bottom-up process to manufacture micron-sized particles is spray drying (SD). Properties of the product are highly dependent on solubility, diffusion rate and surface activity of the drug molecules in the atomised droplets [45]. This process oftentimes results in amorphous pharmaceuticals with a spherical shape which are characterised by a narrow size distribution compared to micronisation by milling [46,47]. Particle properties can be tailored to meet requirements for pulmonary drug delivery by the control of respective process parameters [48]. In addition, the product is characterised by a uniform composition. For these reasons, spray-drying is employed for the manufacturing of API particles in the present work.

Another approach is spray-freeze drying which typically involves a solution that is atomised into a chamber filled with a cryogenic liquid (liquid nitrogen) and is subsequently freeze-dried. By doing so, amorphous low density particles with a high specific surface area are obtained [49]. Although an overall higher yield can be reached compared to conventional spray drying, it is a cost-intensive and rather time-consuming procedure [50].

2.3.2 Carriers in Pulmonary Drug Delivery

In order to increase flowability and processability of an inhalation powder, a coarse carrier is oftentimes added to the drug. A suitable carrier should meet several criteria such as physico-chemical stability, biocompatibility, easy accessibility and production at low costs. Moreover, it must be inert to prevent chemical reaction with the API and should show good flowability. However, the introduction of a carrier causes a significant dependency of the aerodynamic performance on interparticle-interactions between drug and the carrier. Current DPI products are mainly utilising α -lactose monohydrate, while mannitol is continuously gaining interest as alternative excipient.

2.3.2.1 α -Lactose Monohydrate

Despite recent advances in particle engineering, carrier-based formulations are still the most commonly used approach for a targeted drug delivery to the lungs. The carrier of choice is α -lactose monohydrate with a wide range of pharmaceutical grades for inhalation with different physico-chemical properties available [51]. Lactose has been extensively examined as carrier and its beneficial toxicity profile is well-documented [52]. However, it belongs to the class of reducing sugars which are capable of reacting with amine groups of other molecules, e.g. amino acids. As a consequence, an API molecule could undergo a chemical reaction which oftentimes causes a loss of activity [53]. This disqualifies lactose for formulations with peptides or proteins. This drawback, inter alia, has put focus on the exploration of further potential carriers.

2.3.2.2 Other Organic Carriers

Mannitol is a non-reducing sugar alcohol described as being less hygroscopic than lactose [54]. It has been introduced as the most promising candidate as alternative carrier for DPI formulations [55]. Mannitol has an extended osmotic effect, which is why it is employed as active in Bronchitol[®], a currently marketed medicine against cystic fibrosis [56]. Recently, spray drying was presented as a suitable technique to manufacture spherical mannitol carrier particles with good flowability. By that, physico-chemical properties of the product could be modified as well [57].

Further sugars and sugar alcohols such as glucose, sorbitol, maltitol and xylitol have been examined but exhibited only minor respirable fractions, mainly due to their increased hygroscopicity [52,58].

2.3.2.3 Model Carrier System: Glass Beads

Many studies have been presented in which a specific property of lactose was modified to subsequently investigate its impact. However, other material characteristics have been also altered unintentionally during the respective processes. For example, the change of carrier size generally alters surface roughness or varying the polymorphic form can result in a change in both crystal lattice and shape [59]. This essentially complicates interpretation of gained results since potential changes in respirable frac-

tion cannot be explicitly attributed to that respective modification. To overcome this issue associated with the use of conventional carriers, the present work employed glass beads as model carrier system for studies shown in this thesis. These are available in a wide range of size. Moreover, the manufacturing process ensures a uniform spherical shape and a reproducible state of the surface. This qualifies GBs for an ideal system to selectively investigate the impact of carrier modification on interparticle interactions. GBs in the size range of 400 – 600 μm were employed, while the chosen size presents a compromise between the normal diameter of a carrier (50 – 200 μm) and the suitability to conventional inhalation characterisation techniques described in section 3.4. To the authors' knowledge, no studies apart from those within the DFG priority program have been conducted to examine interactions between carrier and API by such a systematic approach. Although GBs are basically only applicable to *in vitro* experiments due to safety concerns, gained results will help to further elucidate explain interparticle interactions in DPI formulation. Consequently, present findings will contribute to further optimise the currently marketed as well as newly developed formulations.

2.3.3 Interparticle Interactions

2.3.3.1 General Considerations for DPI Formulations

The formation of interactive mixtures for dry powder inhalation is generally considered a two-step process of drug deagglomeration and drug adhesion onto the carrier surface [60]. Fracture of larger drug agglomerates is initially obtained by impact of particles with the coarse carrier and the walls of the mixing vessel. After this, drug particles are completely deagglomerated and deposited onto the carrier surface due to forces arising from friction between drug and carrier and/or the mixing vessel [61].

It can be concluded that the blending process depends on the magnitude of cohesive and adhesive forces of the particles. The former refer to interaction between particles of the same kind while the latter describe the interaction between different materials. Cohesive forces of drug particles need to be low enough to be overcome by shear forces created during blending and to prevent reagglomeration [62]. The formation of interactive mixtures is energetically favoured if the adhesive forces are stronger than

cohesive forces of the drug [63]. But as far as adhesion is concerned, excessive forces between carrier and API potentially prevent the latter from being readily detached during inhalation. This would lead to a deposition in the upper airways [64] (Figure 2-3). Nevertheless, a sufficient attraction to the carrier is mandatory to ensure blend homogeneity and impede segregation during handling. In this context, the importance of the cohesive-adhesive balance (CAB) has been acknowledged which is essential to meet the requirements for a DPI formulation [65]. Moreover, the CAB ratio between cohesion of the drug and its adhesion to the carrier has already been used to explain and predict the aerodynamic performance of different interactive mixtures [66,67].

Adhesion and cohesion are dependent on three different kinds of forces: van-der-Waals, capillary and electrostatic forces [68]. The extent to which these occur in the interactive mixture is determined by material characteristics of the components as well as environmental conditions, i.e. temperature and relative humidity (rH) [69]. Adhesive forces are particularly important for DPI formulations. The API exhibits high surface area/mass ratio due to its small size. Therefore, attractive forces are significantly higher than the gravitational separation forces [60]. For a powder blend containing a carrier of 200 μm and an API of 5 μm , for example, the adhesion exceeds the respective separation force by a factor of 3×10^5 .

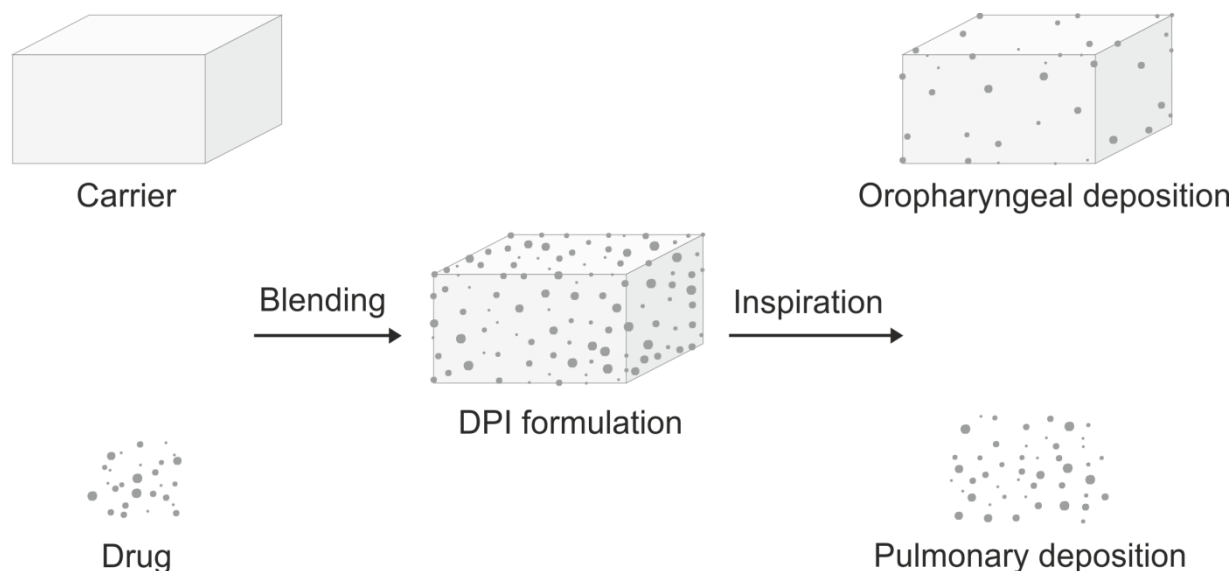


Figure 2-3 Formation and disintegration of an interactive mixture

Van-der-Waals forces are non-covalent interactions consisting of three main components. Firstly, Keesom forces describe interactions between two permanent dipole

molecules. Secondly, Debye interactions between a permanent dipole and a molecule with an induced dipole and thirdly London dispersive forces that arise from molecules with induced dipole moments. Due to mobility of electrons within a certain area (electron cloud), temporary dipoles can be induced within a molecule. Hereafter, this molecule is capable of triggering dipole moments within other molecules. The extent of van-der-Waals forces can be manipulated by limiting contact area which is subject of the present work and/or increasing distance between carrier and API.

At elevated rH, capillary forces arise from the presence of adsorbed water on the particle surface. This is caused by the condensation of water vapour. If such particles come into intimate contact, a concave-shaped liquid meniscus is formed inducing a comparatively strong cohesion/adhesion [70]. Consequently, drug detachment and deagglomeration is impeded. The formation and the extent of these liquid bridges are mainly dependent on ambient conditions and hygroscopic behaviour of the particles. While the development of liquid bridges is generally a matter of minutes to hours, the formation of solid bridges can occur during long term storage at increased rH [71]. This can be the case for materials with enhanced water solubility, where a dissolution and subsequent solidification of molecules on the surface potentially takes place. This leads to either an increase in drug particle size and/or a persisting attachment to the carrier surface, which ultimately impedes the aerodynamic performance.

In contrast, electrostatic forces may prevail at lower rH. These generally occur when two different materials come into contact and separate afterwards [72]. In DPI formulations, carrier and API are generally organic and insulating materials, which is why a net charge of both materials during this process due to electron transfer can be expected. These interfacial charges can increase adhesion between carrier and API. This is especially important for DPI formulations as electrostatic forces were found to be primarily induced by particle-particle and particle-wall friction. This occurs within the device during inhalation manoeuvre and in the mixing container during blending. However, electrostatic charge can be reduced by increasing rH. The resulting absorption of water enhances surface conductivity and triggers electron exchange between particles with an opposite net charge [69].

Both capillary and electrostatic forces are highly dependent on material characteristics. In addition, while certain ambient conditions give rise to one of them, the other

one is reduced. This highlights the importance of a balance of ambient conditions. For this, ideal temperature and rH for processing and storage have to be determined for the formulation components to keep both forces as low as possible.

Forces described above are triggered by a variety of different factors. The most important ones are displayed in Figure 2-4. In the present work, focus was put on carrier surface topography and chemistry, while the impact of API to carrier ratio was investigated as well.

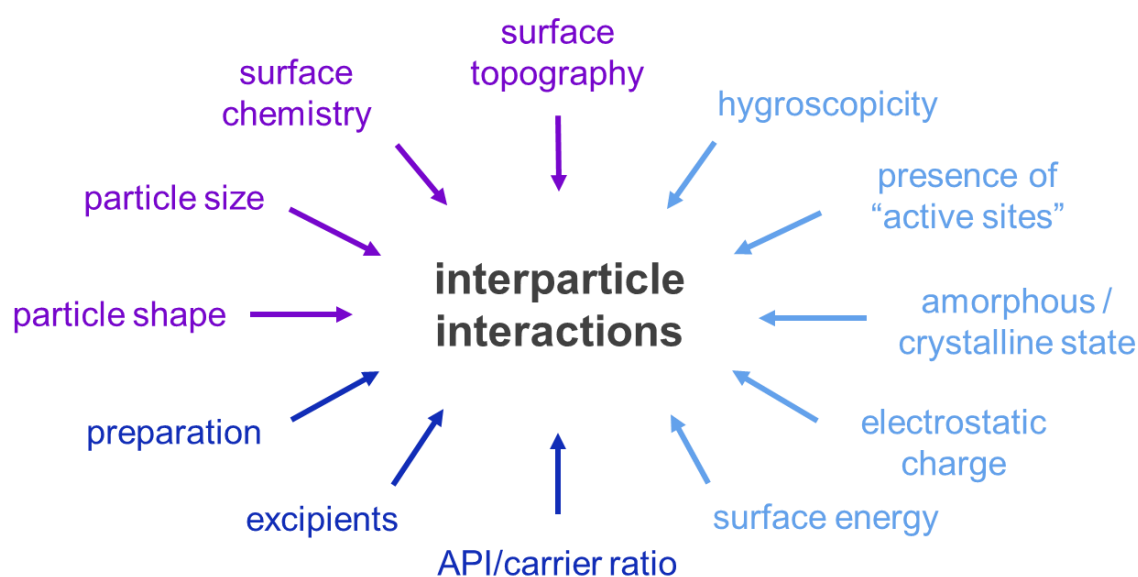


Figure 2-4 Overview of parameters influencing interactions between carrier and API in a DPI formulation: particle characteristics (purple), formulation properties (blue) and further intrinsic properties (light blue) adapted from [73]

2.3.3.2 Impact of Particle Properties on Interparticle Interactions

Material characteristics of carrier and API play an important role in the process of drug deagglomeration and detachment. Here, the control of particle size is crucial. The smaller the drug particles, the higher the adhesive forces due to the decreased surface area/mass ratio provided that other parameters are kept constant. This would actually favour larger particles for an optimal drug detachment. However, these particles would impact in the upper airways due to inertial impaction. The effect of carrier size on aerodynamic performance has been widely investigated with different results. Steckel and Müller found a general reduction of the respirable fraction for larger carriers [74]. This might be ascribed to an increased number of particle collisions and a

higher overall frictional area provided by the smaller carrier. This was also confirmed by another study which noted, however, that a decrease in carrier diameter also forces poor dose uniformity [75]. In contrast, increased aerodynamic performances gained from larger carrier size fractions has also been reported [76]. Since larger carriers showed improved flowability and minimised dose variability, they exhibited an overall enhanced performance. It is assumed that these conflicting results are derived from interdependency between physical properties and also relies on the choice of device. Increased carrier size, for example, might be more favourable when using an inhaler relying on inertial impaction for drug dispersion due to an increased particle momentum.

Carrier morphology can influence the aerodynamic performance as well, since particles with different shapes are affected differently by drag forces. It was shown that an elongated morphology is favourable for an effective drug deposition [77]. This is because an elongated carrier potentially exhibits a considerably smaller aerodynamic diameter compared to a spherical particle with the same volume and mass [78]. Therefore, these particles can follow the air stream for a prolonged period of time so that API particles on the carrier are longer exposed to the detachment forces. The shape of the API might have a substantial influence on adhesion as well, since it determines the contact area with the carrier and therefore interparticle forces. For instance, a perfectly round particle provides fewer contact area compared to elongated ones on a smooth surface. But needle-like particles also showed an enhanced lung deposition due to a smaller aerodynamic diameter compared to spherical particles with similar density [79].

Even though the impact of carrier topography, or more precisely surface roughness, has been investigated, conflicting reports have been published. On the one hand an enhanced drug detachment from carriers holding an irregular surface has been presented [80]. This was confirmed by Zellnitz et al. within the PiKo priority program, where the surface roughness of glass beads has been increased through, inter alia, plasma etching [81]. This beneficial effect was ascribed to a reduction of contact area between carrier and API. On the other hand, a reduced aerodynamic performance of blends consisting of carrier particles with a rough surface was demonstrated as well. Flament et al. attributed this to an increase in contact points of carrier and drug to enhance adhesive forces [82]. These findings were also supported by another

study [78]. One reason for the varying results might be an inaccurate definition of “rough” and “smooth”. Moreover, the oftentimes missing clarification of the scale of roughness might be accountable. But even more important seems a concurrent alteration of other material properties such as size or overall shape triggered by the respective surface modifications. This makes a distinction of the effects resulting from the different modifications very difficult.

In contrast, only little information about the importance of chemical properties for the interaction potential of carrier and API is available at the moment. Traini et al. investigated polymorphic forms of lactose in respect to their surface energies [83]. They found a negative correlation between surface energy and respirable fraction which was attributed to the different extent of adhesion forces (AFs) in the interactive mixture. However, only a narrow range of properties could be examined, since the different lactose grades exhibited rather similar energies.

2.3.4 The Inhalation Device

A typical dry powder inhaler has three main features such as mouthpiece, powder deagglomeration chamber and one or more air inlets. With a few exceptions this applies to all devices regardless of single- or multi-dose. The conception of these parts governs flow properties within the device and determines the prevailing dispersion and detachment mechanisms. This is particularly important as certain properties of the formulation might be beneficial for the aerodynamic performance using one device, but may be ineffective or even disadvantageous for another device.

The Cyclohaler for example is a device with a widely straightforward assembly (section 3.1.6.1). Here, a capsule rotates in the chamber triggered by patient’s inspiratory air flow. By that, the powder blend gets released from the capsule. Drug redispersion is based on drag and lift forces arising from the different velocities of airstream and particles [84]. This device was chosen for impaction analysis in the present thesis for two main reasons: Firstly, a single-dose device was needed as dose-metering systems of available inhalers do not function effectively with the large GB carriers. Secondly, its comparatively simple design enabled numerical simulations within the PiKo priority program by the working group of Professor Sommerfeld from the University of Halle concerning drug detachment in the device [85].

One commonly-used reservoir device is the Novolizer[®] which presents a more sophisticated design. A build-in classifier secures a controlled circulation time of the interactive mixture to optimise the use of the available energy provided by the airstream for dispersion [86]. Due to its conception, drug detachment and deagglomeration are mainly triggered by inertial and frictional forces which are considered as most effective [84]. This is beneficial for rather large carriers.

In general, a device should deliver a precisely metered dose to the target site with a high efficiency. It should also be easy to use and least susceptible to incorrect handling by the patient. In addition, a high independence from the patient's inspiration is desirable to ensure reproducibility of dose and make it available to all patient groups such as children or elderly with limited lung function. In recent years, effort has been made to optimise the inhalation device in respect to these requirements. Friebel, for example, developed a new DPI named the Unihaler which was optimised by using different freely combinable inhaler parts in different dimensions [87]. This so-called modular system (section 3.1.6.2) is also employed as a device system in the present thesis.

3 Materials and Methods

3.1 Materials

The APIs utilised in the present work are common medications in the treatment of asthma bronchiale or COPD. They were selected based on their physico-chemical properties to cover a wide range of hydrophilicity/lipophilicity (Table 3-1). Thus, complexity of interparticle interactions could be elucidated to a further extent. Moreover, the chosen APIs were used in spray dried (sd) and/or micronised (micro) quality depending on the requirements profile of the respective study.

Table 3-1 Physico-chemical properties of used APIs [88–91]

API	Molecular weight, g/mol	Solubility	LogP
Budesonide (BUD)	430.5	Insoluble in H ₂ O Soluble in methylene chloride	2.7
Formoterol fumarate (FF)	478.5	Poorly soluble in H ₂ O Soluble in methanol	1.06
Ipratropium bromide (IB)	430.4	Soluble in H ₂ O	-1.8
Tiotropium bromide (TB)	472.4	Sparingly soluble in H ₂ O	-1.7

3.1.1 Model Drugs

3.1.1.1 Budesonide

BUD belongs to the substance class of inhaled corticosteroids (ICSs). Reducing hyper-responsiveness of the airways as well as decreasing the production of inflammatory mediators and mucus is the proposed effect mechanism of action [92]. Due to its beneficial high ratio of topical anti-inflammatory to systemic activity, it is routinely used in the treatment of asthma bronchiale [93]. Furthermore, *in vitro* tests have shown a 200-fold higher affinity to the glucocorticoid receptor than cortisol [94]. BUD is part of

long-term control medication which patients are supposed to take regularly to keep chronic symptoms to an acceptable minimum and also prevent asthma attacks [95]. It is marketed as single preparation with a dose of 200 µg (children) – 400 µg (adults) or as combination product with formoterol fumarate. The structural formula is illustrated in Figure 3-1.

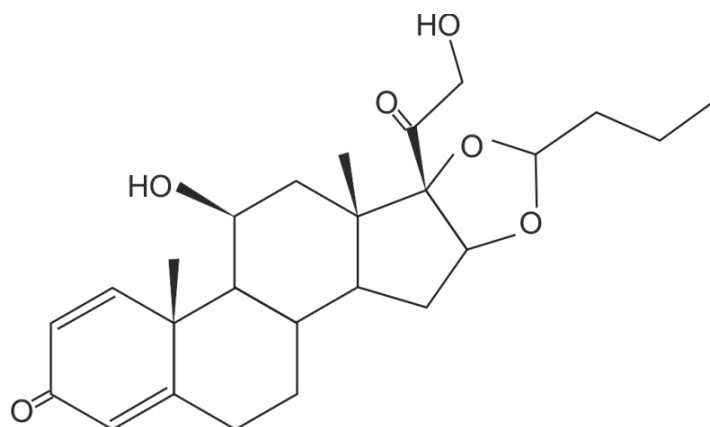


Figure 3-1 Chemical structure of BUD

3.1.1.2 Formoterol Fumarate

FF is a fast-acting β_2 -agonist which additionally has a prolonged effective period of up to 12 hours due to its ability to permeate and be stored in smooth muscle cell membranes. In contrast to other existing β_2 -agonists, it has an enhanced intrinsic efficacy at its receptor [96]. Binding to the β_2 -adrenoceptor leads to bronchial dilatation causing a persisting expansion of the lower airways. FF has gained approval for the therapy of COPD and is also used in the treatment of asthma bronchiale [94]. In case of the latter, it is administered as single or combination product with BUD, for example [97]. In general, only a very low dose of 9 – 12 µg is needed due to its high potency. The chemical structure is shown in Figure 3-2.

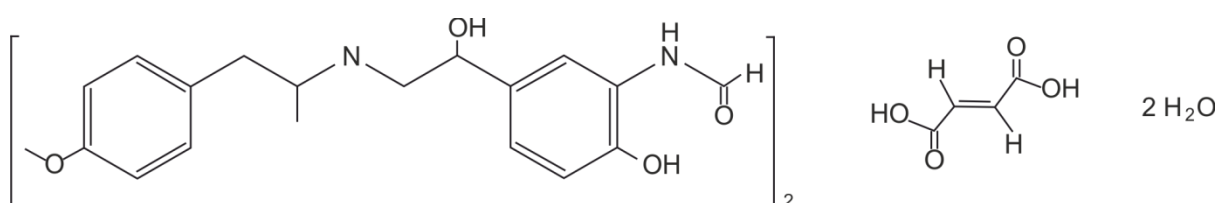


Figure 3-2 Structural formula of FF dihydrate

3.1.1.3 Ipratropium Bromide

IB serves as a short-acting muscarinic antagonist (SAMA) [98]. Administration of IB leads to a dilatation of smooth muscle cells triggered by the antagonism at muscarinic receptors. The combination of IB and salbutamol sulphate (SBS) is well established as medication on demand in 2nd line therapy of asthma bronchiale. It is also indicated in the treatment of COPD [99]. The marketed combination product (Combivent[®]) delivers a dose of 120 µg SBS and 20 µg IB. Its structural formula can be found in Figure 3-3.

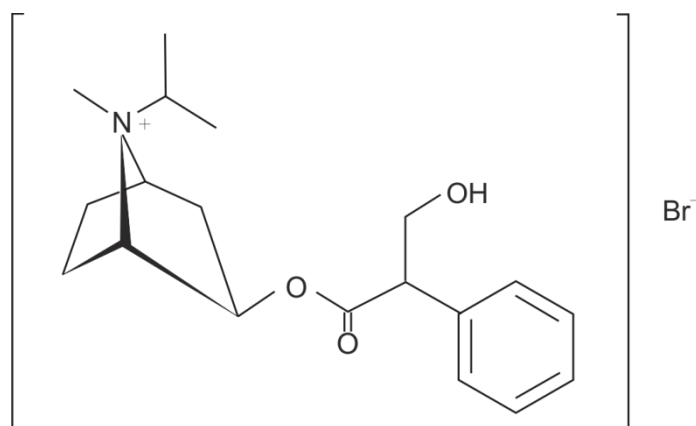


Figure 3-3 Chemical structure of IB

3.1.1.4 Tiotropium Bromide

TB belongs to the drug class of long-acting muscarinic antagonists (LAMAs). A decelerated dissociation from the muscarinic receptor compared to IB ensures a prolonged effective period and allows a once-daily administration. Present guidelines advise the application of, inter alia, LAMAs as first-line treatment of COPD to reduce its symptoms and exacerbations [100]. Additionally, TB has recently been added to the Global Initiative for Asthma Treatment Strategy as an alternative for addition at steps 4 and 5 in adult patients with asthma bronchiale [101]. TB is currently marketed as an aqueous solution for soft mist inhalers and as a DPI formulation with doses of 2.5 µg and 18 µg, respectively. The chemical structure is illustrated in Figure 3-4.

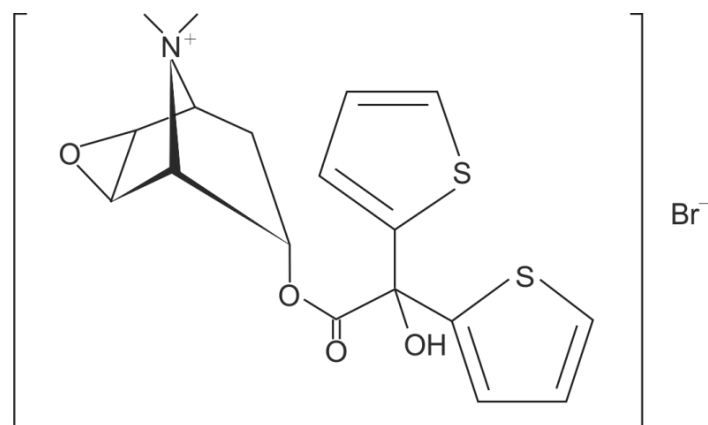


Figure 3-4 Structural formula of TB

3.1.2 Glass Beads

In this study, GBs in the size range of 400 – 600 μm (manufacturer specification) were used as a model carrier system. They are made of soda-lime glass with its main component being silicon dioxide, further consisting of sodium oxide, calcium oxide, magnesium oxide and aluminium oxide [102]. Soda-lime glass accounts for the largest proportion of industrially manufactured glass and is widely used, for example in building or food industry.

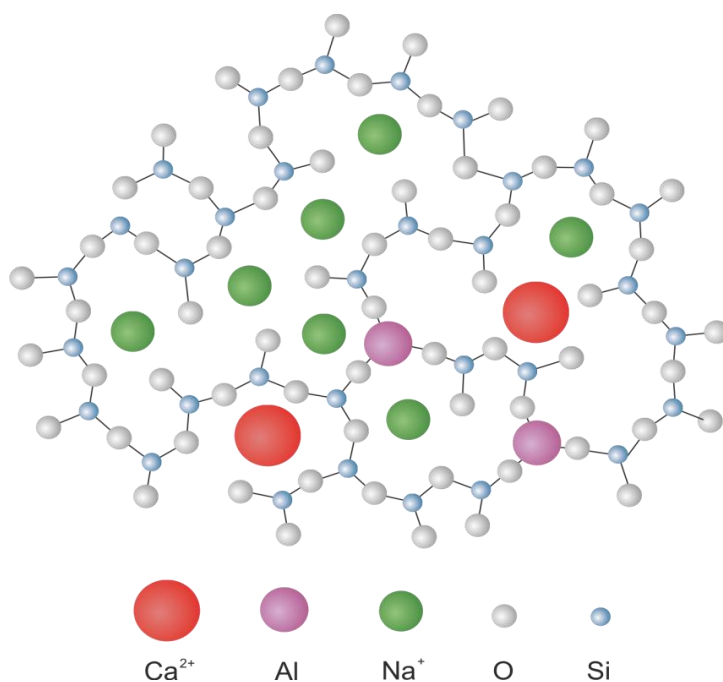


Figure 3-5 Schematic drawing of the structure of soda-lime glass used for GB manufacturing

The GBs (SiLibeads Type S[®], Sigmund Lindner GmbH, Warmensteinbach, Germany) are characterised by a high hydrolytic (class HGB2, based on DIN ISO 720) and acidic (class S2, according to DIN 12116) resistance and additionally show maximum resistance to alkalines (class A1, according to DIN ISO 695) [102]. The glass structure can be taken from Figure 3-5.

3.1.3 Tungsten Carbide

Tungsten carbide (TC) is amongst nature's hardest materials with 9.5 on the Mohs scale of hardness (Diamond: 10.0). Due to its robustness, TC is frequently used in the industry as raw material for the manufacturing of mechanically highly stressed tools like drills or milling machines. These characteristics qualify TC for grinding of the GB carrier surface.

TC powder HTWC 250 (Wolfram Bergbau und Huetten AG, St. Martin i.S., Austria) with a nominal grain size of 25 µm was employed as grinding material for physical surface alteration of GBs.

3.1.4 Hydrofluoric Acid

Hydrofluoric acid (HF) is a common industrial agent for wet chemical etching of metal or glass surfaces. For instance, HF is used in the manufacturing of wafers to control the thickness of the respective silicon layer [103]. Furthermore, it has been presented as a suitable agent to adjust the diameter of optical fibres [104]. This is due to its capability to readily dissolve silicate glass even at room temperature which makes HF a suitable chemical product for the alteration of GB surfaces.

Concentrated HF (40 %) was purchased from Merck Millipore (Darmstadt, Germany).

3.1.5 Capsules

Prior to filling, capsules were stored in a desiccator for 24 hours to maintain a brittle state of the material. Due to the large carrier size, this conditioning step was needed to ensure the release of the interactive mixture during inhalation manoeuvre.

Hard gelatin capsules of size 3 (CAPSUGEL, Morristown, USA) were utilised in the present study.

3.1.6 Inhalation Devices

3.1.6.1 Cyclohaler

The Cyclohaler (Figure 3-6) is a passive inhalation device and is therefore fully relying on the patient's inspiration capacity. It delivers a single dose of powder blend from a hard gelatin capsule [105]. The Cyclohaler belongs to the group of low resistance inhalers, since a very high flow rate has to be applied to reach the mandatory pressure drop of 4 kPa defined by the Ph. Eur. [106].

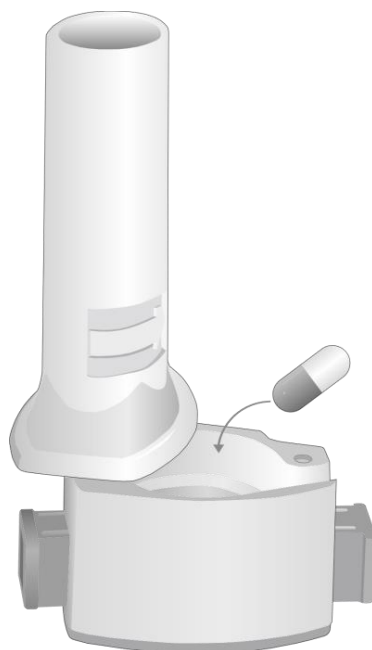


Figure 3-6 Commercially available Cyclohaler

3.1.6.2 Unihaler/Modular Inhaler

The Unihaler was developed by Christian Friebel at Kiel University in the course of his doctoral thesis where several parts of the inhaler including the opening mechanism for the capsule, air-conducting parts, deagglomeration chamber and mouthpiece have been designed and optimised [87]. This ultimately led to the final concept. The optimisation was realised using a so-called modular inhaler system, whereby the differently dimensioned parts could be freely combined (Figure 3-7).

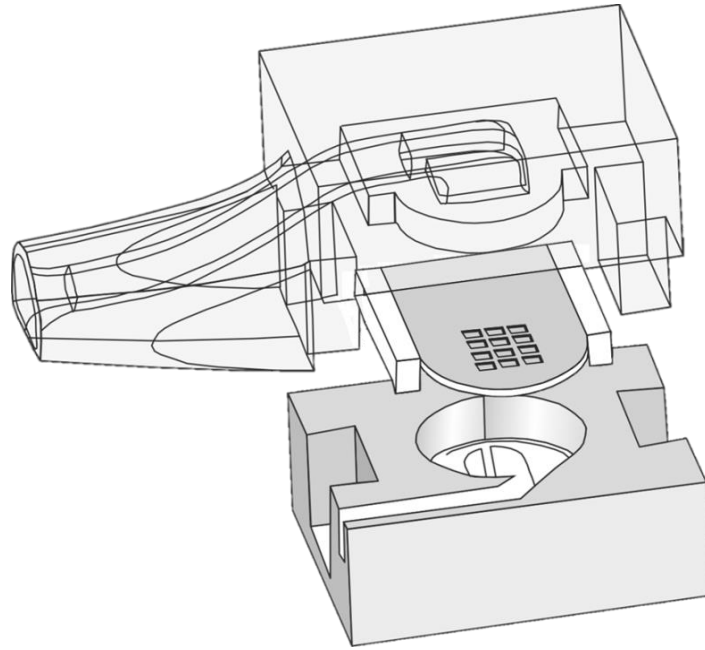


Figure 3-7 Design of the Modular Inhaler with upper part, grid and bottom part

3.2 Statistical Methods

3.2.1 Design of Experiments

Conventional approaches used for the finding of optimal experimental conditions are “trial and error” or changing of just one factor at a time. These methods are usually very time- and resource-consuming and do not lead to the desired outcome at all times. DoEs however, provide the possibility to efficiently evaluate processes which are characterised by a high degree of complexity. For this purpose, various factors and their levels are selectively combined leading to an empirical model. This reflects the influence of the included factors on the defined responses as well as the relation of different factors [107]. Table 3-2 provides an overview of common terms in experimental design.

Table 3-2 Common terms in experimental design

Term	Definition
Factor	Influence quantity selected for the respective trial
Quantitative	Can accept arbitrary values within a certain range, e.g. temperature or concentration
Qualitative	Can solely accept certain values, e.g. "on" and "off"
Factor levels	Values of respective factor used in the study
Response	Objective criterion, e.g. particle size or yield
Effect	Impact of factor on response

In general, a variety of different designs is available whereby the choice of the appropriate one is dependent on the scientific question. For this thesis, a central composite face design (CCF) with three factors varied on three different levels was used. The resulting setup is illustrated in Figure 3-8. Each point represents a single experimental setup. The centre point (CP) was repeated five times to investigate reproducibility and validity of the model resulting in a total of 19 runs. This applies to all DoEs presented

in this work. Initially, every term under investigation was considered. For the present setup with three factors, the respective responses (R) were evaluated based on equation 5:

$$R = c_0 + c_1f_1 + c_2f_2 + c_3f_3 + c_4f_1^2 + c_5f_2^2 + c_6f_3^2 + c_7f_1f_2 + c_8f_1f_3 + c_9f_2f_3$$

This equation also takes possible quadratic relations and interactions between factors into account. Here, c_x and f_n are defined as coefficients and factor levels. To ensure an adequate model fit for the DoE, insignificant terms were disregarded from the respective equation for each response. The quality of the models was evaluated based on criteria listed in Table 3-3.

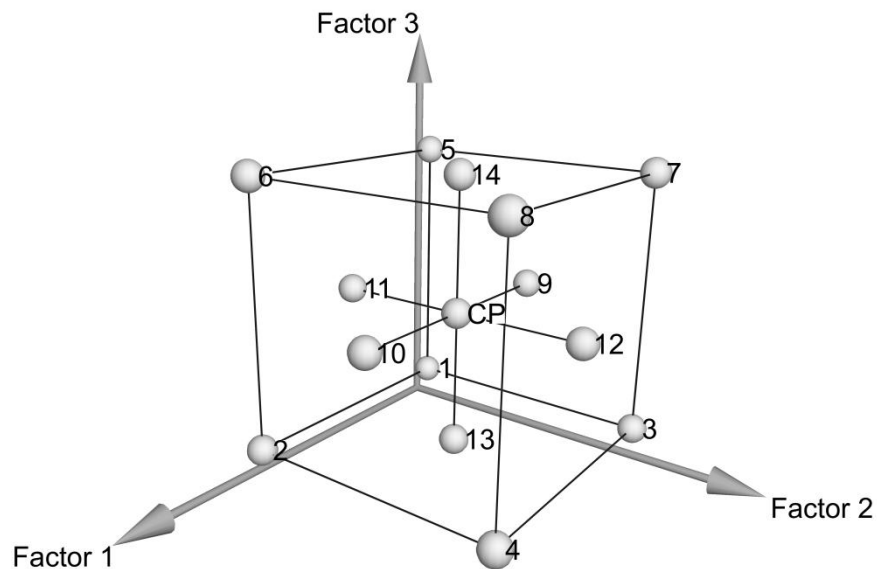


Figure 3-8 Illustration of the CCF design applied for respective DoE approaches in this study

Generation as well as evaluation of DoEs was carried out using the MODDE 10.1.1 software (Umetrics AB, Umeå, Sweden).

Table 3-3 Parameters for the evaluation of design quality

Parameter	Definition	Target value
R2	Shows the model fit and is an indicator for model significance	> 0.5 indicate significant model
Q2	Indicates future prediction precision	> 0.5 is desirable
Model validity	Indicates presence/absence of diverse model problems	> 0.25 is mandatory*
Reproducibility	Variation of replicated centre points compared to overall variability	> 0.5 is desirable

* might be very low due to an artificial lack of fit if reproducibility is > 0.9

3.2.2 General Statistical Considerations

Unless otherwise stated, measurements were performed in triplicate in the present study to determine the mean value and standard deviation (StD), which is represented by error bars in the respective graphs. If necessary, data was subjected to analysis of variance (ANOVA) and Student's t-test (Microsoft Excel 2010 (Microsoft Corporation, Redmond, USA)) with a probability value (p-value) of < 0.05 considered being statistically significant.

3.3 Preparative Methods

3.3.1 Spray Drying of Model Drugs

SD, being a one-step process, is a useful technique to create particles in the size range desirable for inhalation [108,109]. It also allows a selective alteration of not only particle size, but also shape and morphology by modifying process conditions [110]. The final product is typically characterised by a narrow particle size distribution (PSD) which is also considered as beneficial for pulmonary application [111]. Due to a comparatively low heat stress applied, this technique can even be used for thermosensitive biomolecules like peptides [112,113]. Nevertheless, one potential disadvantage of this process is that it often leads to a phase change of crystalline raw material resulting in particles in the amorphous state. This may essentially complicate powder handling [114]. Strategies to cope with this issue are explained in detail in Section 3.3.3.

In the course of SD, an API solution, a suspension or a colloidal dispersion is atomized by a nozzle creating a large number of droplets, while the solvent is quickly evaporated by the co- or anti-current drying gas stream. Solidified API particles are separated in a cyclone based on centrifugal forces and are collected afterwards in a bottom collecting vessel (Figure 3-9 (left)). As the desired particle diameter is 1 to 5 μm , the spray drying parameters inlet temperature (T_{inlet}), feed rate (FR), feed concentration (FC), spray gas flow (SGF) and drying gas flow (DGF) have to be chosen thoughtfully. Based on preliminary tests, fixed and varying parameters as well as their ranges were specified and provided the basis for the DoEs described in the following sections.

All trials were carried out with a B290 Mini Spray Dryer (Büchi Labortechnik AG, Switzerland) equipped with a high performance cyclone (Figure 3-9 A). Aqueous solutions were processed in open cycle mode, where heated air led to solvent evaporation. Due to safety reasons, the B290 was connected to a B295 Inert Loop (Büchi Labortechnik AG) and was operated in closed cycle mode when working with organic solvents (Figure 3-9 (right)). Here, nitrogen was used as drying gas to create inert conditions and prevent the danger of potential explosion. After passing the spray dryer, nitrogen is led into the inert loop, where separation of the organic solvent is taking place at a refrigerator unit while the nitrogen is brought back into the system. The final

products were stored in a desiccator over silica gel (Sigma Aldrich Chemie GmbH, Munich, Germany) immediately until further use.

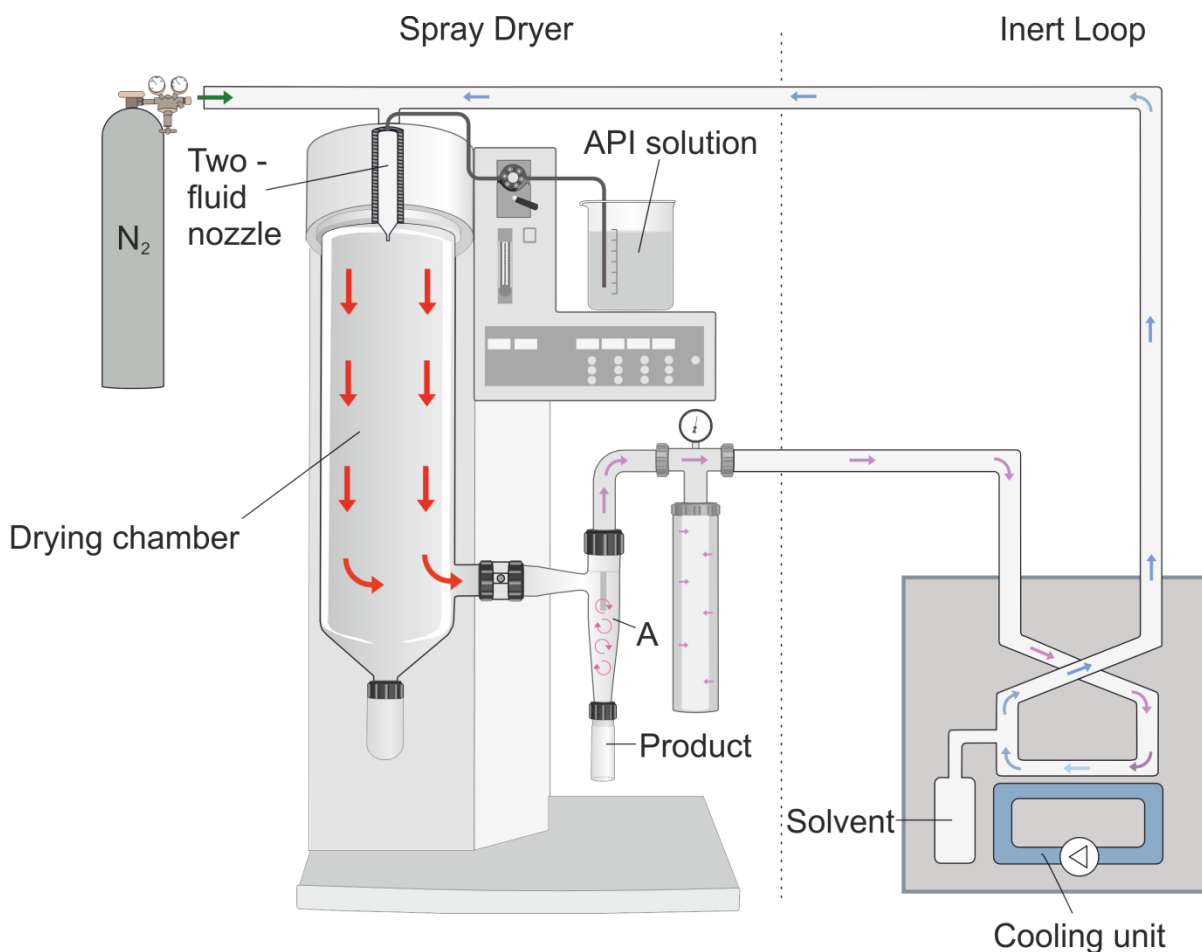


Figure 3-9 Setup of the Büchi B290 Mini Spray Dryer (left) equipped with a B295 Inert Loop (right)

3.3.1.1 Budesonide

In the present study, BUD was used as a hydrophobic model drug in micronised quality (Minakem SAS, Dunkerque, France) and additionally as spray-dried material for research purposes. For the latter, an appropriate amount of drug was dissolved in methylene chloride. In order to obtain particles in the suitable size range, T_{inlet} , FR and FC were varied on three different levels, while SGF and DGF were kept constant. Detailed information about SD conditions for the APIs can be taken from Table 3-4.

Table 3-4 SD conditions for different APIs

API	T _{inlet} , °C	FR, mL/min	FC, %(w/w)	SGF, L/h	DGF, m ³ /h
BUD	80, 100, 120	3.2, 4.3, 5.4	2.5, 5.0, 7.5	414	40
FF	100	2.1, 3.2, 4.3	2.5, 5.0, 7.5	334, 380, 426	40
TB	120, 135, 150	3.7	2, 3, 4	380, 438, 496	40

3.3.1.2 Formoterol Fumarate

FF was engaged as a model drug with intermediate hydrophilicity forming a link between hydrophobic BUD and hydrophilic IB/TB. It was used as micronised (Vamsi Labs Ltd., Maharashtra, India) and spray-dried material. For the latter FR, FC and SGF were varied to obtain inhalable particles. The SD solution was prepared by dissolving the adequate amount of FF in methanol, wherefore the process was performed in closed cycle mode as well.

3.3.1.3 Tiotropium Bromide

Furthermore, the present study included TB (Hangzhou Hyper Chemicals Ltd., Zhejiang, China) as a hydrophilic model drug. SD of aqueous solutions of the drug was performed in open cycle mode aiming at the manufacturing of particles in the size range of 1 – 5 µm. Here, T_{inlet}, FC and SGF were adjusted at constant FR and DGF.

3.3.1.4 Ipratropium Bromide

IB served as an additional hydrophilic model drug in the present study. As a consequence of inadequate processability by SD, IB was solely used in micro quality (Boehringer Ingelheim Pharma AG & Co. KG, Ingelheim, Germany).

3.3.2 Modification of Glass Beads

In order to investigate the effect of carrier surface characteristics on interparticle interactions and consequently on effective drug loading (TSC) and aerodynamic per-

formance, different methods for selective surface modification have been introduced. Before the actual process, GBs were incubated with a standard cleaning solution ($\text{H}_2\text{O}_2:\text{NH}_4\text{OH}:\text{H}_2\text{O}$ 1:1:5) to erase any organic residues and maintain comparable surface conditions. This applies to all modification procedures.

3.3.2.1 Chemical Surface Modification

For alteration of chemical surface properties, untreated GBs (GB_UT) were incubated with ethanolic solutions of various silanes in three different concentrations of 0.005 M, 0.05 M or 0.5 M for 30 min. Structural formulas of the respective silanes can be taken from Figure 3-10. Afterwards, GBs were rinsed several times with double-distilled water (ddH_2O) and put in a drying chamber at 60 °C to remove residual moisture.

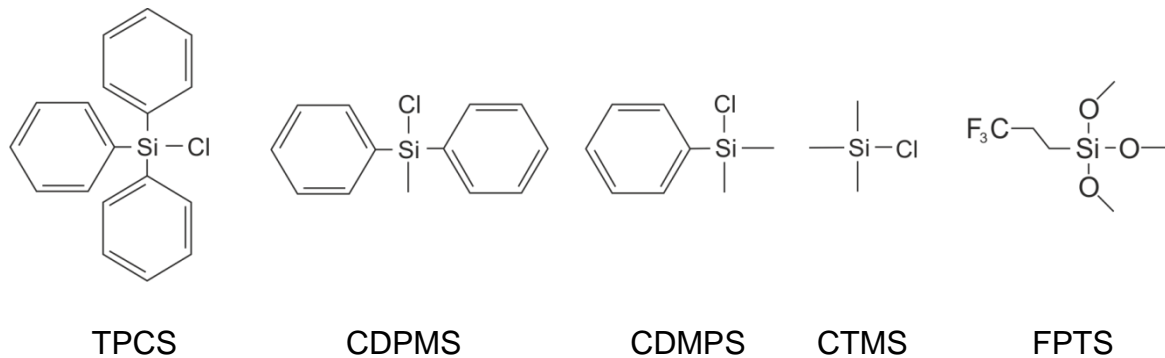


Figure 3-10 Silanes used for chemical surface modification: Chlorotriphenylsilane (TPCS), Chloro(methyl)diphenylsilane (CDPMS), Chloro(dimethyl)phenylsilane (CDMPS), Chlorotrimethylsilane (CTMS) and Trimethoxy(3,3,3-trifluoropropyl)silane (FPTS)

This work was carried out by cooperation partners of the DFG priority program at the Department of Mechanical Process Engineering (Otto von Guericke University, Magdeburg).

3.3.2.2 Alteration of Surface Topography

HF Treatment

100 g of GBs were incubated with HF for 10 minutes. After filtration, GBs were rinsed several times with ddH_2O to wash off acid residues followed by drying and storage in a plastic container until further use.

Ball Milling

The second processing method engaged a planetary ball mill where a grinding jar rotates in the opposite direction to a counterweight (Figure 3-11). That induces high dynamic energies caused by frictional and impaction forces [115].

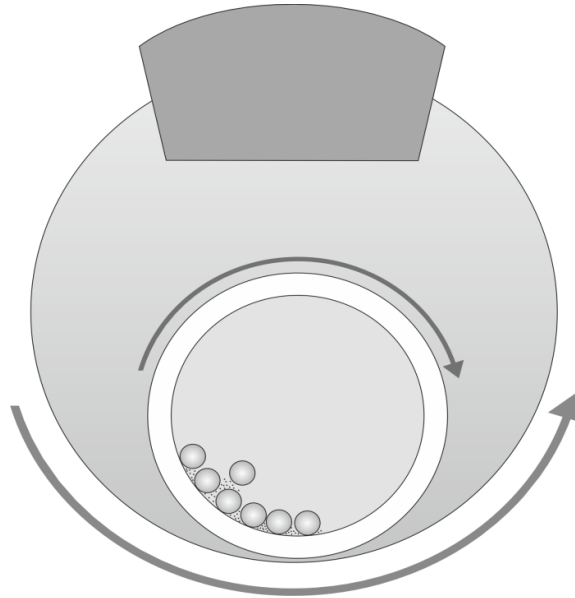


Figure 3-11 Working principle of the ball milling process

For surface alteration purposes, conventional grinding balls were replaced by TC as grinding media (small particles). 100 g of GBs (large spheres) were filled into a zirconium oxide grinding jar with a volume of 500 mL together with the same amount of TC and processed with a PM 100 ball mill (Retsch Technology GmbH, Haan, Germany). Milling time was set to four or eight hours and rotation speed was adjusted to 424 rpm. The whole process was conducted in a cold storage room at 1 – 3 °C to counteract the heat development created through extensive frictional forces during milling. Afterwards, a stainless steel sieve with a mesh size of 355 μm was used to separate GBs from the major portion of TC. GBs were then put in a glass vessel filled with $\text{d}_2\text{H}_2\text{O}$ and placed in an SONOREX SUPER RK ultrasonic bath (Bandelin Electronic GmbH & Co.KG, Berlin, Germany) to detach remaining TC from the glass surface.

3.3.3 Working Under Controlled Ambient Conditions

Preparation (section 3.3.5) and impaction analysis (section 3.4.2.3) of interactive mixtures were performed under controlled conditions to maintain stability of the drugs. Furthermore, this procedure ensured comparable environmental conditions for all experiments. The parameters temperature and rH were chosen thoughtfully for each API based on performed dynamic vapour sorption (DVS) measurements (section 3.4.1.7). An overview can be taken from Table 3-5.

Table 3-5 Ambient conditions adjusted for different APIs used in the present study

API	Temperature, °C	Relative humidity, %
BUD sd	21	35
BUD micro	21	45
FF sd	21	30
FF micro	21	45
TB sd	21	20
IB micro	21	45

Therefore, blending and impaction analysis were conducted in a climate chamber (Imtech GmbH, Hamburg, Germany).

3.3.4 Calculation of Carrier Surface Coverage-Theoretical Considerations

As already mentioned, an overarching objective of the present study was to investigate the interparticle interactions between API and carrier. In the course of this, the effect of carrier surface modification on drug loading and consequently the influence of drug loading on aerodynamic performance should be elucidated. As the use of spray-dried, spherical particles provided the opportunity to determine the amount of API necessary to cover a certain degree of carrier surface, different so-called theoretical or calculated surface coverages (CSCs) were determined. This was achieved by calculating the amount of API needed to be weighed in to cover a defined percentage

of the total free carrier surface [81]. Assuming densest sphere packing of API particles on the GB surface, the projected area of two equilateral triangles, where side length is the diameter of a single API particle, equals the space occupied by a single drug particle (Figure 3-12).

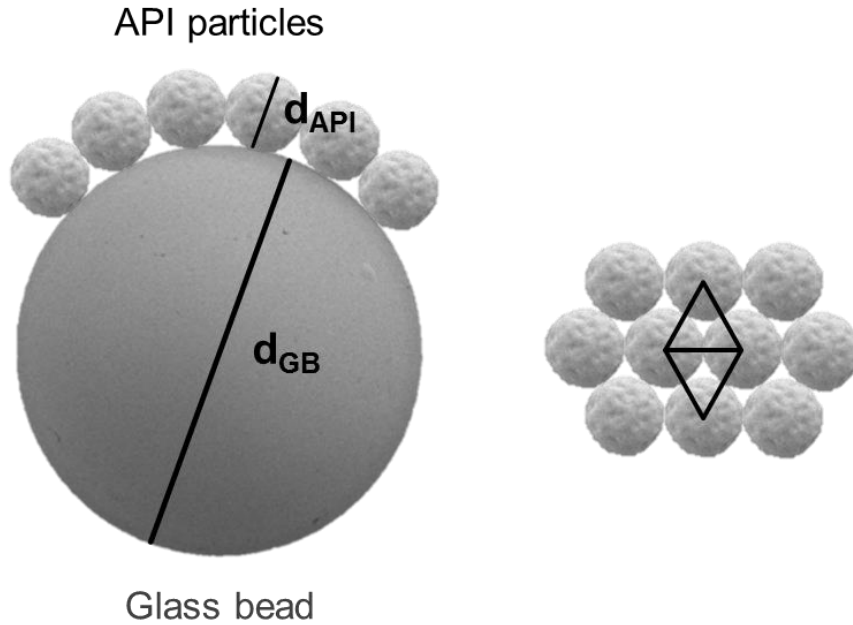


Figure 3-12 Schematic illustration of CSC determination adapted from [81]

The surface area (SA_{GB}) of a single GB and the projected area on a GB occupied by a single API particle (pA_{API}) were calculated based on equation 6 and equation 7. Here, d_{GB} and d_{API} represent the diameters of a single GB and an API particle, respectively. In order to determine the total number of API particles needed to cover 100 % of the surface of one GB, the resulting value from equation 6 was divided by the surface area occupied by a single API particle. For other CSCs (50 % and 25 %), the resulting value was adjusted accordingly.

$$SA_{GB} = (d_{GB} + d_{API})^2 * \pi \quad \text{equation 6}$$

$$pA_{API} = \left(\frac{d_{API}^2}{4} * 3^{0.5} \right) * 2 \quad \text{equation 7}$$

$$m_{GB} = V_{GB} * p_{GB} = \pi * d_{GB}^3 * \frac{p_{GB}}{6} \quad \text{equation 8}$$

$$\frac{m_{API}}{GB} = \pi * d_{API}^3 * \frac{p_{API}}{6} * \chi \quad \text{equation 9}$$

In a third step, the mass of one single GB particle (m_{GB}) was calculated based on equation 8 (V_{GB} : volume of one GB) to determine the number of GBs present in 15 g (by dividing 15 g by m_{GB}). Equation 9 provides the mass of API particles per GB, which is multiplied by the calculated number of GBs to display the amount of API needed to weigh in for the desired CSC. χ represents the number of API particles per GB for the desired CSC. For illustration purposes, a scheme has been added, where calculation steps can be comprehended more easily (Figure 3-13).

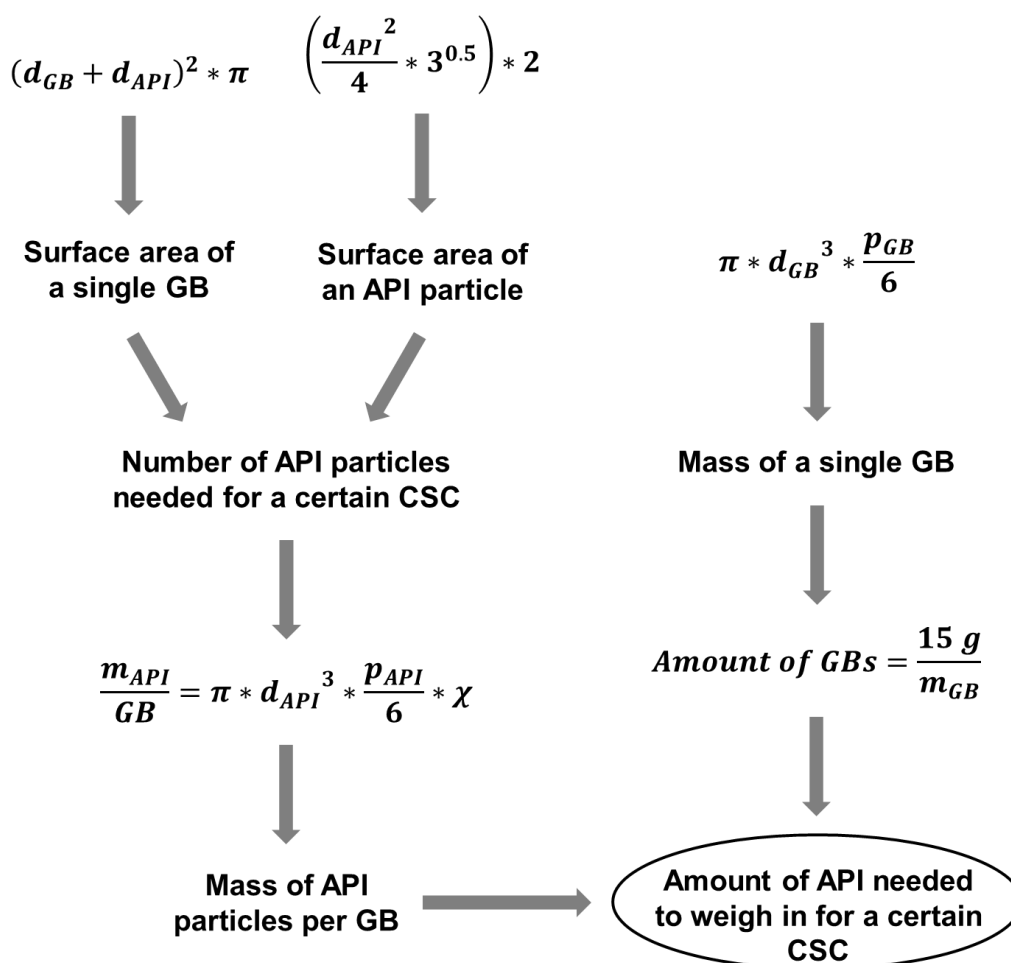


Figure 3-13 Illustration of arithmetic steps for determining API net weight for a certain CSC

3.3.5 Preparation of Interactive Mixtures

Manufacturing of interactive mixtures employed a Turbula blender T2C (Willy A. Bachofen AG, Muttenz, Switzerland), where the mixing container is subjected to

rotation, translation and inversion to obtain sufficient homogeneity [116]. The basic principle is illustrated in Figure 3-14.



Figure 3-14 Rotational movement of the Turbula blender

For spray dried or micronised API qualities, 15 g or 14.75 g of GBs and the appropriate amount of drug were weighed into a stainless steel mixing vessel using the double sandwich method (Carrier/API/Carrier/API/Carrier) resulting in a filling volume of around 20 %. For each API, preliminary tests were conducted to determine optimal blending parameters, namely time and rotation speed to obtain sufficient blend homogeneity (section 3.4.2.2) as well as to ensure integrity of spray-dried and micronised API particles. Blending protocols can be taken from Table 3-6

Table 3-6 Blending parameters for different APIs

API	Blending time, min	Rotation speed, rpm
BUD sd	30	20
BUD micro	20	30
FF sd	30	20
FF micro	30	42
TB sd	45	20
IB micro	20 followed by 10	30 followed by 20

3.4 Analytical Methods

3.4.1 API and Carrier Characterisation

3.4.1.1 Laser Diffraction

Laser diffraction is a frequently used technique in the pharmaceutical industry and in research for investigations concerning particle sizes as it can be applied to solid and liquid samples [117,118]. The measuring principle is based on the varying potential of particles to diffract laser beams according to their size, whereby larger particles lead to higher intensities at smaller measuring angles. Gained data is subsequently transformed into the equivalent particle diameter (volume based) utilising the Mie or the Fraunhofer theory [119].

Laser diffraction was applied to determine PSDs of spray-dried and micronised drugs. Therefore, a Helium Neon Laser Optical System (HELOS[®], Sympatec GmbH, Clausthal-Zellerfeld, Germany) was equipped with a RODOS[®] dry dispersion module (Sympatec GmbH) and an R2 lens with a measuring range of 0.25 – 87.5 µm. Samples were fed manually to obtain an optical concentration between 1 and 5 %, while powders were dispersed towards the measurement chamber by compressed air (3 bar). Data evaluation was performed with the Windox 5 software (Sympatec GmbH) based on the Fraunhofer Enhanced equation to determine cumulative frequency (Q3) and probability density function (q3*). Additionally, characteristic variables of the PSD, namely x_{10} , x_{50} and x_{90} , i.e. the volume based equivalent diameter at which 10 %, 50 % or 90 % of particles under investigation are smaller, were provided. The span value served as a measure for PSD width (equation 10).

$$\textit{Span} = \frac{x_{90} - x_{10}}{x_{50}} \quad \textit{equation 10}$$

3.4.1.2 Dynamic Image Analysis

In order to determine size and shape of GBs, particles were analysed using image analysis equipment. Here, particles are accelerated in a fall shaft by gravitation, while they are dispersed due to particle-wall and particle-particle collisions. A high-speed

camera records the particles on up to 450 images/s. This setup allows size determination between 1 and 20000 μm .

Measurements were performed with the QICPIC system (Sympatec GmbH) at a recording speed of 300 Hz. For sample dispersion, a VIBRI vibrating chute (Sympatec GmbH) was coupled with GRADIS gravity disperser (Sympatec GmbH). On the one hand, this provided information about PSDs. On the other hand, images were used to determine particle sphericity (Sph) as the measure for overall shape. Sph is defined as the ratio of the perimeter of the equivalent circle (P_{EQPC}) to the real perimeter (P_{real}). This is described in equation 11, where A is the area of the particle. Sph can accept values between 0 and 1, whereby 1 shows a perfect spherical shape.

$$Sph = \frac{P_{EQPC}}{P_{real}} = \frac{2\sqrt{\pi*A}}{P_{real}} \quad \text{equation 11}$$

3.4.1.3 Scanning Electron Microscopy

This method is based on electrons which are emitted by a wolfram cathode and are accelerated in an electric field at a high voltage [120]. The created electron beam is focused onto the specimen surface via solenoids. Depending on interactions between electrons and atoms of sample surface, different signals including the emission of secondary electrons are recorded. Hereby, a magnification of up to 500,000-fold can be achieved. The process is typically performed under high vacuum to avoid interactions with airborne molecules and atoms.

All measurements of scanning electron microscopy (SEM) were conducted using a Zeiss Ultra 55 Plus (Carl Zeiss NTS GmbH, Oberkochen, Germany) at a working voltage of 2kV. Signals were recorded by a SE-2 detector. Since nonconductive samples tend to build up electrostatic charge during scanning, samples were fixed onto carbon stickers and sputtered with a Bal-Tec SCP 050 Sputter Coater (Leica Instruments, Wetzlar, Germany) for 65 s prior to analysis. This ensured electrical conductivity and grounding to minimize imaging faults.

3.4.1.4 Contact Angle Measurements

Determination of contact angle (CA) employing the sessile drop method was conducted to investigate chemical surface properties of different modified GBs. In general, water is used as the liquid component in this setup. Therefore a low CA can be associated with a hydrophilic surface since increased potential for interaction between the surface and the water drop causes spreading of the water drop. This consequently decreases the measured angle of contact.

Experiments were carried out with an OCA 20 contact angle meter (DataPhysics Instruments GmbH, Filderstadt, Germany) equipped with a USB CCD-camera. A water drop of $< 1 \mu\text{l}$ was generated manually and placed onto the GB surface. This procedure was repeated on 20 GBs to calculate the mean CA and StD.

3.4.1.5 Atomic Force Microscopy

Surface Topography

Atomic force microscopy (AFM) is a versatile tool for the characterisation of surface properties like morphology, polarity or roughness [121–123]. In contrast to conventional visualisation techniques, AFM generally relies on direct interaction with the specimen. The basic setup for surface imaging is illustrated in Figure 3-15. For analysis purposes a cantilever with a sharp tip at the end raster-scans the surface of the sample which is fixed onto a piezo-motorised stage. As the tip scans across the specimen surface, present irregularities cause twisting and bending of the cantilever. This leads to specific extents and angles of deflection of the laser beam, which is focused onto the cantilever. These signals are detected by a photo diode and can be transformed by a processing unit to provide information about surface topography [124]. This technique is used to visualize sample surfaces on three-dimensional height images in a highly detailed fashion even on nano-scale. In addition, it provides the opportunity to quantify the degree of surface roughness and therefore allows direct comparison of different samples.

Initially, carrier particles under examination were fixed onto a commercially available glass slide using a two-component adhesive (UHU, Buehl, Germany). Carrier imaging as well as determination of surface roughness were performed with a NanoWiz-

ard I (JPK Instruments AG, Berlin, Germany) equipped with an OMCLAC 160 TN-W2 cantilever (Olympus K.K., Tokyo, Japan). Three areas of $100 \mu\text{m}^2$ ($10 \mu\text{m} \times 10 \mu\text{m}$) each on three different GBs were measured for every type of carrier with tapping mode imaging. From gained data, carrier surface roughness, expressed as the root mean square roughness (R_{rms}), was calculated with the help of Gwyddion 2.42 data analysis.

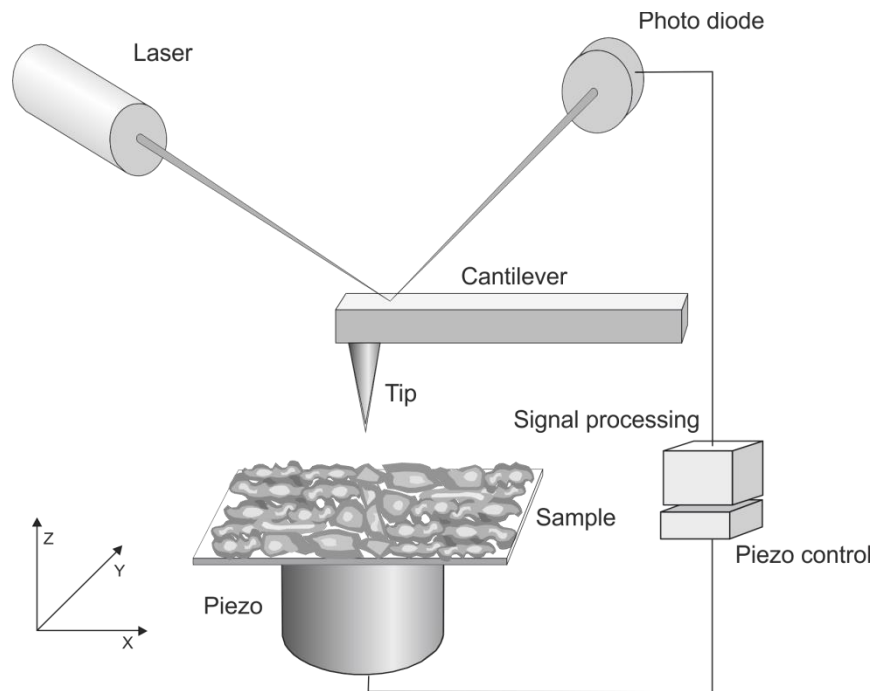


Figure 3-15 AFM setup for surface characterisation

The R_{rms} was calculated based on equation 12, where n is the number of data points and x_i is the vertical distance of the i^{th} data point from the mean value of the corresponding scan line [125]. Due to the sphericity of samples under investigation, the overall curvature was taken out of the equation by subtracting from each AFM picture before the actual calculation.

$$R_{\text{rms}} = \sqrt{\frac{1}{n} \sum_{i=1}^n x_i^2} \quad \text{equation 12}$$

Adhesion Forces

Colloidal probe AFM was used to investigate AFs between physically modified GBs and BUD sd. Here, a tiplless cantilever is equipped with a single particle (Figure 3-16) which is brought into and out of contact with the specimen surface. The AF is calcu-

lated from those measurements based on Hooke's law [126], where x and k represent the cantilever displacement induced by interparticle forces and the spring constant, respectively (equation 13). The latter is considered a measure for the cantilever stiffness. Since the spring constant is specific for each cantilever, it was determined in a preliminary test each time. This method provides the possibility to measure forces between an API particle and the carrier surface directly as the AF is equivalent in magnitude to the force required to detach the respective particle [127].

$$AF = k * x \quad \text{equation 13}$$

Therefore, a single API particle was glued onto a NSC 12 cantilever (Anfatec Instruments AG, Oelsnitz, Germany) with the help of a NMO-203 micromanipulator (Narishige Group, Tokyo, Japan). Figure 3-16 presents exemplary an SEM picture of a prepared cantilever. A grid of $5 \times 5 \mu\text{m}$ was laid on the scan area of the carrier resulting in 25 measuring points. On each scan point, the force needed to detach the API particle from the carrier surface was monitored 50 times, leading to 1250 force curves for a single GB. This procedure was repeated three times with a new set of API and carrier for every type of GB. Mean values and standard deviations were calculated based on AFs determined on the total of 75 measuring points for every type of GB. Measurements were conducted with a JPK NanoWizard I as well. Force curves of adhesion were evaluated using a self-written LabVIEW program developed by Dr. Michael Kappl (Max Planck Institute for Polymer Research, Mainz, Germany).

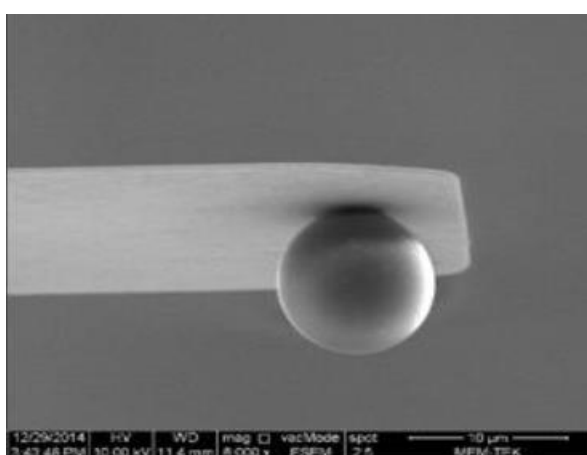


Figure 3-16 Exemplary SEM micrograph of a spherical glass particle attached to an AFM cantilever taken from [128]

3.4.1.6 Density Measurements

Gas pycnometry was used to investigate the density of spray-dried powders. For its characterisation, the volume of inert gas displaced by the sample is measured. As this equals the sample volume, the density can be calculated by implementing the sample weight [129]. Generally, helium is used as inert gas since it is able to permeate in small pores up to a minimal diameter of 2 Å. Hereby the volume of open pores on the surface can be taken into account, while closed pores remain unrecognised.

Density of samples was measured with a Pycnomatic ATC helium pycnometer (Porotec, Hofheim, Germany). For this, the measuring vessel was filled up to about 80 % with the sample powder, carefully placed inside the instrument and analysed in 10 cycles.

3.4.1.7 Dynamic Vapour Sorption

The measuring principle is based on absorption and desorption processes of solvents at defined rH [130]. Since amorphous materials are characterised by a higher potential to absorb moisture compared to those in the crystalline state and since recrystallisation is accompanied by water loss, transitions from amorphous to crystalline state, inter alia, can be investigated [131]. Hence, DVS was used as an additional method of characterisation for the different APIs. Findings also contributed to define optimal ambient conditions for blending and impaction analysis in order to avoid recrystallisation of spray-dried APIs.

DVS measurements were carried out using a DVS-HT (Surface Measurement Systems Ltd., London, UK) applying the following method under isothermal conditions (25 °C):

Step 1: Increase of rH from 0.0 to 0.9 followed by decrease to 0.0 again

Step 2: Repetition of step 1

After reaching equilibrium, where no significant change in mass (< 0.0005 %/min) was noticed, rH was increased or decreased by 0.1 to the next stage.

3.4.1.8 X-Ray Powder Diffraction

X-ray powder diffraction (XRPD) is commonly used for characterising the degree of crystallinity and identifying crystal polymorphs. Here, X-rays are generated in a tube by a cathode while electrons are accelerated towards the anode and in direction of the sample by applying high voltage. Diffraction of X-rays from probe atoms can be detected and processed into diffraction patterns that provide information about the crystal structure. Amorphous samples do not lead to distinct diffraction patterns, but only create background signalling (halo), hence, this technique was used in the present work to check for amorphicity.

Powder examination was performed by XRPD (Stadi P diffractometer, Stoe & Cie GmbH, Darmstadt, Germany). An operating voltage of 40 k V was applied and measuring range was set to $\theta = 8 - 35^\circ$ with a step rate of $2\theta = 0.05^\circ$.

3.4.1.9 Inverse Gas Chromatography

Inverse gas chromatography (iGC) is a versatile technique to investigate physico-chemical properties of various materials. Contrary to conventional gas chromatography, the probe under investigation is filled into a chromatographic column to provide the stationary phase (Figure 3-17). Different alkanes varying in their chain length are injected as mobile phase into the probe-packed column at a constant carrier gas flow rate [132]. As retention time of the eluents (detected by a flame ionisation detector (FID)) is, amongst other factors, highly dependent on potential for interaction between eluents and sample molecules, gained data serves for further characterisation of surface and bulk properties [133].

The dispersive part of surface energy (γ_s^d) and γ_s^d profiles were investigated with an SMS Inverse Gas Chromatograph (Surface Measurement Systems Ltd., London, UK). For analysis, about 0.2 g of API or 4.5 g of GBs were filled into silanised glass columns (Surface Measurement Systems, 300 mm x 6 mm outer diameter) with an inner diameter of 3 or 4 mm, respectively and sealed with silanised glass wool. After a pre-compaction step of 10 minutes utilising the column-packing accessory (Surface Measurement Systems) samples were initially equilibrated at 303 K and 0 %rH for two hours to ensure a comparable state of the samples. For examination of γ_s^d , al-

kanes (hexane, heptane, octane, nonane, decane) were injected at infinite dilution (0.03 p/p^0), while methane (0.01 p/p^0) was used to determine the dead volume. Calculation of γ_s^d from gained data was performed with the help of the iGC Advanced Analysis Macro V1.41 (Surface Measurement Systems) using Microsoft Excel 2010. A profound overview of applied arithmetic operations can be taken from [134].

To compile γ_s^d distribution profiles, the appropriate alkanes were injected at different concentrations ranging from 0.03 to 0.95 p/p^0 . By doing so, isotherms for each alkane were created to subsequently acquire information of surface energy profiles of the specimen [135,136]. Again, methane was used to identify the dead space volume. Data was evaluated with SMS Isotherm Macros Version 1.4 Advanced and Microsoft Excel 2010.

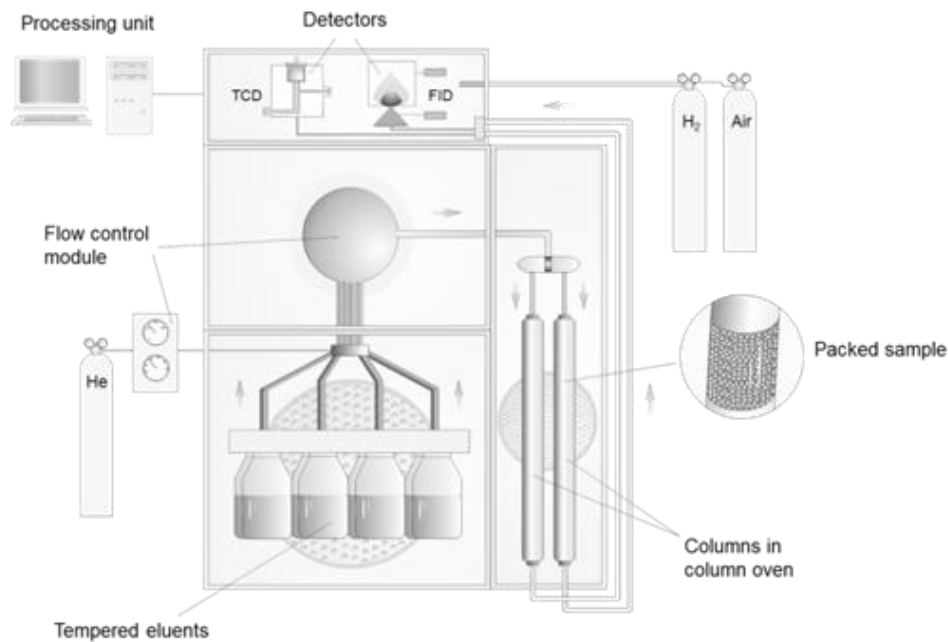


Figure 3-17 Setup of the iGC Instrument

3.4.1.10 Powder Rheometry

The purpose of these measurements is the investigation of powder properties of practical relevance, i.e. fluidization, flowability, cohesiveness and compressibility. Furthermore, it provides the possibility to examine interactions between pharmaceutical powders and different materials facilitating the choice of powder processing equipment.

Basic Flowability Energy

Basic flowability energy (BFE) is an important criterion for flow properties of powder samples. In general, a high value for BFE can be considered as a sign for suboptimal flowability. However, it is also influenced by particle properties, namely size, shape and morphology and additionally by powder compressibility [137].

In a first step, a conditioning cycle is applied to ensure a comparable state of the sample in terms of packing density. Afterwards, the twisted blade (A) performs a downward traverse while rotating anticlockwise at a tip speed of 100 mm/s through the test vessel (B) (Figure 3-18). The BFE can be calculated from the work required to move the blade from top to bottom of the vessel.

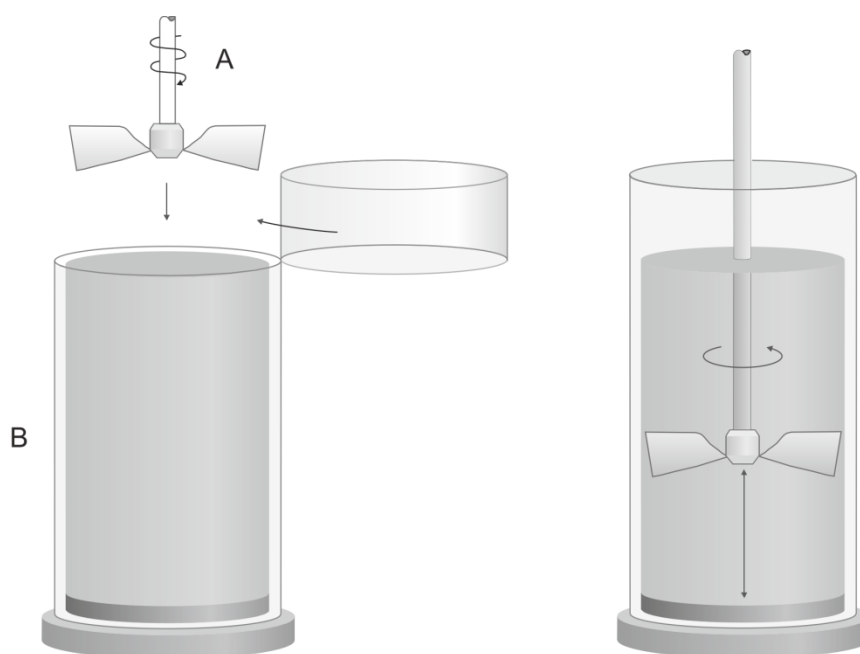


Figure 3-18 Schematic setup for the BFE test

Wall Friction

This setup is used to investigate interactions between the sample and wall material, e.g. different modified GBs and the inhaler wall in this study. The vessel is filled with sample material which is brought into contact with a disc mounted onto the wall friction piston. A normal stress is applied by the piston and the energy required for rotation of the disc is recorded [138].

For the determination of the wall friction angle (WFA), the measurement piston was equipped with a plate in appropriate size and of the same material as the inhalation device. By monitoring the energy, which was required to move the plate across the sample surface, the kinematic WFA was quantified. Calculations are based on equation 14, where τ_x and σ_x are the shear stress and the normal stress on the wall material, respectively.

$$WFA = \tan^{-1} * \left(\frac{\tau_x}{\sigma_x} \right) \quad \text{equation 14}$$

In the present study all measurements were conducted using a FT4 Powder Rheometer[®] (Freeman Technology, Tewkesbury, UK). It provides various methods to characterise powder behaviour under different conditions [139], whereby those methods can be tailored to the user's need.

3.4.2 Characterisation of Interactive Mixtures and *in vitro* Deposition

3.4.2.1 Evaluation of Drug Content

The content of each API in its respective mixture was determined by reversed-phase high performance liquid chromatography (RP-HPLC) with a Waters HPLC system (Waters Corporation, Milford, USA) equipped with the appropriate column (section 3.4.2.1). Standard solutions of the respective drug in concentrations from 1 $\mu\text{g}/\mu\text{L}$ to 100 $\mu\text{g}/\mu\text{L}$ provided the calibration curve. The injection volume was set to 100 μl and each standard solution was analysed in duplicate. Detailed information about HPLC methods are listed in section 8.1.

3.4.2.2 Determination of Content Uniformity

After blending, the interactive mixture was spread over a sheet of paper (Din A4) and 10 samples of 150 mg \pm 10 % each were taken from different spots to receive representative information about blend homogeneity. Samples were dissolved in the appropriate solvent and analysed via HPLC analysis. Only interactive mixtures with a coefficient of variation (relative standard deviation, rStD) of < 5 % were used for further experiments.

3.4.2.3 Impaction Analysis

Impaction analysis is the method of choice for *in vitro* testing of aerodynamic performance of preparations for inhalation. It needs to be noted that an impactor cannot be seen as an artificial lung model due to e.g. lack of possibilities to display physiological conditions in the human lung [140]. However, it can be used to determine the aerodynamic particle size distribution (APSD). Since particles are separated due to gravitational forces in this setup, the aerodynamic particle size is influenced by particle shape and mass.

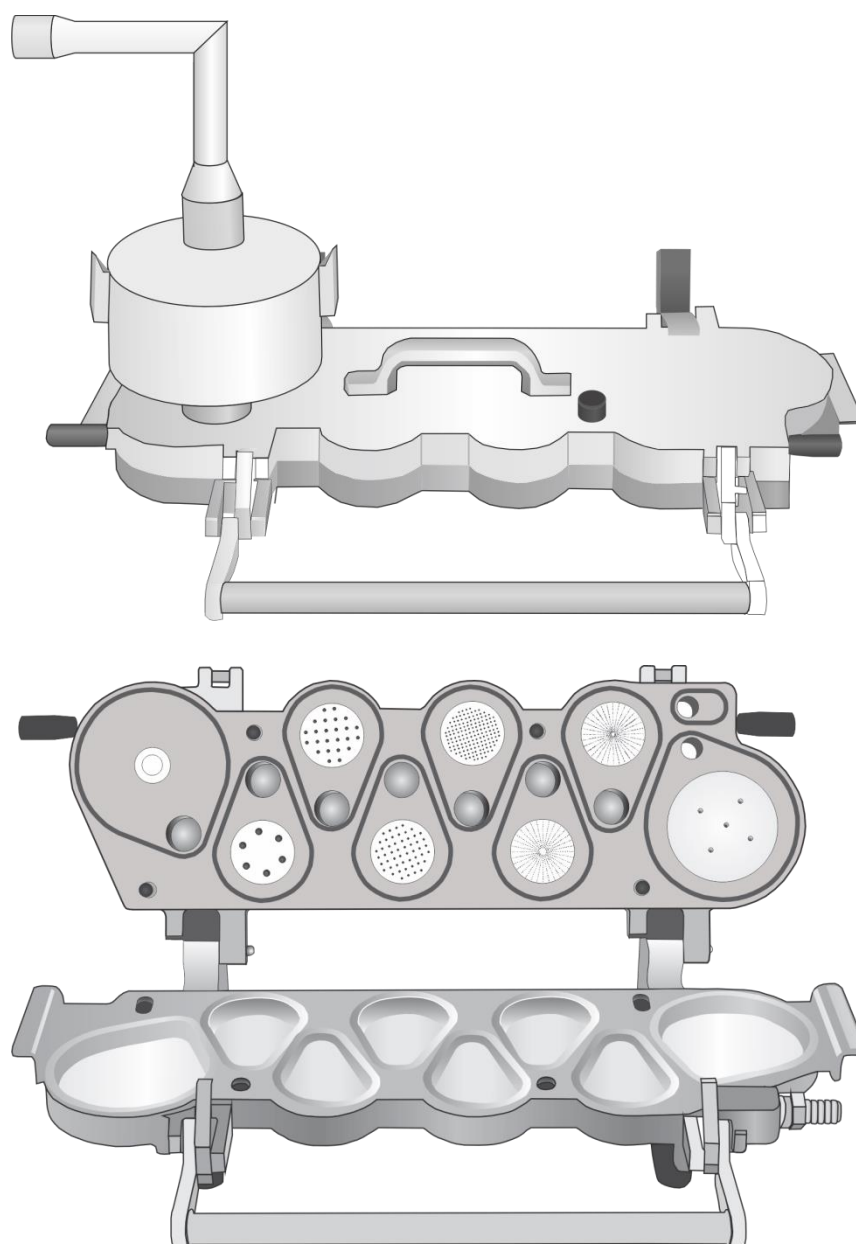


Figure 3-19 Setup of a closed NGI equipped with Induction Port and Preseparator (top) and an open NGI with collection cups and the MOC (bottom)

The Next Generation Pharmaceutical Impactor (NGI), described as Apparatus E in the Ph. Eur. [106], was used to investigate APSDs (Figure 3-19). Therefore, each of the seven stages, the micro-orifice collector (MOC) and the impaction plate of the preseparator were coated with stage coating consisting of ethanol (51 %), glycerol (34 %) and Brij[®] 35 (15 %) and allowed to dry completely. By that, a potential erroneous deposition profile caused by particles bouncing off the stages was prevented. 250 mg of blend under investigation were filled into hard gelatine capsules size 3 with a spatula. Prior to impaction analysis, capsules and inhalation device were deionised with a Static Line LC discharging bar (HAUG GmbH & Co. KG, Leinfelden, Germany) to minimize electrostatic charging. When using interactive mixtures with CSCs of 100 % or 50 %, three capsules were used for each NGI run. Investigations concerning blends with a CSC of 25 % made it necessary to release the content of five capsules to guarantee quantifiable amount of drug across the whole impactor. After inhalation manoeuvre, the device was rinsed with 20.0 mL of the appropriate solvent (section 8.1) followed by washing of capsule shells with this solution on orbital shaker 3005 (Gesellschaft für Labortechnik GmbH, Burgwedel, Germany) for one minute. Drug located in the induction port including mouthpiece and preseparator was dissolved with 15.0 mL and 30.0 mL, respectively. Stages and MOC were rinsed with 5.0 mL each. Drug content was quantified via HPLC analysis.

Table 3-7 Overview of parameters for the implementation of aerodynamic assessment with different inhalation devices

Inhalation device	Flow rate, L/min	Valve opening time, s
Cyclohaler	100	2.4
Unihaler & Modular Inhaler	60	4.0

The appropriate flow rate for the used inhaler (Table 3-7) was adjusted with the help of a digital flowmeter DFM3 (Copley Scientific Ltd., Nottingham, UK) to obtain a pressure drop of 4 kPa across the inhalation device as required by the Ph. Eur. [106]. Valve opening time was set in respect to the corresponding flow rate to obtain an inhaled volume of 4 L. This is considered as the average lung volume of an adult. Data evaluation was performed with the Copley Inhaler Testing Data Analysis Software 3.0 (Copley Scientific Ltd.). Hereby, delivered dose (DD) in µg signifies the

amount of API recovered from the entire NGI (induction port, preseparator, stages and MOC). Additionally, the mass median aerodynamic diameter (MMAD) was defined as the aerodynamic diameter at which 50 % of the particles are larger with regard to mass [141]. Fine particle dose (FPD) in μg and fine particle fraction (FPF) in %, being the amount of drug with an aerodynamic diameter $< 5 \mu\text{m}$ and the fraction of API $< 5 \mu\text{m}$ in proportion to the DD, respectively, were utilised to evaluate aerodynamic performance of interactive mixtures (equation 15).

Capsule retention (CR) in % was calculated based on equation 16, where $w_{capsule}$ is the amount of drug found in the capsules and RD is the recovered dose, defined as the total mass of API recovered from the impactor plus the fraction recovered from the capsule.

$$FPF = \frac{FPD}{DD} * 100 \% \quad \text{equation 15}$$

$$CR = \frac{w_{capsule}}{RD} \quad \text{equation 16}$$

3.4.2.4 Determination of Specific Device Resistance

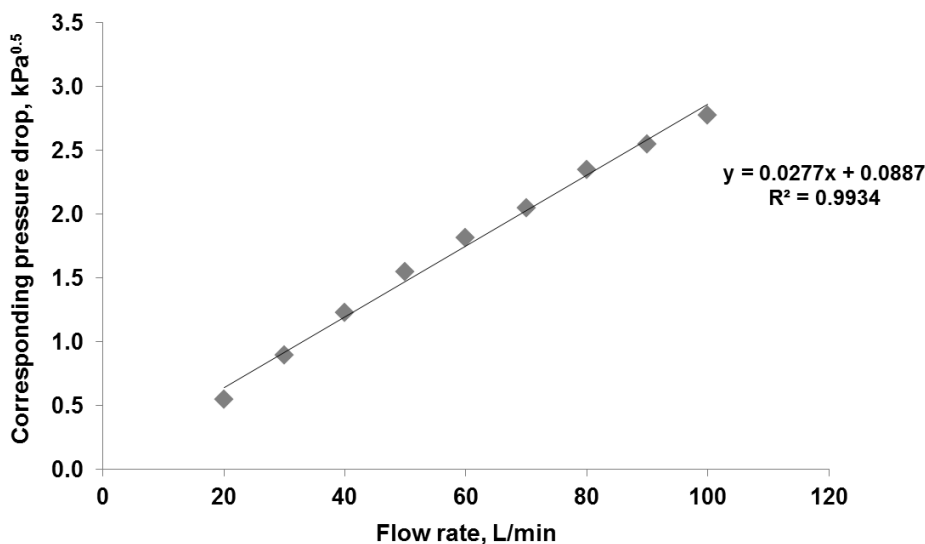


Figure 3-20 Exemplary illustration of the mathematical determination of SDR

Specific device resistance (SDR) can be used to compare resistance behaviour of different inhalation devices. Investigations were conducted implementing a method based on the setup for determination of delivered dose uniformity. As a first step, the resulting pressure drops within the inhaler at adjusted flow rates (20 – 100 L/min)

were measured. By plotting flow rate against square root of the corresponding pressure drop, SDR in $\text{kPa}^{0.5} \cdot \text{min/L}$ resulted from the slope of the regression line [142]. Consequently, the steeper the slope, the higher the resistance of the inhaler is. Figure 3-20 presents a resulting graph in exemplary manner.

Air flow was generated by a HCP5 vacuum pump (Copley Scientific Ltd) and pressure drops and flow rates were measured with a Critical Flow Controller Model TPK (Copley Scientific Ltd.) and Flow Meter Model DFM2 (Copley Scientific Ltd.), respectively.

3.4.2.5 Calculation of True Surface Coverage

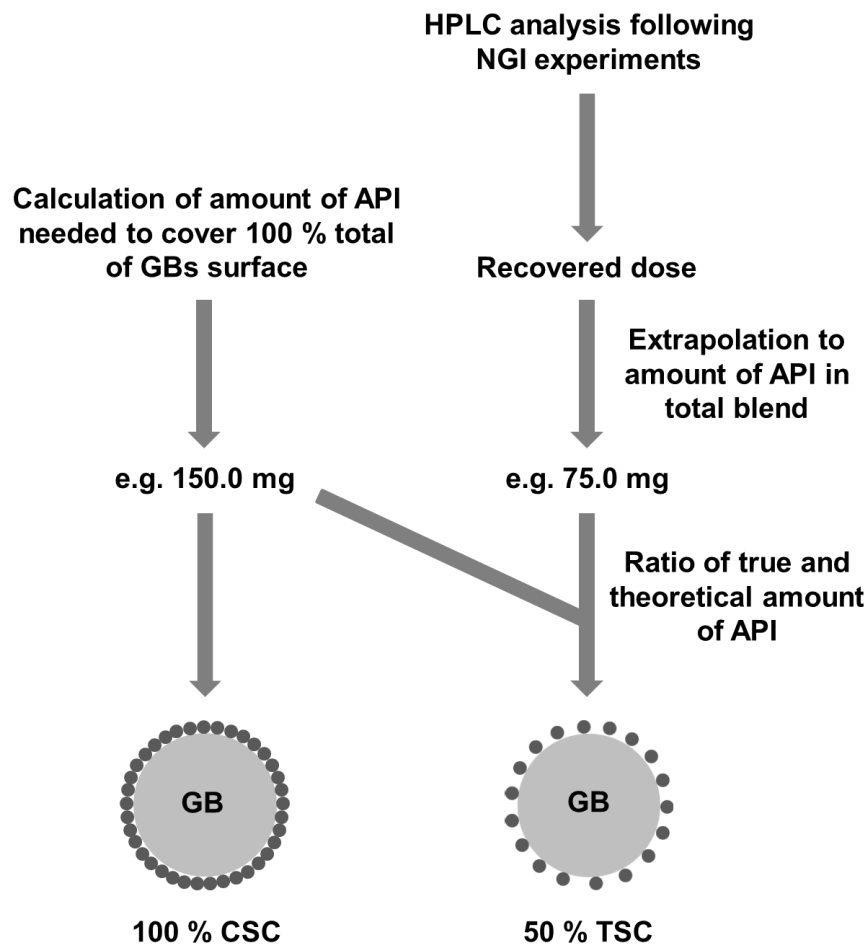


Figure 3-21 Applied methodology for the determination of TSC

The effective drug loading, expressed as TSC in this study was determined based on data from impaction analysis. As a first step, RD was quantified for the respective NGI experiments via HPLC. By knowing the initial mass of interactive mixture in the capsules, the amount of API was extrapolated to the total mass of blend. Dividing this

mass by the original net weight of API provided TSC for the respective blend. Figure 3-21 gives an illustration of calculation steps for TSC.

4 Results and Discussion

4.1 Spray Drying of Different APIs

For the present study, drug particles with certain properties such as the suitable size range for inhalation, uniformity and a spherical shape were needed. As described in section 3.3.4, interactive blends should be prepared by utilising the exact amount of API to cover a certain percentage of the total carrier surface. However, calculations require both carrier and API in a spherical shape. SD was chosen as the appropriate technique to produce micron-sized particles with the desired characteristics for dry powder inhalation. Its main advantage is the ability to alter process parameters to determine product properties, e.g. size, shape and morphology [143]. Previous studies have reported the feasibility of obtaining a size range of 1 to 5 μm by SD [144,145]. In general, the product is also characterised by a narrow size distribution which is beneficial to achieve an enhanced respirable fraction [146]. Moreover, the particles were usually of spherical shape when processing starting material in solution [109,147].

Within the DoEs, the impact of factors on particle size (x_{50}) and width of the PSD (span value) was examined to subsequently select optimal SD conditions to meet product requirements mentioned above (PSD, shape). An efficient process is also desired, wherefore the product yield, defined as the relation between initial mass weighed in and product mass, was determined. Based on preliminary trials, constant and varying parameters as well as their range were selected for the respective DoE setups. Drying gas was kept at a maximum flow rate of 40 m^3/h for all experiments to obtain products with minimum residual moisture. Increased gas velocity within the spray dryer is also known to trigger major collection and separation efficiency of the cyclone [143]. Since the present study aimed at elucidating the influence of carrier surface characteristics for a wide range of drugs, BUD, FF and TB with extensively differing chemical properties were chosen.

Hereafter, DoEs and their outcome for the three APIs are subsequently discussed followed by characterisation of the final products which were utilised to manufacture interactive mixtures. However, only valid and significant models are presented. Detailed information about the different DoE setups can be taken from section 8.5.

4.1.1 Budesonide

For the first DoE, preliminary trials suggested the variation of inlet temperature (T_{inlet} , 80 – 120 °C), feed rate (FR, 3.2 – 5.4 mL/min) and feed concentration (FC, 4 – 10 %) at a constant spray gas flow (SGF, 414 L/h) within the given ranges. Particle size of BUD was solely influenced by the FC, while x_{50} values varied from $1.2 \pm 0.0 \mu\text{m}$ to $3.3 \pm 0.1 \mu\text{m}$, as seen in Figure 4-1. For yield and span value, no significant models could be established.

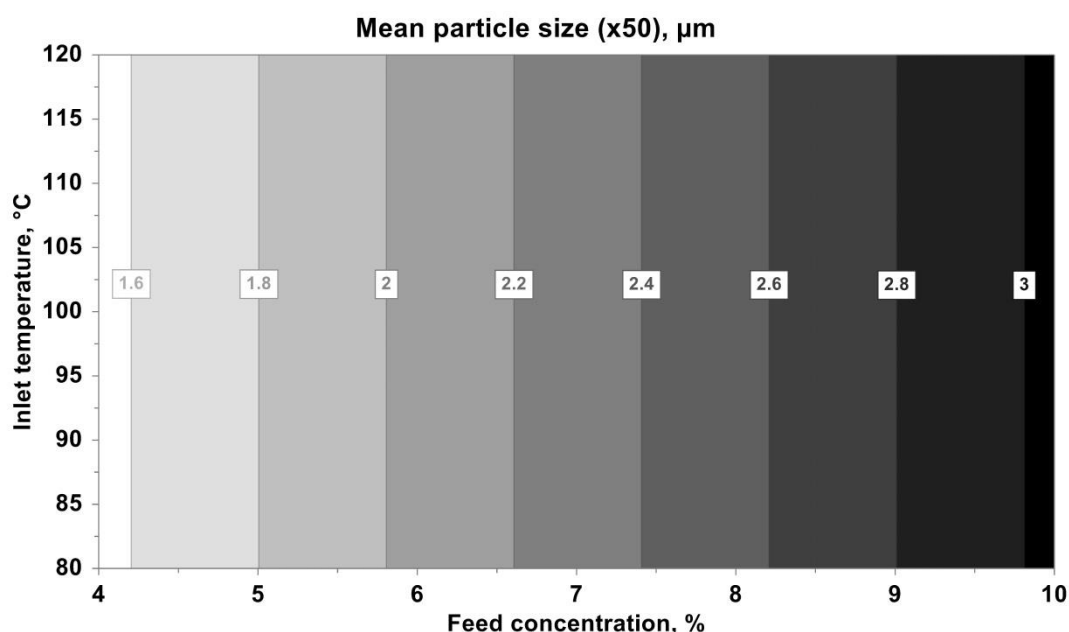


Figure 4-1 Contour plot of the mean particle size for BUD as a response of the factors FC on the x-axis and InT on the y-axis

FC had a significant effect on particle size as the increase of the FC by 3 % induced a size increase of $0.75 \pm 0.08 \mu\text{m}$. During SD, each atomised droplet forms one particle. By increasing the solid concentration, an extended amount of drug molecules will be present in each droplet. As the solvent gets evaporated, a larger particle forms compared to a solution with a lower drug concentration. This effect has also been described for a range of other substances [148,149].

Based on gained data, optimal process parameters were predicted using the MODDE software as well. Since particle size was the only response where a significant model was established and it was merely affected by FC, the following equation could be applied which is derived from the general equation 5 (section 3.2.1):

$$\text{Particle size} = c_0 + c_1FC$$

This suggested a FC of 10 % to manufacture the final product for further investigations. As the x_{50} value was found to be independent of FR and T_{inlet} , these factors were minimised to 3.2 mL/min and maximised to 120 °C, respectively, for the final product to evaporate most of the solvent present in the respective atomised drops and maintain a dry powder.

4.1.2 Formoterol Fumarate

Here, FC (2.5 – 7.5 %), FR (2.1 – 4.3 mL/min) and SGF (334 – 426 L/h) were altered at a constant T_{inlet} of 100 °C based on preliminary trials. Particle size was significantly governed by concentration and gas flow in a positive and negative manner, respectively (Figure 4-2). The process resulted in x_{50} values between $1.0 \pm 0.0 \mu\text{m}$ and $4.3 \pm 0.2 \mu\text{m}$. Significant models were also established for product yield and span value. A linear term (positive) as well as a quadratic correlation (negative) of the concentration was shown for the yield. It was also affected in a negative way by the gas flow (Figure 4-3). Span value was governed FC (positively). Here the SGF showed a linear term as well as a quadratic correlation (both negative) (Figure 4-4).

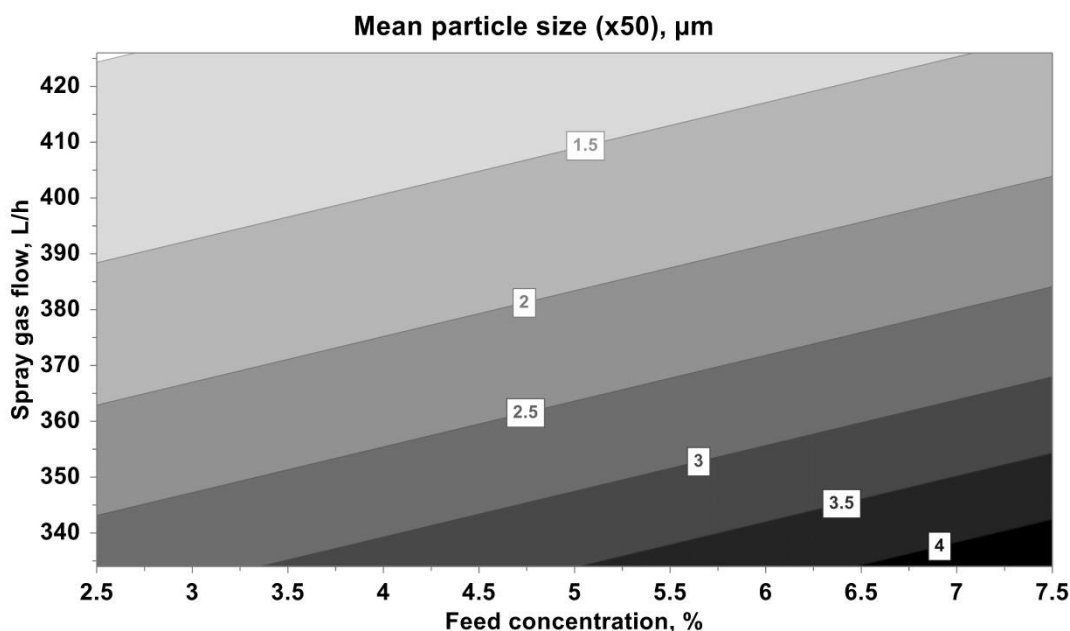


Figure 4-2 Contour plot of the particle size for FF as a response of the factors FC on the x-axis and SGF on the y-axis

The influence of FC on particle size has been discussed earlier. For the SGF, a negative correlation was determined. An increase of gas flow supplies more energy to the nozzle which forces a smaller diameter of atomised droplets [148]. In consequence, less drug molecules are present in a single droplet resulting in smaller particles.

Product yield was, inter alia, determined by the SGF as well. In general, a low flow rate led to superior API recovery from the process while increasing flow reduced product yield. When the SGF is increased, a considerable amount of spray-dried particles will be of comparatively low size $< 0.5 \mu\text{m}$ due to the small droplet size at these conditions. This fraction is separated from the airstream by the cyclone with only minor efficiency. Therefore, a certain amount of particles within this size range remains in the airstream and will be carried out of the system. Consequently, this fraction does not add to the powder collected in the product vessel forcing an insufficient yield. Similar considerations apply to the impact of API concentration. Initially, product yield increases with FC since larger particles are produced which can be separated more easily. At higher API concentrations, a certain percentage of particles has a larger diameter and is partly collected in the primary separation flask on the bottom of the drying chamber and therefore does not contribute to the final yield.

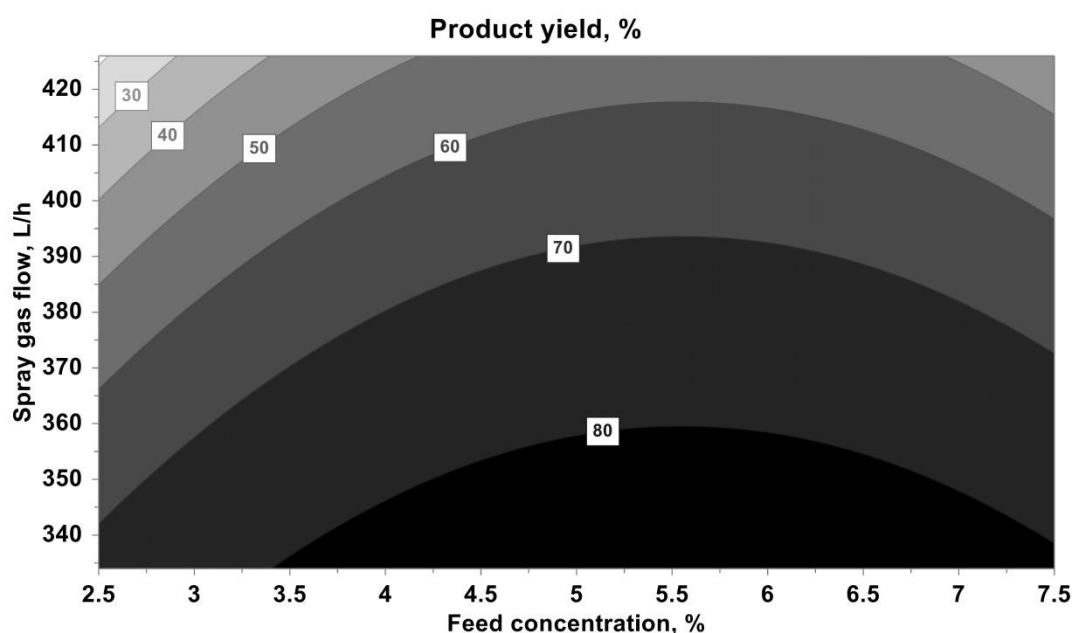


Figure 4-3 Contour plot of the product yield for FF as a response of the factors FC on the x-axis and SGF on the y-axis

The increase of SGF triggered a narrow PSD, since overall smaller particles were produced. The majority of larger particles got separated from the collected product which was therefore characterised by a lower span value. Furthermore, an enhanced API concentration generally lowered the efficiency of the SD process and led to overall larger particles simultaneously limiting the fraction of $< 0.5 \mu\text{m}$.

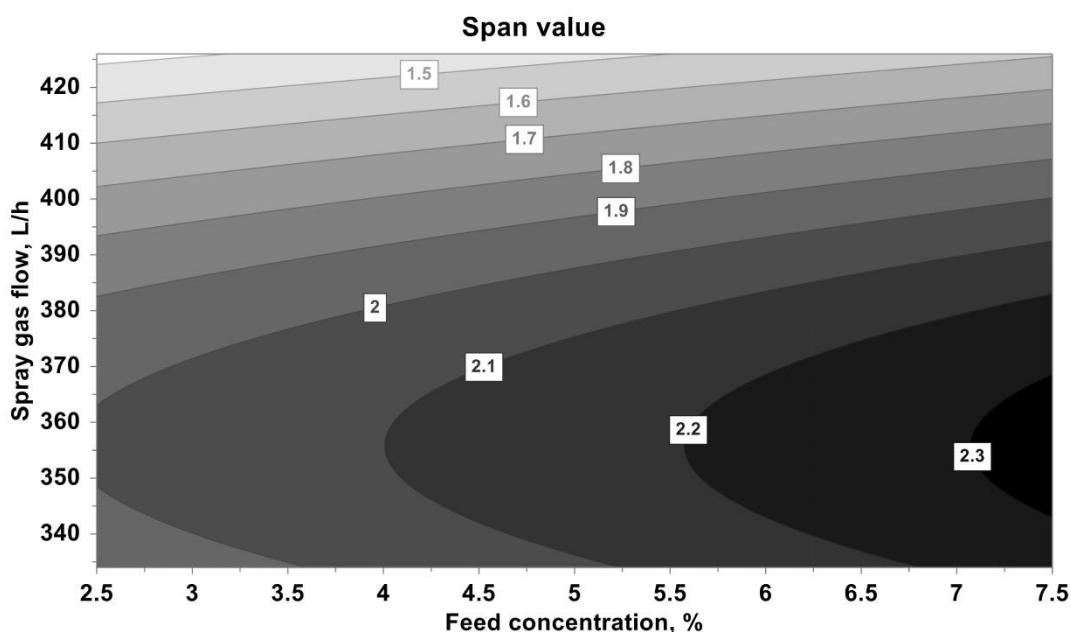


Figure 4-4 Contour plot of the span value for FF as a response of the factors FC on the x-axis and SGF on the y-axis

As significant model could be shown for particle size, yield and span value (with the significant factors mentioned above), SD conditions were optimised based on equations describing these conditions:

$$\text{Particle size} = c_0 + c_1FC + c_2SGF$$

$$\text{Yield} = c_0 + c_1FC + c_2SGF + c_4FC^2$$

$$\text{Span} = c_0 + c_1FC + c_2SGF + c_5SGF^2$$

Consequently, concentration was set to 4.5 %, while FR and SGF were fixed at 2.1 mL/min and 357 L/h, respectively. Additionally, a T_{inlet} of 120 °C was applied to minimise residual moisture in the final product.

4.1.3 Tiotropium Bromide

Implementing findings from preliminary trials, SD experiments for the hydrophilic model drug TB employed a variation of FC (2.0 – 4.0 %), T_{inlet} (120 – 150 °C) and SGF (380 – 496 L/h). FR was adjusted to 3.7 mL/min for all experiments. By doing so, a valid model was established concerning the mean size (Figure 4-5). Again, concentration and gas flow had a significant impact. An interaction of the two was also observed leading to a mean particle size of $1.9 \pm 0.0 \mu\text{m} - 4.85 \pm 0.1 \mu\text{m}$.

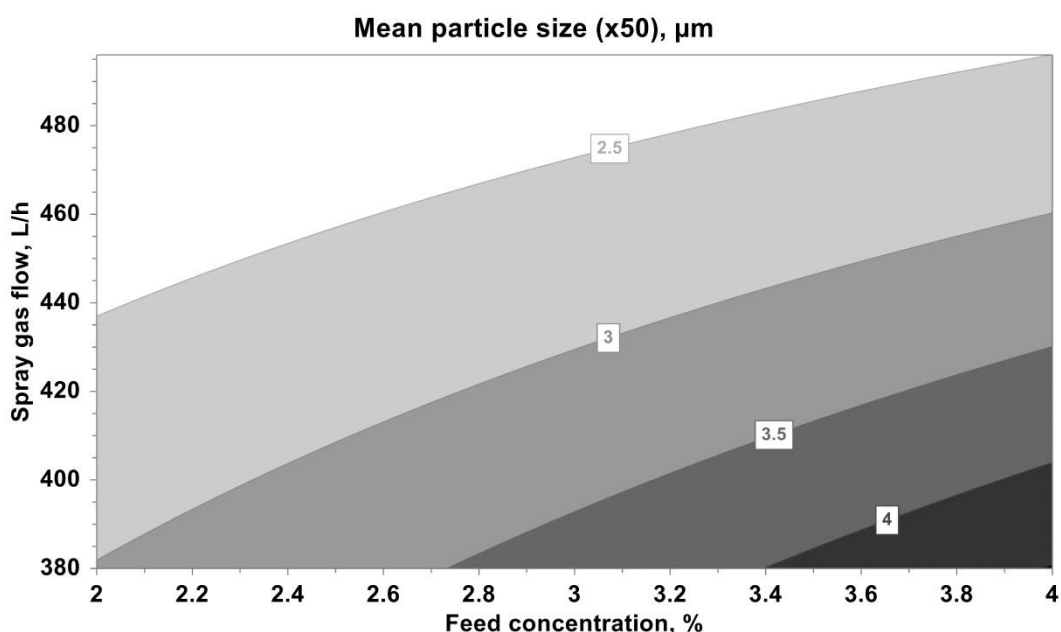


Figure 4-5 Contour plot of the particle size for TB as a response of the factors FC on the x-axis and SGF on the y-axis

For TB, a significant model was established for particle size and consequently optimal parameters were determined from the following equation:

$$Particle\ size = c_0 + c_1FC + c_2SGF + c_7FCSGF$$

This suggested an API concentration of 4 % and a SGF of 451 L/h. T_{inlet} was set to 150 °C and FR to 3.7 mL/min.

4.1.4 Characterisation of the Final Products

After the SD process, drug powders were characterised by different measurement techniques to understand their physico-chemical properties (Table 4-1). In the course of this, particle size, span value and γ_s^d were of particular interest. In addition, bulk properties were investigated. Density of the powder samples was determined, since it was needed for calculations of CSC. Samples were also subjected to XRPD to investigate the crystallinity. Examination of sorption behaviour was performed to receive information about sample stability and hygroscopicity.

Although a slight batch to batch variability of the spray-dried products was experienced in terms of particle size and span value due to the manufacturing process, e.g. minor fluctuations in drying gas pressure, other properties remained constant. For that reason, the following chapter representatively displays examination of batches of spray-dried APIs utilised for experiments to study the impact of chemical surface properties of the carrier described in section 4.2.

Table 4-1 Summary of physico-chemical properties and StDs of spray-dried APIs utilised for the manufacturing of interactive mixtures (n=3)

API	x_{50} , μm	Span value	Density, kg/m^3	γ_s^d , mJ/m^2
BUD	2.9 ± 0.1	2.4 ± 0.0	1250 ± 10	48.5 ± 0.3
FF	2.7 ± 0.1	2.1 ± 0.1	1720 ± 10	34.0 ± 0.6
TB	2.7 ± 0.1	2.0 ± 0.0	1730 ± 20	48.1 ± 0.9

4.1.4.1 Particle Size

These investigations were performed via laser diffraction. Size is a critical parameter of inhaled particles since it determines region particle deposition within the respiratory tract during inhalation (in interplay with density and shape).

FF and TB showed x_{50} values of $2.7 \pm 0.1 \mu\text{m}$ each and narrow PSDs of 2.1 and 2.0, respectively. The latter can be linked to a largely monomodal size distribution for both APIs. Mean particle size of BUD was determined to be marginally larg-

er ($2.9 \pm 0.1 \mu\text{m}$) with a span value of 2.4. This is shown by the PSD curves displaying a slightly bimodal distribution for the hydrophobic model drug (Figure 4-6).

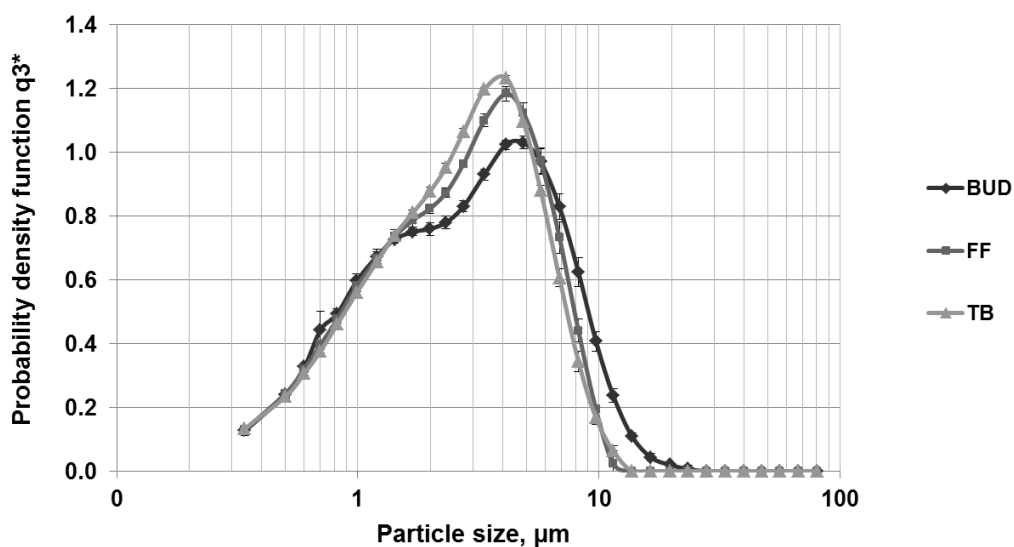


Figure 4-6 PSDs (+StD) with logarithmic scaling on the x-axis of BUD, FF, and TB (n=3)

4.1.4.2 Particle Shape and Morphology

Apart from size, drug shape was examined via SEM. SD is known to produce round particles which is also true for BUD, FF and TB (Figure 4-7). For BUD, two particle populations of about $> 2 \mu\text{m}$ and of about $< 1 \mu\text{m}$ were observed. This is in agreement with its slightly bimodal PSD described earlier. On the contrary, FF and TB particles were found to be more evenly distributed and a major quantity of particles was in the range of 2.0 to $3.5 \mu\text{m}$.

As further displayed in Figure 4-7, BUD sd and FF sd were characterised by a smooth surface without any irregularities. SD of TB led to a limited amount of microscopic indentations on some particles $> 2.5 \mu\text{m}$. In literature, drying rate, viscosity and surface tension of the solvent were described to govern morphology of spray-dried amorphous substances [150]. Nevertheless, the overall spherical shape was maintained and no indentations were present on particles $< 2.5 \mu\text{m}$.

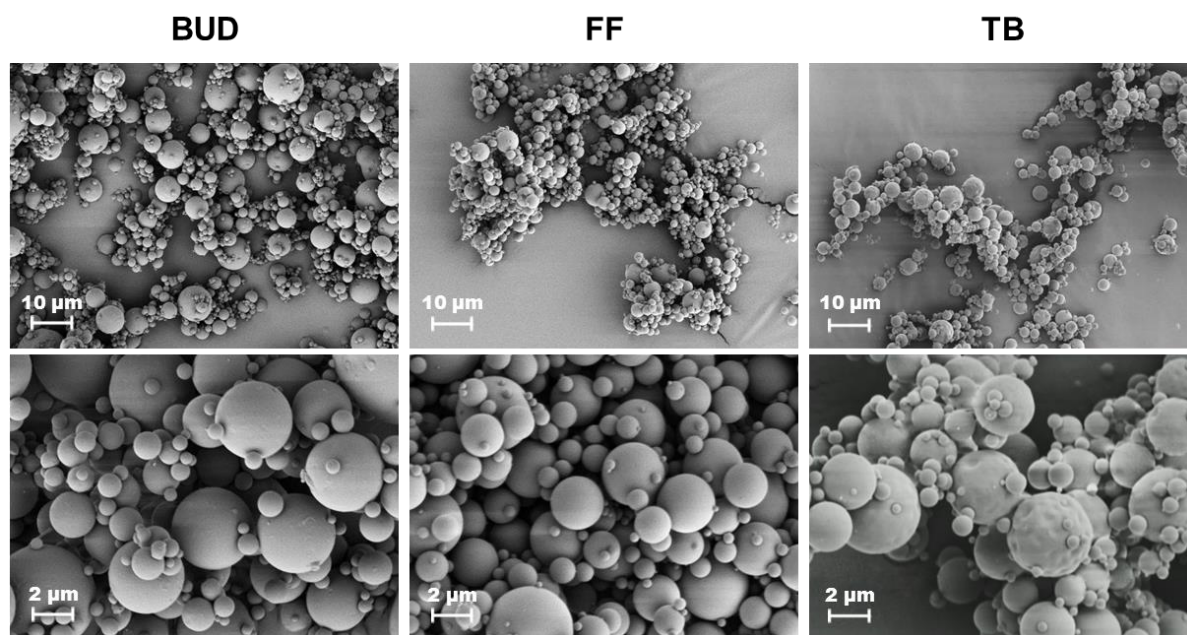


Figure 4-7 SEM micrographs of spray-dried APIs at respective magnifications of 1000x (top) and 5000x (bottom)

The overall smooth surface of the APIs ensured a defined and comparable contact area between drug particles and the carrier within interactive mixtures investigated in the following.

As shown in the present chapter, widely different SD conditions were needed to maintain particles of the three APIs with comparable properties such as size, morphology and shape. This can partly be ascribed to the used solvents. BUD and FF were processed in organic solvents which show a comparatively low surface tension. This was described to alter particle morphology and also decrease particle size [151]. It conclusively explains why an overall lower FC and SGF had to be employed for TB which was dissolved in d_dH_2O compared to BUD and FF. In addition, particle size and PSD were also found to be influenced by the drying temperature. That had to be adjusted in the present study due to the different solvents used for the APIs [152]. Another factor potentially influencing material characteristics of the spray-dried product is the type of drying gas, while nitrogen or compressed air were used for processing of BUD, FF or TB [153]. The extent to which these factors influence the product, however, is highly dependent on material characteristics of the raw material and is oftentimes difficult to predict [154].

4.1.4.3 Stability and the Impact of Ambient Conditions

With the help of XRPD and DVS measurements, crystallinity and moisture sorption isotherms were evaluated in order to estimate stability of the spray-dried drugs and to determine optimal ambient conditions for sample handling and impaction analysis. The importance of drug stability on aerodynamic performance has been emphasised in literature before. An occurring recrystallisation within the interactive mixture was shown to trigger intraparticle solid-bridging [155]. Furthermore, a control of temperature and rH is mandatory as liquid bridges form under certain conditions as result of an interparticle moisture condensation [156]. The consequent rise of capillary forces extends interactions between carrier and API. This impedes drug detachment.

XRPD diffractograms of the three spray-dried APIs are depicted in Figure 4-8, presenting the absence of a specific diffraction pattern, which would indicate crystalline regions. Instead, samples exhibited so-called halos linked to background signalling. This suggests amorphicity after the SD process.

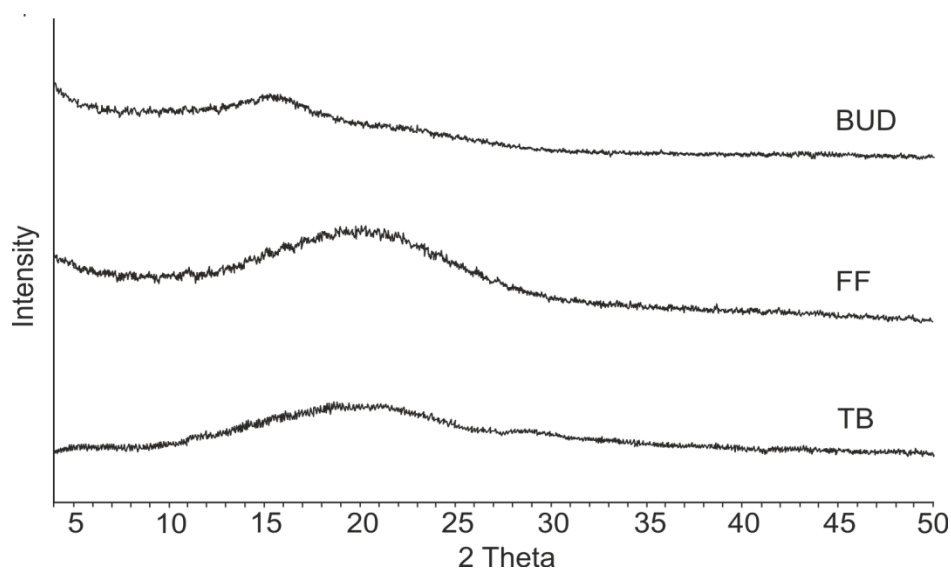


Figure 4-8 XRPD diffractograms of spray-dried APIs

The behaviour of the fully amorphous samples under different relative humidities was examined via DVS in a two cycle program (0 – 90 – 0 %rH each) with water (section 3.4.1.7). In general, samples in the crystalline state show a largely different moisture uptake compared to amorphous materials [157]. Additionally, recrystallisation is accompanied by a rapid water loss of the specimen which enables the identification of state changes occurring at certain ambient conditions [158].

Mass of all samples increased steadily when raising the rH up to 90 % (Figure 4-9). BUD displayed the lowest mass change of + 4.7 %. Sorption isotherms of the two sequent cycles showed no significant difference. For FF, a mass increase of 12.9 % was detected, while a rapid mass loss becomes apparent at 90 %rH. The second cycle induced solely a negligible water uptake. As far as TB is concerned, an accelerated moisture sorption was observed up to an increase in mass of 8.1 %. At 70 %rH, a sudden decrease in mass occurred. When further lowering the rH, initial mass was reached again. The second cycle only induced a mass increase of 3.0 %.

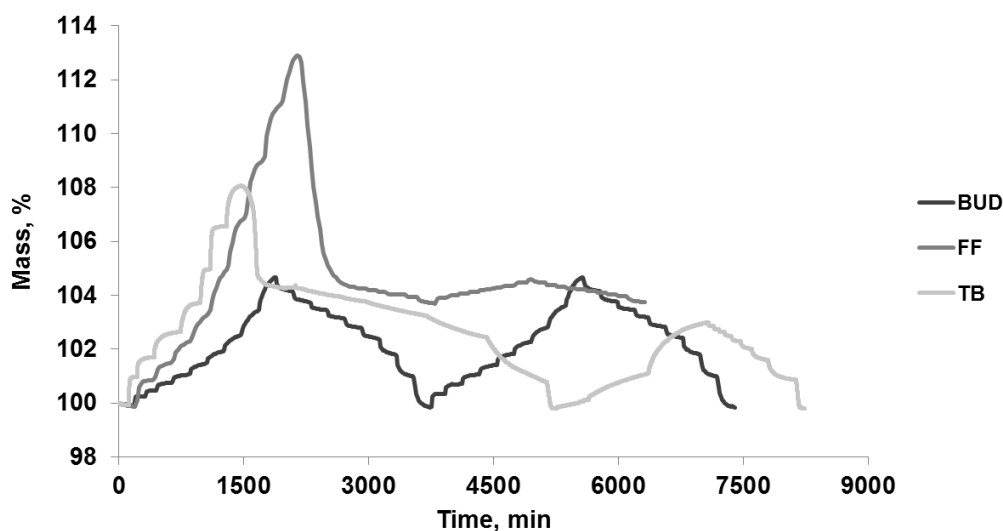


Figure 4-9 Absorption behaviour of spray-dried BUD, FF and TB when subjected to a two cycle DVS program (0 – 90 % rH) with water

The behaviour of FF during analysis indicates a recrystallisation event, underlined by the abrupt mass change in the first cycle. Amorphous, hydrophilic materials are known to adsorb water at their surface [159]. Unlike crystalline materials, they additionally tend to absorb water inside the particles forcing a higher moisture uptake [160]. Due to the ability of water to act as a plasticiser, this increases molecular mobility within the particles ultimately inducing recrystallisation [161]. During this process, a major loss of water occurs. As a consequence, sorption behaviour of FF during the second cycle significantly differs from the first one as a result of the recrystallisation. Similar observations were made when examining TB, where a recrystallisation event could be detected at a rH of 70 %. This is supported by a diminished increase in mass during the second cycle. Here, hygroscopic nature of TB becomes also apparent as an uptake of water of 3.2 % was observed compared to only 1.1 % for the

recrystallised FF. Hydrophobic BUD presented lower overall affinity towards water vapour compared to the hydrophilic model drugs. Neither recrystallisation nor a different behaviour was observed during or between the two sorption cycles underlining the stability of BUD sd at a moderate temperature of 25 °C.

Moreover, it can be taken from Figure 4-9 that absorption and desorption of vapour as well as the release of water happened at a different pace for the three APIs. This could be monitored due to the experimental setup. Only after reaching equilibrium of the sample (< 0.005 %/min change in mass) the next step within the two-cycle program was initiated.

Based on these findings, optimal ambient conditions for material processing and impaction analysis were defined. BUD showed extended stability regardless of the rH and therefore moderate conditions of 21 °C and 45 %rH were chosen to mainly ensure a comparable experimental setting. FF and TB displayed recrystallisation events at elevated humidity, which is why rH was set to 30 % and 20 %, respectively at standard 21 °C to guarantee maintaining of the amorphous state.

4.1.4.4 Dispersive Surface Energy

The dispersive part of the surface energy was examined in order to receive information about the extent of non-polar interactions potentially formed between carrier and API.

As displayed in Figure 4-10, energies of 48.5 ± 0.3 mJ/m² and 48.1 ± 0.9 mJ/m² were determined for hydrophobic BUD and hydrophilic TB in spray-dried condition, respectively. FF showed a γ_s^d of 34.0 ± 0.6 mJ/m².

Despite extensively different chemical properties, solely marginal differences in γ_s^d were experienced for spray-dried BUD and TB, while fairly hydrophilic FF was characterised by reduced interactions with the aliphatic eluents. In consequence, no clear correlation between API chemistry and surface energy could be established. In general, the γ_s^d was always higher for the micronised material. This can be attributed to the high energy input of the micronisation process leading to particles with an increased surface energy.

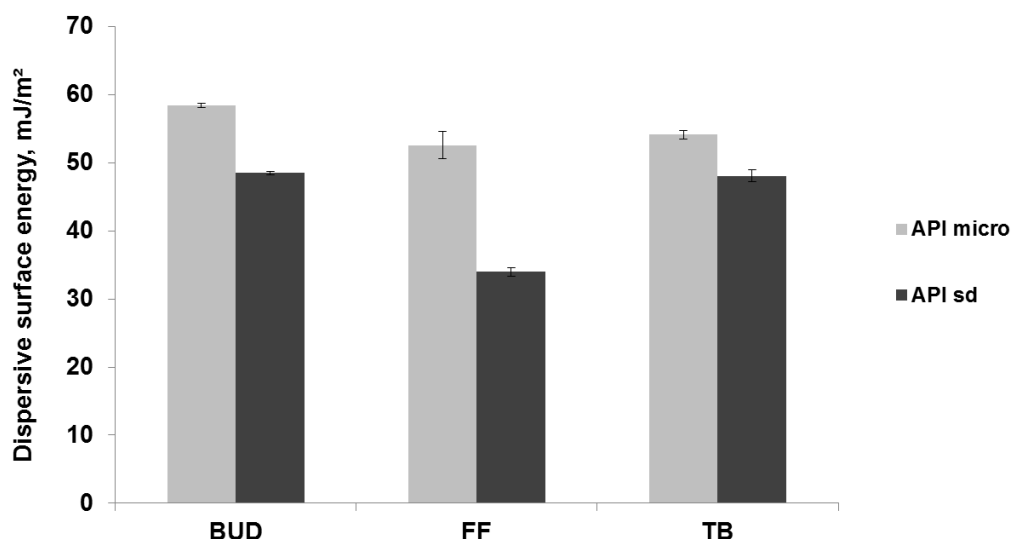


Figure 4-10 Dispersive surface energies (+StD) of different APIs in spray-dried (black bars) and micronised form (grey bars) (n=3)

It needs to be noted that the γ_s^d merely displays the dispersive or non-polar surface energy which is exhibited by any material. For polar probes, the so-called polar part also contributes to the total surface energy and displays interactions such as hydrogen bonding or acid-base forces [134]. This especially applies to FF and TB in the present study. Consequently surface energies for these APIs could not be completely described with the used technique as the iGC instrument did not allow the determination of those forces. Nevertheless, dispersive surface energy is generally considered as a valuable parameter to assess properties of pharmaceutical powders [162]. Thus, results from iGC experiments were employed to further characterise the spray-dried APIs in this thesis.

4.2 Chemical Modification of Glass Beads

As already pointed out (section 2.3.3.2), very little research has been made on the importance of chemical properties of carrier and API for the performance of interactive powder blends for inhalation. To examine this scientific question, GBs were incubated with different silanes which varied in their functional groups, in three concentrations of 0.5 M (1), 0.05 M (2) or 0.005 M (3). This aimed at creating a broad range of hydrophobicity on the carrier surface. The effect of the silanisation process was determined by CA measurements and by iGC to subsequently select four different types of modified GBs exhibiting a range of different surface characteristics. Other material properties, i.e. flow properties as well as particle size and shape were examined to ensure that no significant changes in those had occurred. Hereby, observed effects of chemical modification on the TSC and aerodynamic performance could be directly correlated to the determined carrier characteristics. Chosen carriers were blended with three different APIs differing in chemical properties for their part, namely hydrophobic BUD (sd), FF (sd) and hydrophilic TB (sd). In order to find optimal blending parameters for the APIs, preliminary trials were conducted with varying blending conditions. Qualities of the blends were determined by content uniformity (section 3.3.5) to evaluate homogeneity and also by visual examination of SEM micrographs to assure the integrity of spherical API particles.

4.2.1 Characterisation of Glass Beads

4.2.1.1 Contact Angle

CA measurements were implemented as one technique to characterise carrier properties before and after modification. It allowed direct determination of hydrophilicity/hydrophobicity through the angle measured between a water drop and the respective surfaces. The silanisation process generally led to increased CAs compared to GB_UT (Table 4-2). Except for FPTS and CTMS, the CA increased with higher concentrations of the respective silanes. Additionally, highest overall CAs were found for TPCS among all GBs.

Table 4-2 Measured CAs of GB_UT and GBs incubated with silanes in different concentrations of 0.5 M (1), 0.05 M (2) and 0.005 M (3); LogP values of the silanes were determined based on mathematical operations described by Wildman et al. [163] (n=20)

Modification	Contact angle, °	Standard deviation, °	LogP value
GB_UT	24.0	4.9	/
FPTS_1	58.3	6.2	2.00
FPTS_2	67.8	3.5	2.00
FPTS_3	47.3	6.6	2.00
CTMS_1	73.8	5.1	2.27
CTMS_2	40.6	7.2	2.27
CTMS_3	44.4	13.7	2.27
CDMPS_1	75.6	5.7	2.34
CDMPS_2	49.5	9.0	2.34
CDMPS_3	32.4	8.2	2.34
CDPMS_1	80.3	3.2	2.72
CDPMS_2	54.0	5.9	2.72
CDPMS_3	49.2	12.9	2.72
TPCS_1	86.1	3.1	2.89
TPCS_2	66.8	6.8	2.89
TPCS_3	41.2	8.1	2.89

In general, a low CA indicates a hydrophilic specimen as the water drop spreads widely on the surface in that case. The low CA of GB_UT can be explained by the presence of free silanol groups that confer polarity to the surface. Thus, GB_UT can be considered as most hydrophilic carrier in the present study. During incubation, a chemical reaction covalently binds silanes to the GB surface (Figure 4-11). Characteristics of the so-altered surface can be attributed to functional groups of the respective silanes which correspond well to their respective logP values (Table 4-2). Consequently, particles treated with rather hydrophilic FPTS showed comparatively low CAs

among the modified GBs. Hydrophobicity was enhanced by replacing methyl groups of the silanes by more hydrophobic phenyl groups leading to highest CA for GBs treated with TPCS. These GBs also exhibited the highest logP value. However, this is only true for the highest concentrations (0.5 M). Here, the major part of the carrier surface reacted with silanes in solution. Lowering the silane concentration diminished the amount of silane molecules available which in consequence decelerated the chemical reaction. The total number of molecules might also not have been high enough to saturate the free silanol groups on GB surfaces in the first place. To conclude, the resulting chemical characteristics of GBs were governed by the silane itself and by its concentration as well. When evaluating present results, it needs to be noted that the determination of CA was originally designed for larger and flat surfaces, where the respective angles can be measured with the naked eye in a satisfactory manner. As GBs are round and only about 500 μm in diameter, measurements are presumably not as precise as conventional ones, e.g. on compressed powder. This also justifies extended standard deviations of the measurements.

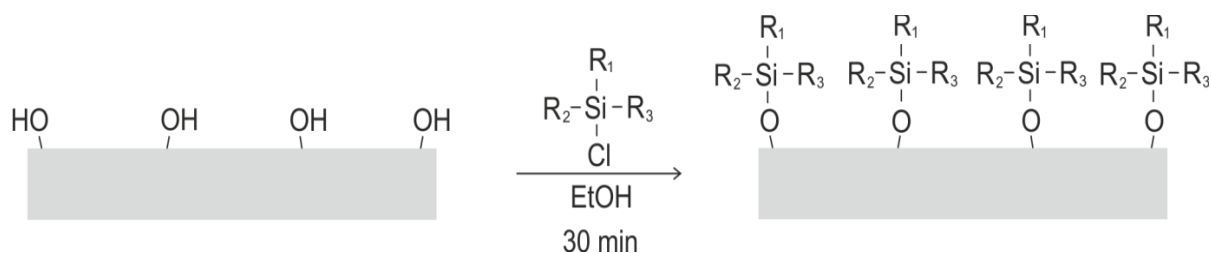


Figure 4-11 Schematic illustration of the silanisation process on GB surfaces adapted from Taglietti et al. [164]

4.2.1.2 Surface Energy

iGC served as the second technique of surface characterisation. It enabled the examination of unmodified and chemically modified GBs in regard to surface energy which arises from acid-base interactions and nonspecific van-der-Waal forces [165]. The latter were of particular interest for GB where hydrophobicity has been increased and were examined by determination of γ_s^d . This was done by injecting a homologous series of alkanes at infinite dilution. Under these conditions solute molecules (decane, nonane, octane, heptane and hexane) solely cover < 1 % of the sample surface. Table 4-3 displays γ_s^d ranging from 28.0 ± 1.0 to $79.4 \pm 1.5 \text{ mJ/m}^2$ for silanised GBs. Analysis of GB_UT gave an intermediate γ_s^d of $42.7 \pm 1.6 \text{ mJ/m}^2$. Results generally

illustrate lower energies at higher silane concentration which applies to each modification.

Table 4-3 Dispersive surface energies of untreated and GBs incubated with silanes in different concentrations of 0.5 M (1), 0.05 M (2) and 0.005 M (3).

Modification	Dispersive surface energy, mJ/m ²	Standard deviation, mJ/m ²
GB_UT	42.7	1.6
FPTS_1	28.0	1.0
FPTS_2	54.3	0.7
FPTS_3	/*	
CTMS_1	61.3	4.1
CTMS_2	79.4	1.5
CTMS_3	/*	
CDMPS_1	33.2	0.8
CDMPS_2	49.6	1.1
CDMPS_3	/*	
CDPMS_1	34.4	0.2
CDPMS_2	35.0	0.1
CDPMS_3	/*	
TPCS_1	44.2	0.2
TPCS_2	61.4	1.1
TPCS_3	/*	

* no determination possible due to technical issues

Based on results gained in this section and in section 4.2.1.1, four differently modified GBs, namely FPTS_1, FPTS_2, CDPMS_2 and TPCS_2 were selected, while GB_UT served as a control. Hereby, a wide range of CAs as well as dispersive surface energies was covered (Figure 4-12). Further investigations presented in this chapter will focus on these five carriers.

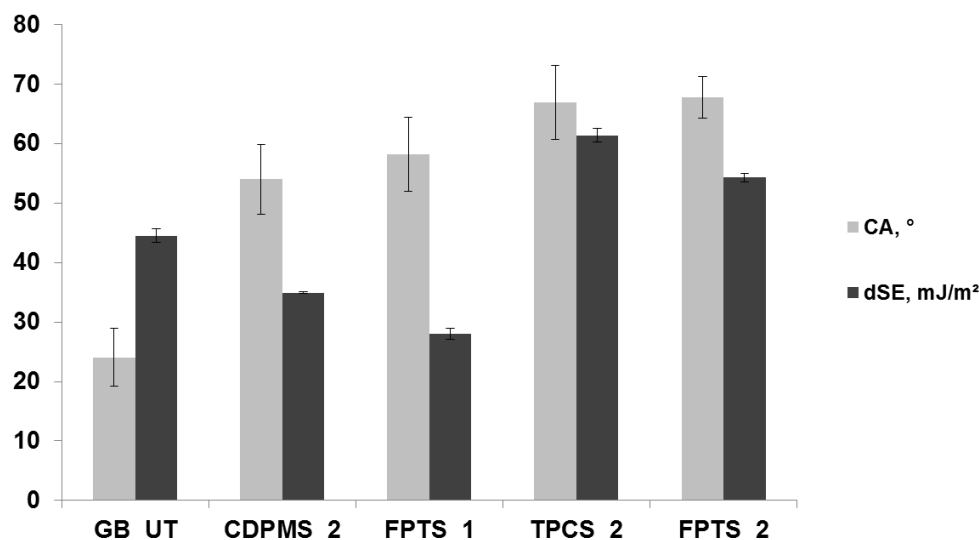


Figure 4-12 Overview of GB characteristics (+StD) sorted by ascending CAs (n=3)

Even though measurements conducted at infinite dilution are generally reliable since they are characterised by major sensitivity, they only represent the highest proportion of γ_s^d present on the respective sample [166]. For that reason, iGC was also employed to generate distribution profiles to investigate the dispersive surface energy distribution across the whole carrier surface. Therefore, increasing volumes of same alkanes used to determine the γ_s^d were injected and adsorption isotherms were measured. As a result, surface energies at particular surface coverages (n/n_m) are displayed (Figure 4-13). Chemically modified GBs showed a steep negative slope at low coverages, while a widely constant energy was measured when coverage was increased. It needs to be noted that the extent of decrease differed significantly for the different modified GBs. GB_UT on the other hand presented a constant decrease of γ_s^d .

Each type of GB exhibited a heterogeneous distribution profile regardless of the modification indicated by varying dispersive surface energies at higher surface coverages. It can also be taken from Figure 4-13 that chemically modified GBs reached a constant γ_s^d above a certain surface coverage. In contrast, the surface energy profile of GB_UT decreased across the whole range of surface coverages.

Heterogeneity of distribution was least pronounced for GB_UT, where γ_s^d only varied from 36.0 mJ/m² to 42.5 mJ/m². A constant reduction of surface energy indicates a statistically even distribution of high and low energy sites [167]. Widely differing distribution profiles were experienced for modified GBs. On TPCS_2, sites of high ener-

gy (63.0 mJ/m^2) were determined. A comparatively low γ_s^d of 37.8 mJ/m^2 was measured on other regions of the surface. These observations confirm the presence of active sites on each type of carrier. But the silanisation process did not alter the whole carrier surface the same way. This is indicated by the increase of heterogeneity of surface energy distribution through chemical modification. In addition, differences in the extent of γ_s^d decrease indicate that the impact of silanisation is highly dependent of the respective agents.

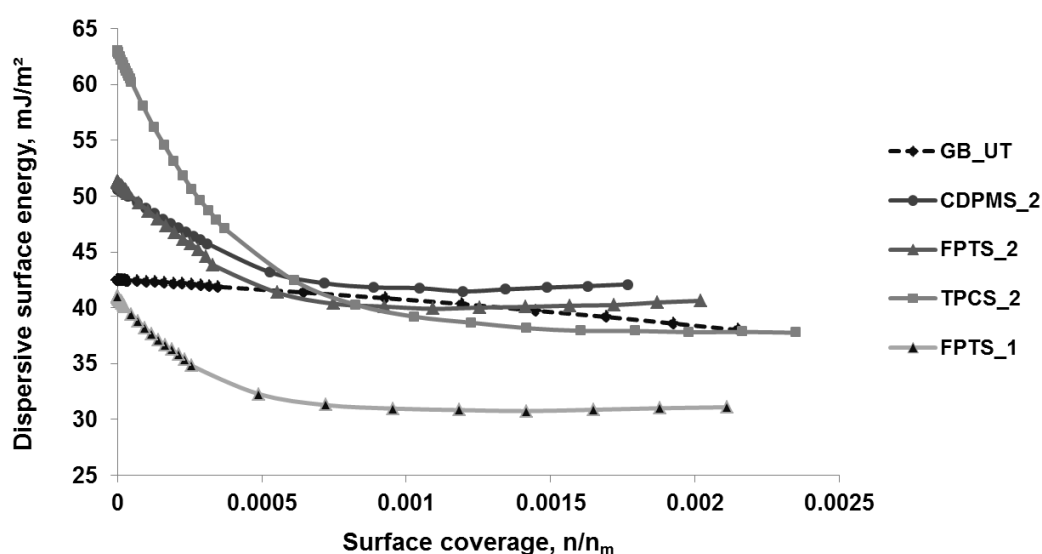


Figure 4-13 Dispersive surface energy profiles of GB_UT and silanised GBs

4.2.1.3 Particle Size and Shape

After silanisation, modified GBs were examined with respect to possible alteration in their size and shape compared to GB_UT. Those factors have been proven to impact the respirable fraction to a certain extent (section 2.3.3). As merely investigating the impact of a specific surface alteration was the overarching goal in this study, no significant change in other characteristics was defined as fundamental requirement for a suitable surface modification technique.

It can be taken from Figure 4-14 (top) that chemical modification did not alter the PSD of GBs significantly. Furthermore, particle sphericity remained unaffected by the silanisation process (Figure 4-14 (bottom)). These findings provide the basis for further experiments, as any changes observed in drug loading or aerodynamic performance could directly be correlated to the respective modification.

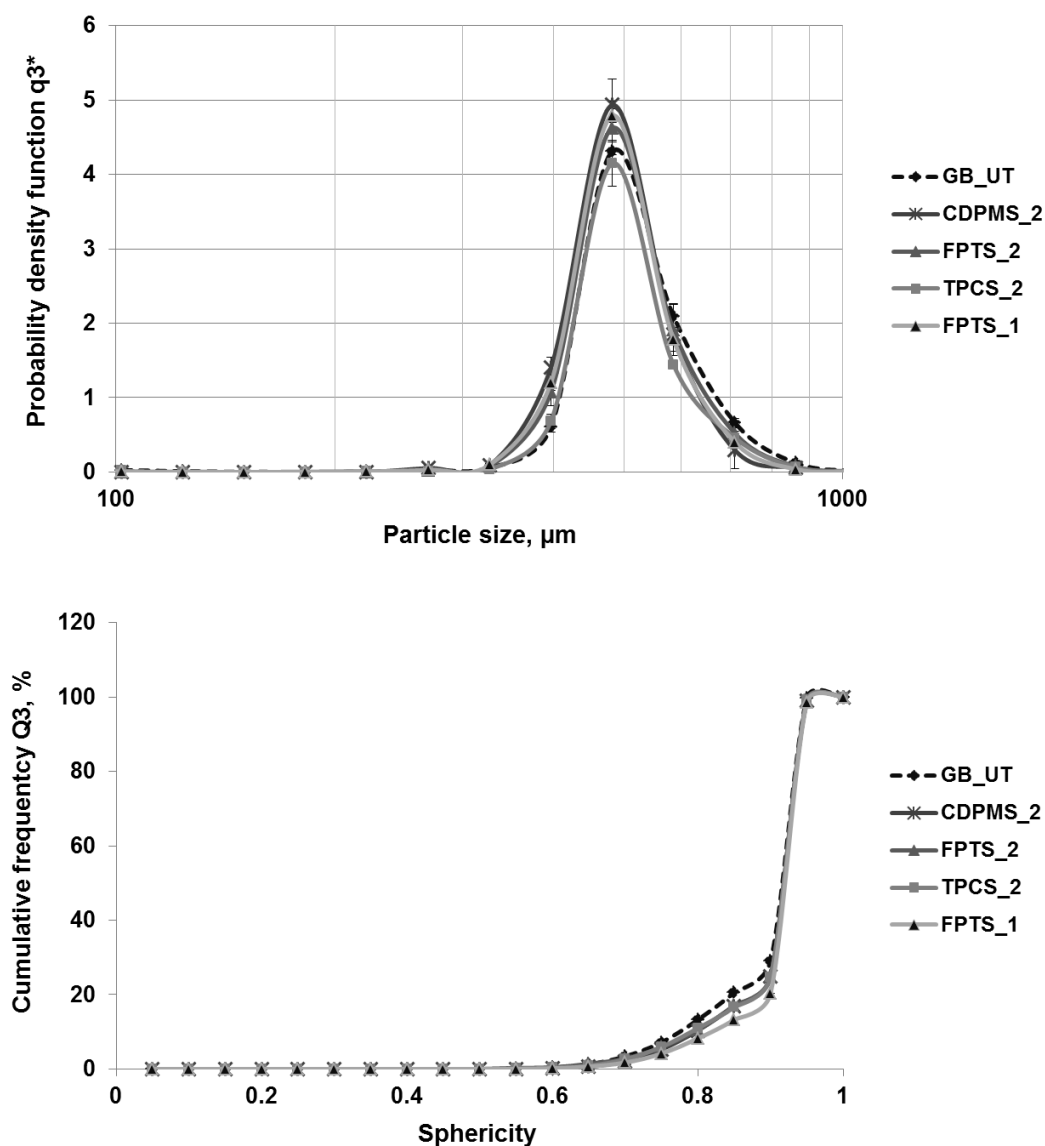


Figure 4-14 PSDs (+StD) with logarithmic scaling on the x-axis (top) and particle sphericities (bottom) of GB_UT and silanised GBs (n=3)

4.2.1.4 Flow Properties

Potential changes of flow properties induced by silanisation were also of interest. Investigations included determination of BFE, which is defined as the energy required inducing a certain flow pattern in a defined and conditioned volume of powder.

Incubation of GBs with silanes in a concentration of 0.05 M slightly reduced flowability as seen for CDPMS_2, FPTS_2 and TPCS_2 (Figure 4-15). FPTS_1 exhibited a significant decrease in BFE (165.0 ± 7.0 mJ) compared to GB_UT (184.7 ± 11.0 mJ) substantiating the suggestion that solely a high silane concentration of 0.5 M was sufficient to ensure saturation of the entire GB surface. In general, a low BFE is desirable

as it indicates proper flowability. This ensures processability, e.g. precise dosing during capsule filling.

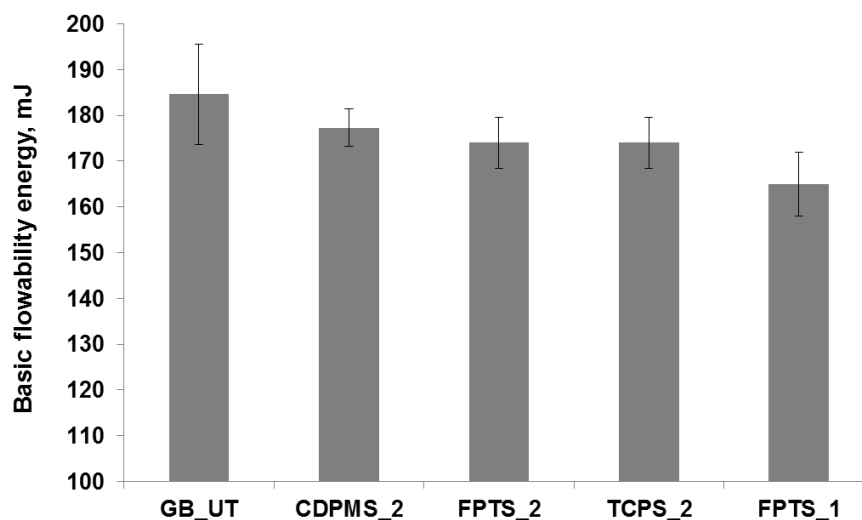


Figure 4-15 BFEs (+StD) of untreated and modified GBs (sorted descending) (n=10)

4.2.2 Influence on True Surface Coverage

Based on mathematical operations presented in section 3.3.4, blends consisting of untreated or modified GBs and API were prepared with different CSCs of 100 %, 50 % and 25 %. In general, drug loading can be seen as an important factor for aerodynamic performance, as it was described to influence the amount of API delivered to the lungs [74]. This highlights the necessity to examine the TSC of the blends used for impaction analysis. Potentially varying drug loadings at a constant amount of API originally weighed in (CSC) were investigated in regard to the respective surface modifications.

TSCs of BUD were found to be lower than the corresponding CSCs (Figure 4-16). This is true for GB_UT and also for modified GBs. Furthermore, the effective drug loading was highly dependent on the amount of API originally weighed in, whereby a CSC of 100 % led to the highest TSC in any case. Fewest overall amount of drug was attached to GB_UT at 47.6 ± 1.9 % TSC after blending and extended drug load was reached by TPCS_2 at 78.6 ± 2.2 % for 100 % CSC.

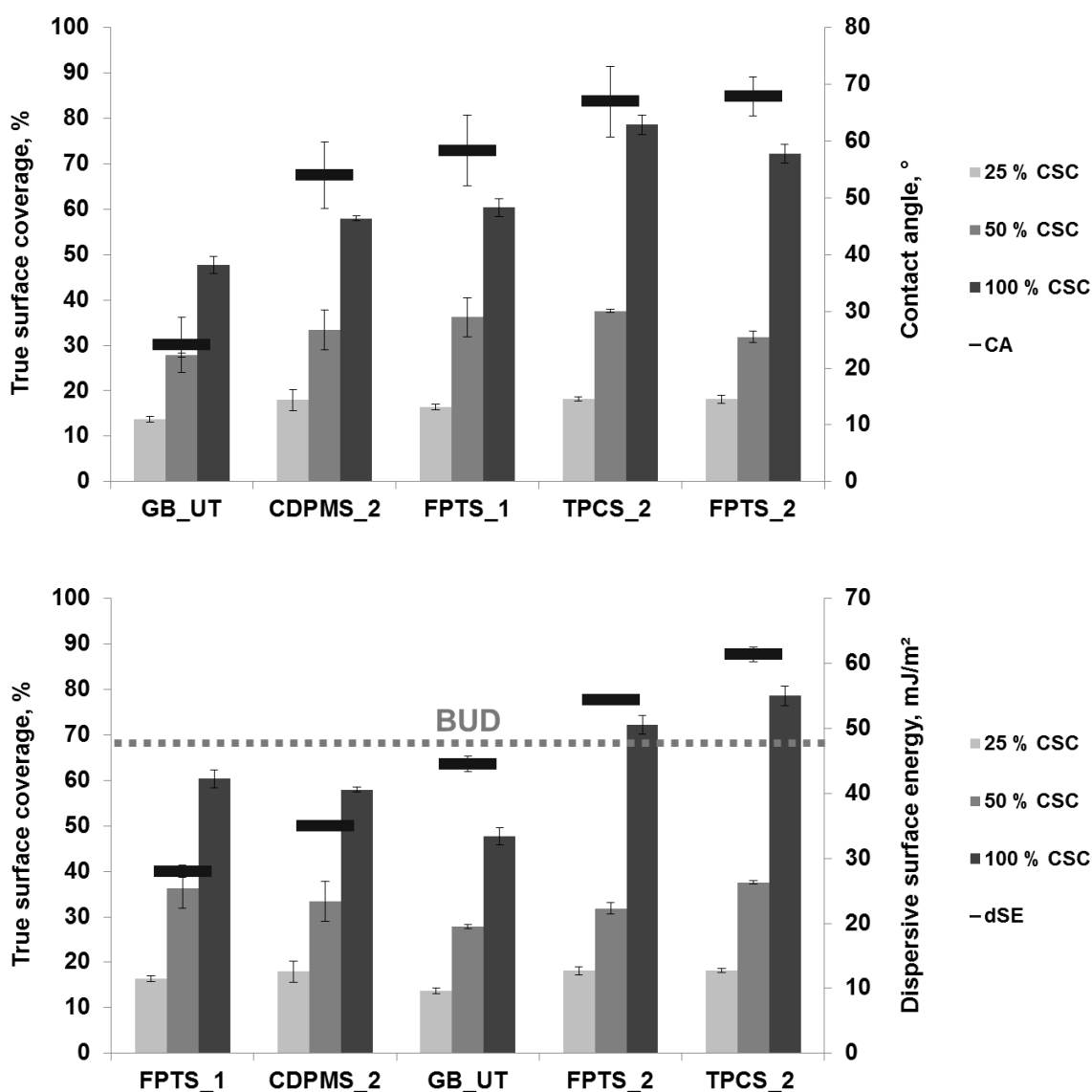


Figure 4-16 Resulting TSCs (+StD) for the different CSC of 100 %, 50 % and 25 % of BUD plotted against CA (top) and γ_s^d (bottom); sorted ascending according to the respective CAs or γ_s^d ; the dotted line represents γ_s^d of BUD (n=10)

The decreased TSCs compared to the respective CSCs indicate that not the entire quantity of API was attached to the carrier during blending. This is supported by pictures taken from the mixing vessel after blending (Figure 4-17). A substantial fraction of drug was located inside the mixing vessel whereby a thin layer covered its inner walls. This can be ascribed to processes taking place during blending. Here, particle-wall collisions and frictional forces occur. This triggers an opposite net charge of mixing container wall and particles within the interactive mixture leading to a persisting attachment of the small API. The following paragraphs will examine the extent to which the API was attached to the different GBs in relation to surface modifications.

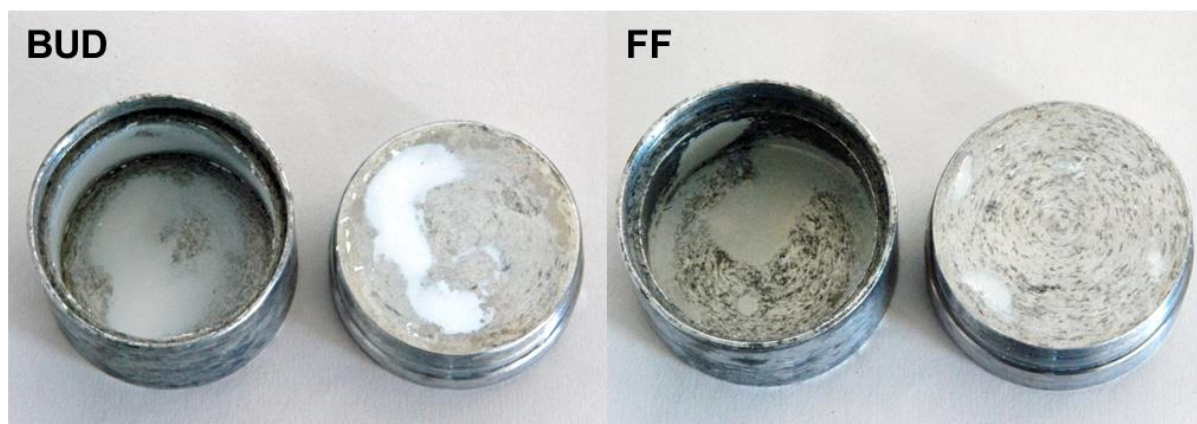


Figure 4-17 Mixing vessels after blending of GB_UT with BUD (left) or FF (right)

Figure 4-16 (top) displays the correlation between CA and TSC. Here, GB_UT exhibited the lowest drug loadings. By increasing surface hydrophobicity, which is expressed by an increase in CA, the amount of API located on the carrier was enhanced step-wise.

Findings can conclusively be linked to physico-chemical properties of carrier and API. While BUD is a very hydrophobic model drug, free silanol groups convey extended hydrophilicity to the GB surface. Attractive forces between BUD and this GB type are presumably limited leading to a smaller proportion of API being attached to carrier surface during blending. Carrier hydrophobicity was subsequently increased through the incubation with different silanes, which is displayed by higher CAs. By that, attractive forces between carrier and BUD were enhanced to ultimately increase the TSC. These observations generally hold true for each TSC but are most explicit for a CSC of 100 %.

Prima facie, no clear correlation between TSC and γ_s^d could be established (Figure 4-16 (bottom)). If, however, the γ_s^d of BUD (48.5 mJ/m²) is taken into account, a specific pattern emerges. While a small difference in dispersive surface energy between API and carrier appeared to be unfavourable, a substantial difference was beneficial for an efficient drug loading as FPTs_2 and TPCS_2 showed highest TSCs. Those findings will be interpreted and put into context in the following.

As far as FF is concerned, a TSC of 100 % could not be reached here either regardless of the carrier modification (Figure 4-18).

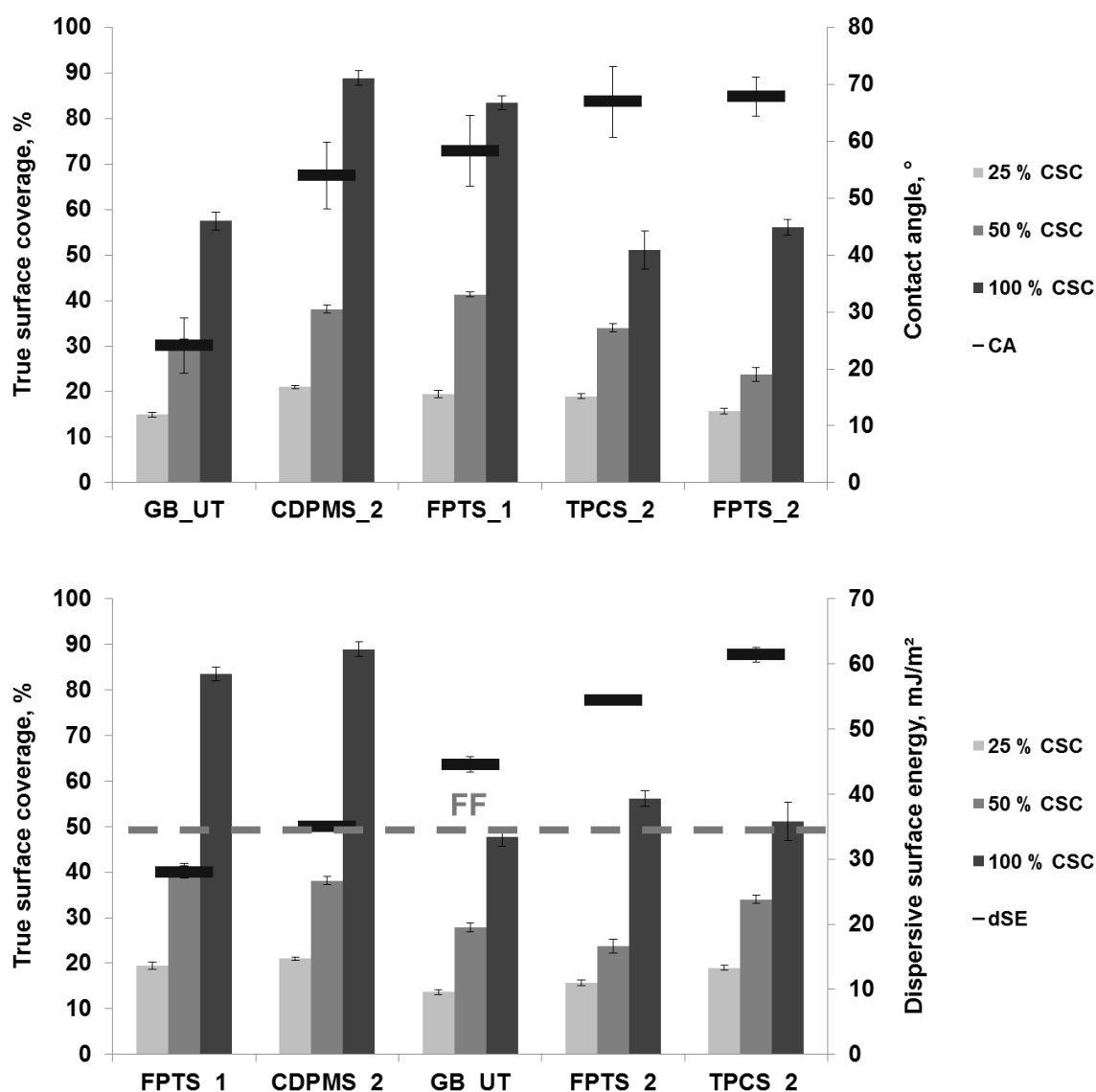


Figure 4-18 Resulting TSCs (+StD) for the different CSC of 100 %, 50 % and 25 % for FF plotted against CA (top) and γ_s^d (bottom); sorted ascending according to the respective CAs or γ_s^d ; the dashed line represents γ_s^d of FF (n=10)

The same applies to the other blends with 50 % or 25 % CSC where the effective drug load was always lower than the targeted one. Furthermore, silanisation showed a considerable impact as varying TSCs between 47.6 ± 2.0 % and 88.9 ± 1.7 % were obtained (for 100% CSC), whereby lowest amount of drug were located on GB_UT. The largest quantity of drug was attached to CDPMS_2.

Here, no clear correlation between TSC and CA could be established (Figure 4-18 (top)). It might be argued that, as far as only modified GBs are concerned, higher drug loadings were found for more hydrophilic material (low CA) and accordingly lower TSCs for GBs with the highest CAs. This is conclusive in terms of FF being more

hydrophilic than BUD. Following this reasoning, the presence of extended attractive forces between hydrophilic carriers and FF enhanced the drug loading, whereas extended hydrophobic properties impeded the attachment of FF.

Figure 4-18 (bottom) takes the respective dispersive surface energies into account. Again, this did not lead to any distinct dependence to the drug loading. Nevertheless, a correlation could be established by implementing the γ_s^d of FF (34.0 mJ/m²). Interestingly, a small difference between the γ_s^d was advantageous as blends containing CDPMS_2 exhibited the highest TSC which is contradictory to findings obtained for BUD. It needs to be noted that only the dispersive part of surface energy was taken into account in this study. But the total surface energy also comprises the acid-base component which described polar interactions. This could potentially put findings in a broader context. Nevertheless, Traini et al. investigated the role of surface energy on FPF and found the same inverse relationship between the two for the dispersive as well as the total surface energy [83]. This validates the present conclusions.

4.2.3 Impaction Analysis

The introduced modification technique has proven to be suitable to alter GB properties on a chemical level (section 4.2.1). As other material properties of the carrier remained mostly unaffected, the impact of the alteration of chemical surface properties, could be directly correlated to aerodynamic performance determined by impaction analysis (NGI). The FPF provided a measure for the effectiveness, with which the API could reach the lungs. Additionally, FPD was determined to receive information of the total dose of particles with an aerodynamic diameter < 5 μm .

In general, CSC substantially affected the respirable fraction and a CSC of 100 % always led to the highest FPF (Figure 4-19). This applies to all types of GBs and is true for both APIs. For BUD, FPFs between 11.2 ± 1.0 % and 19.5 ± 2.4 % were obtained among the different carriers (for 100 % CSC). Best overall aerodynamic performance was exhibited by blends containing GB_UT and lowest FPFs were identified for FPTS_2 (Figure 4-19 (top)). For FF, respirable fractions ranging from 14.9 ± 1.9 % (CDPMS_2) to 26.6 ± 0.7 % (FPTS_2) were observed in impaction analysis (Figure 4-19 (bottom)).

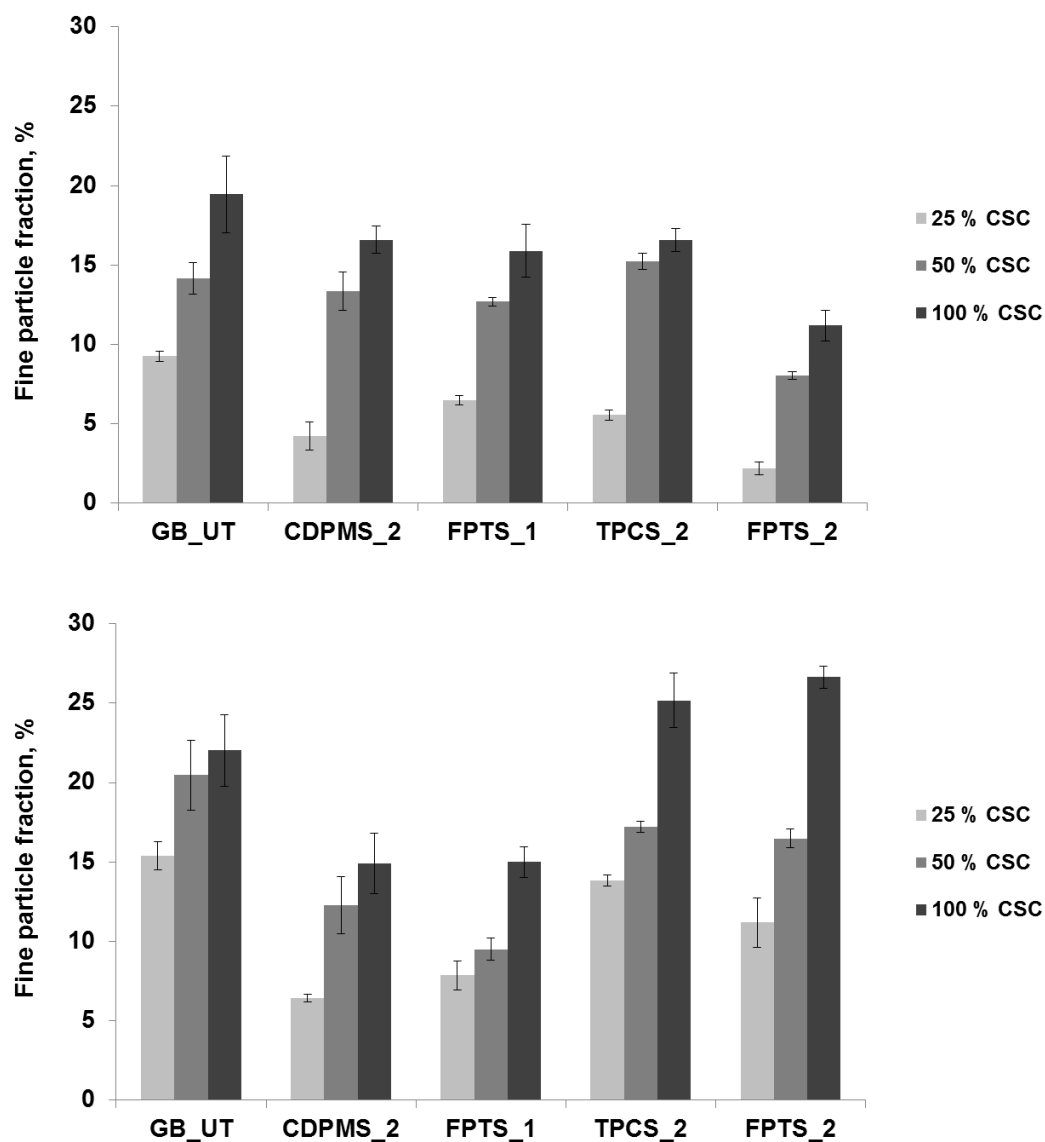


Figure 4-19 FPFs (+StD) of blends containing different GBs and BUD (top) or FF (bottom) for CSCs of 100 %, 50 % and 25 % (n=3)

Relatively low FPFs were gained when using interactive mixtures containing GBs as carriers compared to those prepared with commonly used lactose [168,169]. The observation can be linked to fundamental differences between properties of lactose and GBs. It is well recognized that carrier size is an important parameter for aerodynamic performance of DPI formulations [74,76]. This was, inter alia, ascribed to higher fractions of API persistently attached to larger carrier particles during inhalation, which were recovered from the preseparator [13]. Smaller carrier particles such as present in lactose would also lead to more frequent carrier-carrier collisions and an increased frictional contact area triggering drug detachment [23]. Although previous studies employed conventional carriers, considerations also hold true for GB as well. This is

substantiated by findings from Ooi et al., where blends containing polystyrene spheres in different sizes were utilised as carrier [59]. Again, more drug particles remained on larger spheres resulting in diminished aerosol performance.

Previous studies based the influence of drug loading on the FPF on a heterogeneous surface energy distribution on the carrier surface [170]. First and foremost, this leads to a preferable binding of drug particles to certain areas, characterised as highly energetic, on the carrier surface during blending. This was initially described by Hersey [171], while those areas were introduced as so-called active sites [172]. Secondly, active sites convey extended binding energies oftentimes forcing a persisting attachment to the carrier during inhalation [173,174]. As a result, the following conclusions can be drawn: At high drug loading, only a limited percentage of API is attached to those active sites where AFs are potentially higher than the energy imparted in the course of inhalation. Most of the drug will be present elsewhere (low energy sites). Consequently, sufficient drug detachment is observed during inhalation. In contrast, a substantial fraction of API will be located on high energy sites at low drug loading, leading to a decreased FPF compared to a high drug load (Figure 4-19). This is representatively supported by SEM micrographs of blends containing GB_UT or CDPMS_2 and FF for the other interactive mixtures (Figure 4-20). At a high effective drug loading of 88.9 ± 1.7 % (CDPMS_2, 100 % CSC), the API appears to be fairly even distributed across the carrier surface. As the TSC decreases, preferential binding to certain areas becomes visible (50 % and 25 % CSC). Due to a low effective drug load of GB_UT, inhomogeneous distribution arises at the highest CSC of 100 %. It has been reported for conventional carriers like lactose that active sites are created during manufacturing or by surface-alteration of the particles [175]. In the present study, iGC measurements have already proven the presence of high energy spots on any type of GB (section 4.2.1.2), to which observed results can be linked in a coherent way.

It needs to be noted, however, that the aerodynamic performance can only be enhanced up to a certain point by increasing the drug loading [176]. It reaches a plateau, where further addition of API does not increase respirable fraction. Instead, agglomeration of drug particles and the formation of multilayers on the carrier surface occur to ultimately reduce the FPF and FPD [173].

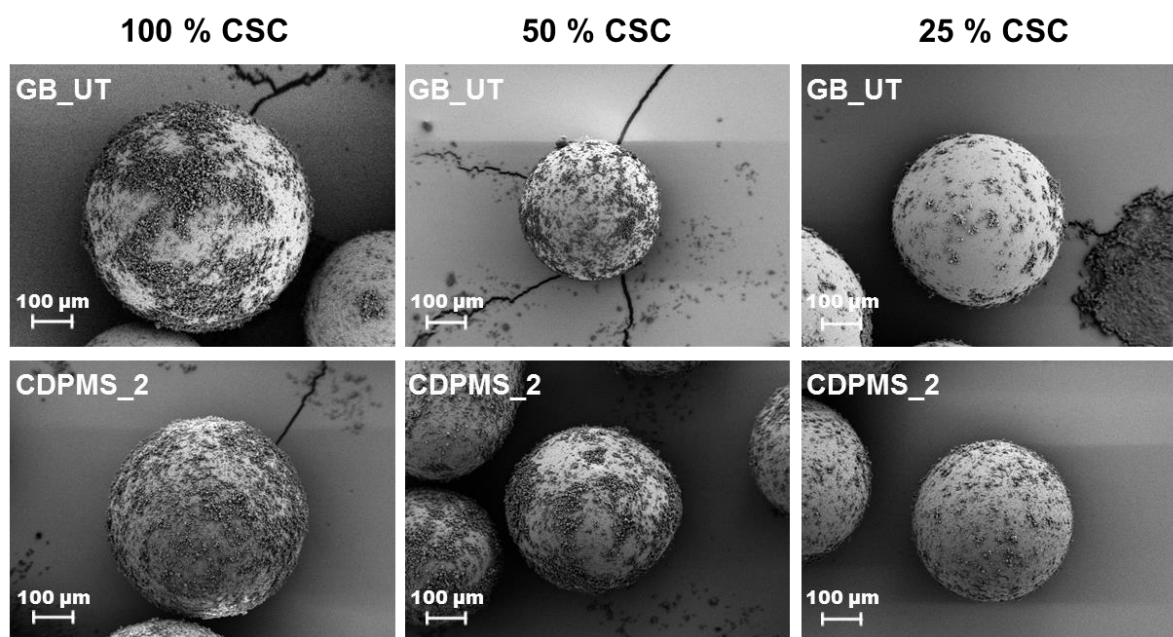


Figure 4-20 SEM micrographs of blends containing FF and GB_UT (top) or CDPMS_2 (bottom) at different CSCs

Section 4.2.2 highlighted the surface modification governing TSC. Furthermore, it has been reported in the previous section that drug loading had a crucial impact on aerodynamic performance. Therefore, the introduction of a standardisation technique becomes mandatory in order to profoundly compare the different interactive mixtures regarding their FPFs. As a first step for this, obtained TSCs for CSCs of 100 %, 50 % and 25 % were plotted against their resulting FPFs, exemplary illustrated in Figure 4-21 for the blends containing GB_UT and BUD. The second step comprised calculating the FPF for a fictive TSC set at 30 %. This drug load was chosen for comparative purposes since on the one hand each API-carrier combination reached this particular TSC despite notable differences observed in drug adhesion. On the other hand, the absence of larger drug agglomerates and no partial multi-layer formation could be presumed under these conditions.

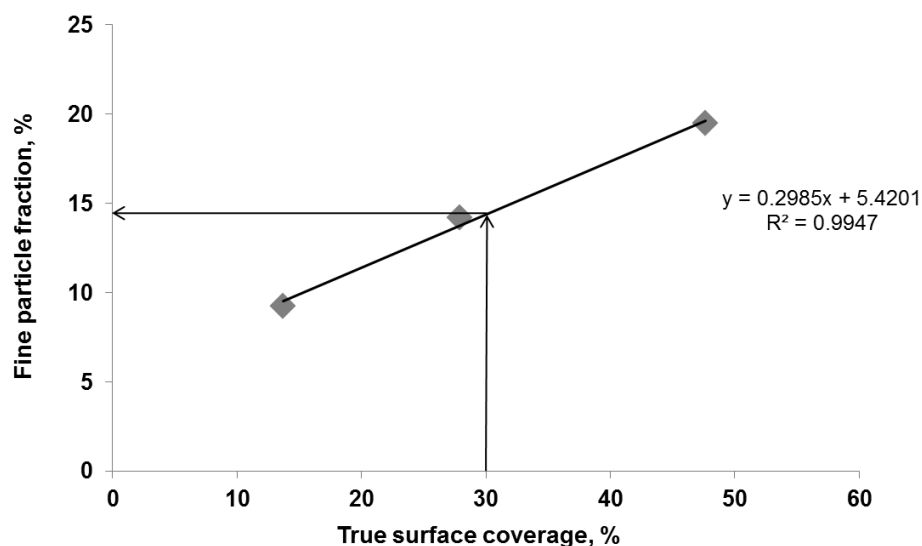


Figure 4-21 Illustration for the mathematical determination of FPF exhibited by a blend with a defined TSC of 30 % exemplary for GB_UT and BUD

By doing so, gained calculated FPFs were comparable and could directly be correlated to carrier surface characteristics. In the course of this, CA had a distinctive effect on the respirable fraction of BUD, while the highest FPF of 14.4 % was achieved by hydrophilic GB_UT (Figure 4-22). In addition, respirable fraction of BUD decreased with increasing CA of the carrier. This displayed a reverse trend compared to the relationship between CA and TSC.

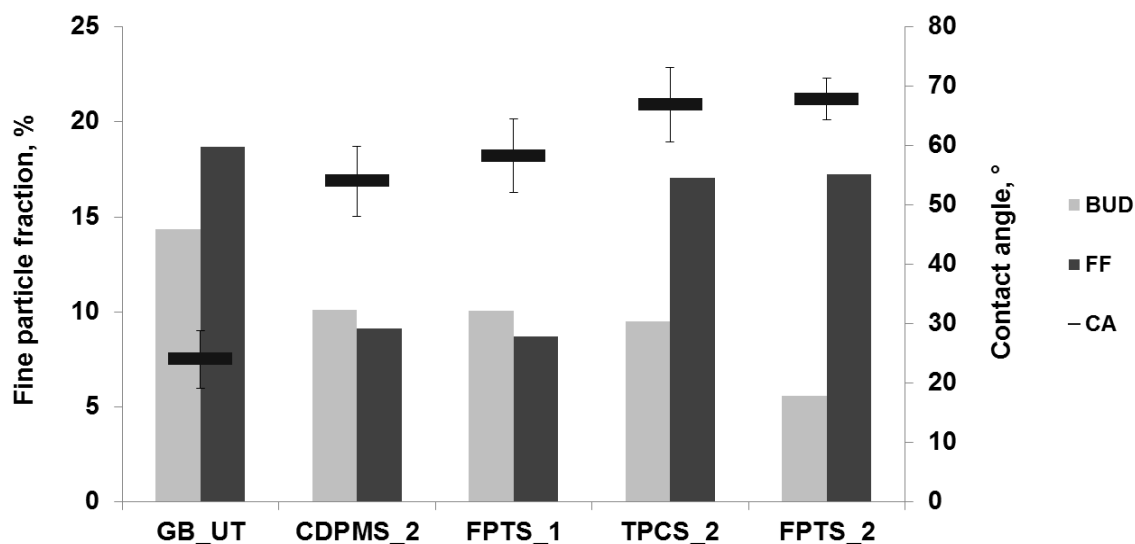


Figure 4-22 Resulting FPFs of blends containing BUD or FF and different GBs at a defined TSC of 30 % plotted against their corresponding CAs; sorted in ascending order according to CA

Observations can be dedicated to API and carrier characteristics in a coherent way. During inhalation, adhesive forces present in interactive mixtures must be overcome to initiate drug detachment. These forces appear to be highly dependent on chemical properties. The potential for interaction between BUD and GB_UT was already described as the lowest among the GBs (section 4.2.2). Although these limited interactive forces led to a low TSC on the one hand, it facilitated drug detachment on the other. By introducing hydrophobicity to the carrier surface, FPF was significantly decreased to 5.6 % for BUD, while adhesive forces were increased accordingly.

Figure 4-23 displays the correlation between γ_s^d and FPF, which becomes apparent upon implementing γ_s^d of the respective APIs (BUD: 48.5 mJ/m²; FF: 34.0 mJ/m²). For BUD, a negligible difference between carrier and API was desirable to ensure proper respirable fractions, while the opposite effect of was observed when γ_s^d varied considerably.

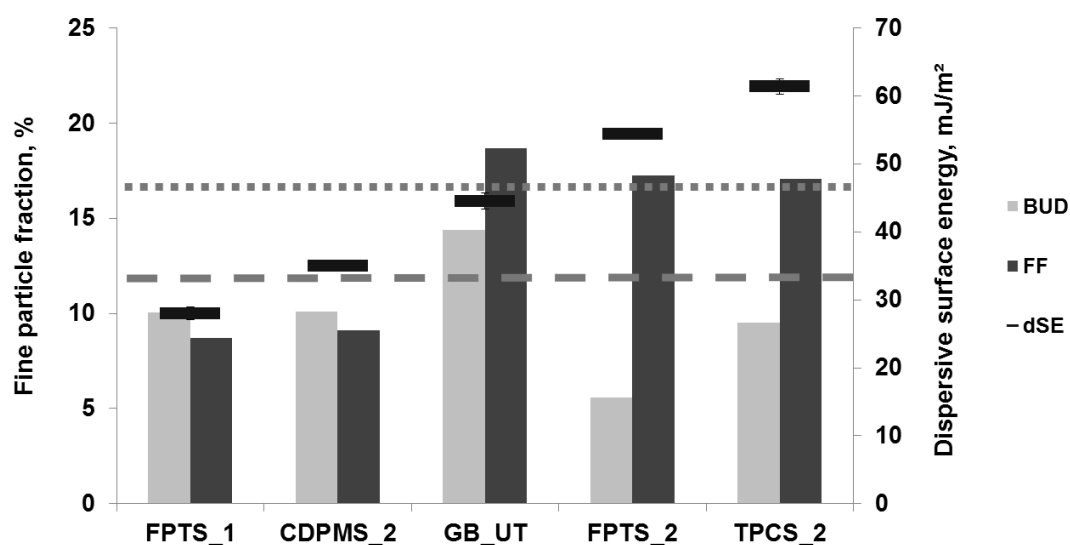


Figure 4-23 Resulting FPFs of blends containing BUD or FF and different GBs plotted against their corresponding γ_s^d ; sorted in ascending order according to γ_s^d ; dotted and dashed lines represent γ_s^d of BUD and FF, respectively

Interestingly, this displayed the opposite trend compared to the effect of γ_s^d on drug loading. Although the impact on TSC and also on FPF could not entirely be explained by evaluating them separately, combining the findings provides a plausible conclusion. For a hydrophobic API like BUD it might be assumed that similar dispersive surface energies induce low adhesive forces consequently leading to a limited TSC, but

an enhanced FPF. In contrast, substantial differences in γ_s^d generate more potential for interaction affecting the TSC and FPF in a contradictory way.

FF showed distinctively different behaviour in terms of respirable fractions (Figure 4-22) exhibiting FPFs in the range of 8.7 % – 18.8 % for FPTTS_1 or GB_UT, respectively. As far as only blends containing modified GBs are taken into account, FPF was correlated to the CA in a positive manner. Here, reverse considerations compared to those for BUD are applied. It is hypothesised, that the detachment of rather hydrophilic FF was facilitated when carrier hydrophobicity was increased (as indicated by higher CAs) leading to this opposite trend.

Not only CAs but also γ_s^d triggered differing respirable fractions (Figure 4-23). A slight difference between carrier and FF proved to adversely influence the FPF. This might also be explained in accordance with findings of the TSCs. For rather hydrophilic FF, approximately equal γ_s^d of carrier and API potentially express enhanced adhesive forces, indicated by maximum drug load but minimum FPF due to impaired detachment.

In addition to BUD and FF, blends containing GBs and TB sd were examined (data not shown). Results demonstrated that no correlation between surface characteristics and neither drug loading nor aerodynamic behaviour could be established. It needs to be noted here that despite the incubation with partially hydrophobic silanes, carrier surfaces remained rather hydrophilic, as CAs below 90° equal hydrophilic materials by definition. It is presumed that distinctive differences in drug loading and aerodynamic performance of polar APIs can solely be observed when implementing very hydrophobic materials. This would enable the investigation of an even broader range of chemical properties. As another consequence, the characteristics and behaviour of blends containing hydrophobic BUD could completely be linked to carrier properties. As hydrophilicity of the API was increased by implementing FF, fewer correlations could be established compared to BUD.

Up to this point, focus has been put on the efficiency with which the drug was delivered to the lower airways expressed as the percentage charge of particles with an aerodynamic diameter < 5 μm (FPF). This is generally considered adequate if a single preparation with a constant API content is tested on different inhalation devices, for

example. In the present study, blends with varying drug loading were examined, since the total amount of drug delivered to the lungs expressed as FPD needs to be taken into account as well.

As expected, a CSC of 100 % led to the highest amount of fine BUD particles regardless of the modification (Figure 4-24). Blends containing CDPMS_2, FPTS_2 or GB_UT resulted in comparable FPDs (100 % CSC). Highest and lowest FPDs were reached for TPCS_2 ($325 \pm 25 \mu\text{g}$) and FPTS_1 ($164 \pm 43 \mu\text{g}$), respectively.

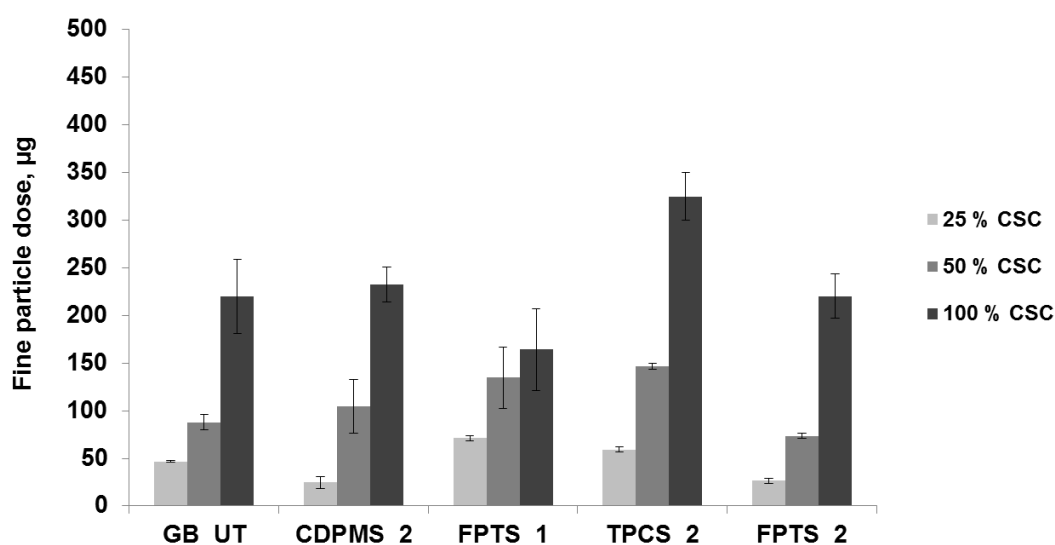


Figure 4-24 FPDs (+StD) of blends containing different GBs and BUD at CSCs of 100 %, 50 % and 25 % (n=3)

Although blends containing TPCS_2 did not show optimal efficiency, i.e. they did not distribute the most API to the target site percentage-wise, they were able to deliver the highest total amount of drug overall due to the maximum drug loading displaying a greater balance of adhesive forces between carrier and API. This identifies TPCS_2, or more precisely the chemical properties of TPCS_2 as being optimal for a carrier-based formulation of BUD.

Consequently, the carrier used to form an interactive mixture with BUD should exhibit the same or at least very similar properties compared to TPCS_2 in terms of hydrophobicity and dispersive surface energy. This ensures that the majority of API is attached to the carrier during blending while a sufficiently low detachment energy is required for drug dispersion.

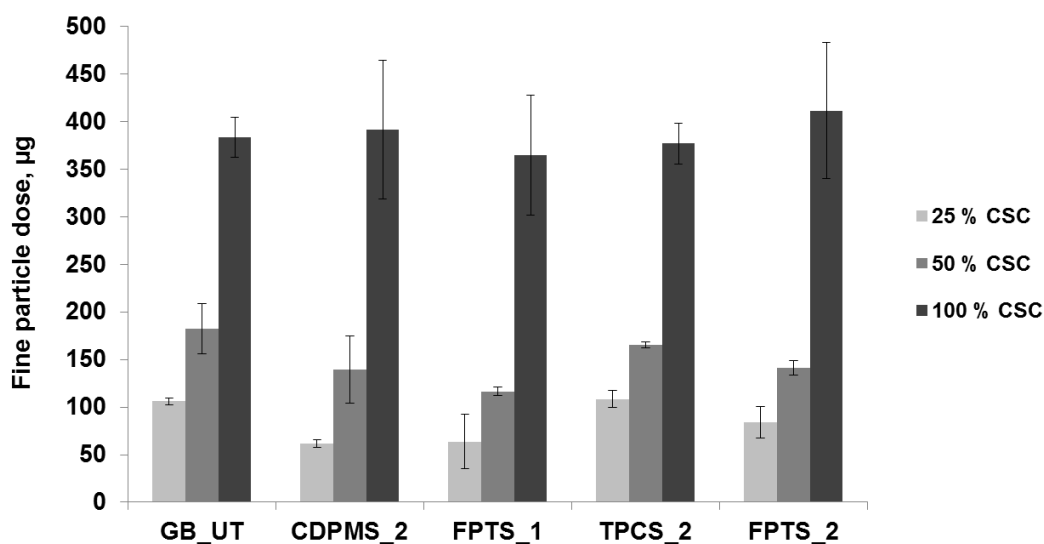


Figure 4-25 FPDs (+StD) of blends containing different GBs and FF at CSCs of 100 %, 50 % and 25 % (n=3)

Figure 4-25 illustrates the resulting FPDs obtained from blends with different GBs and FF. Here, no significant difference was observed between any of the GBs. This implies for the use of rather hydrophilic APIs that chemical surface properties in the examined range do not impact the overall performance of the interactive mixture. Instead, the positive impact of adhesive forces on drug loading and its negative effect on respirable fraction appeared to outbalance each other.

4.3 Alteration of Carrier Surface Topography

In this chapter, different techniques to modify topographical parameters of GBs are presented. This approach aimed at a targeted introduction of roughness to the surface on micro- and nano-scale as well as a combination of both. The effect of these modifications is subsequently correlated to TSC and aerodynamic performance. Initially, untreated and physically modified GBs were blended with BUD or FF, both in spray-dried quality, at different CSCs of 100 %, 50 % and 25 %. Again, only blends with a sufficient content uniformity ($rStD < 5\%$) were employed.

4.3.1 Characterisation of Glass Beads

The effect of modification techniques on the carrier surface described in section 3.3.2.2 was investigated using two different methods, namely SEM and AFM. Figure 4-26 shows representative SEM micrographs of untreated and modified GBs at 100-, 500- and 2500-fold magnifications. GB_UT presented an overall smooth surface with occasional irregularities (clefts and ridges) that become visible at the highest magnification. The incubation of GBs with HF led to micro-scale indentations on the surface. It can be taken from micrographs of HF10min, HF+TC4h and HF+TC8h that introduced cavities were of various shapes. While some looked crescent-like, others appeared nearly hemispherical. Additionally, they significantly differed in depth and diameter. Grinding with tungsten carbide caused numerous nano-scale irregularities, e.g. seen for TC4h. At the same time, the number of ridges present on GB_UT was reduced to a large extent. It also becomes obvious that an extended milling time of eight hours intensified the effect as the surface of TC8h was abraded to a greater extent area-wise compared to TC4h. GBs which have been subjected to both modification steps showed both micro-scale, HF induced, and nano-scale, TC milling induced, roughness (HF+TC4h and HF+TC8h).

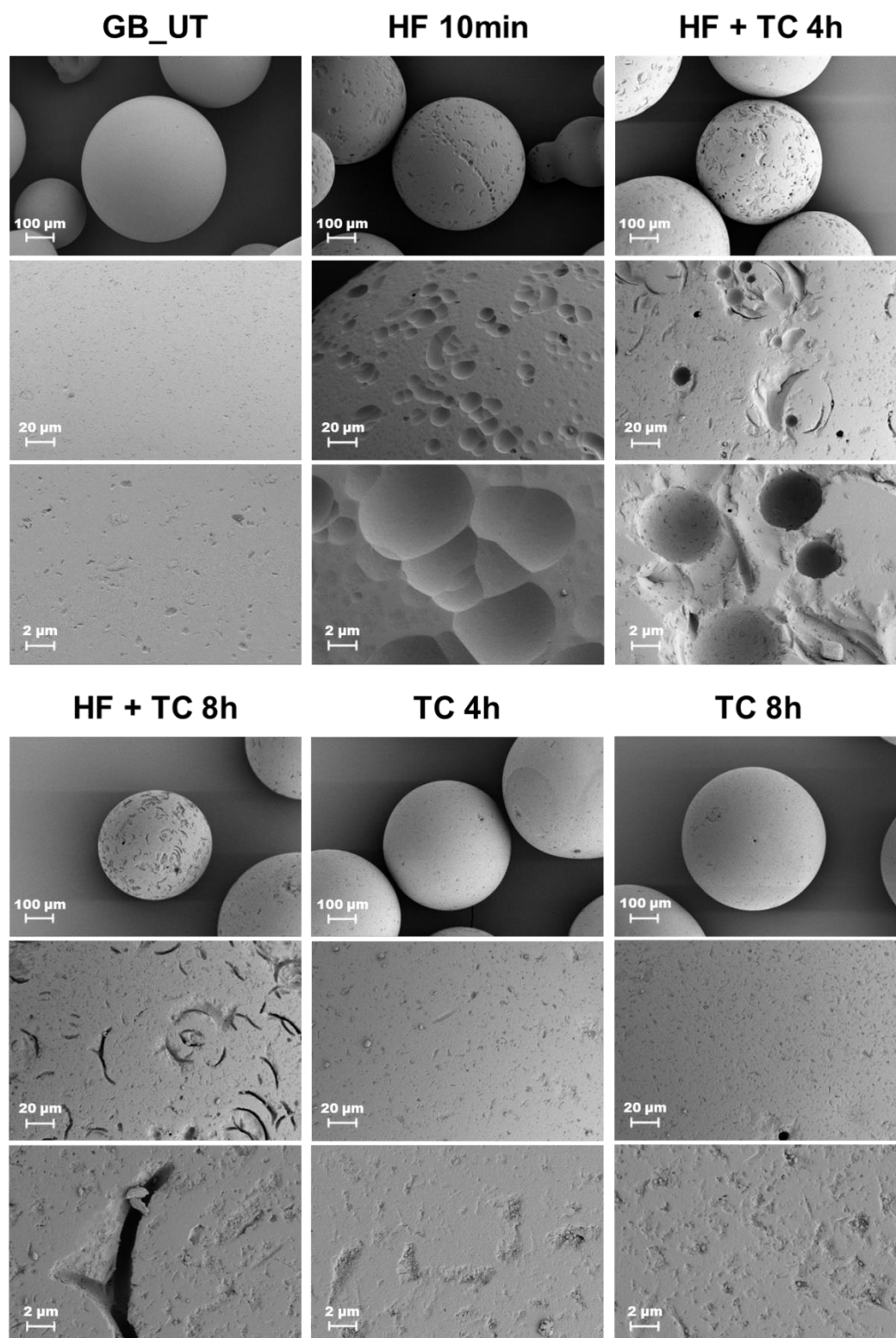


Figure 4-26 SEM micrographs of GB_UT and surface modified GBs at 100-fold, 500-fold and 2500-fold magnification (top, middle and bottom, respectively)

AFM enabled a more precise visualisation of GB surfaces and also allowed the quantification of micro- or nano-scale roughness by mapping the surface in tapping mode

to consequently calculate the corresponding R_{rms} values. As already observed by SEM, GB_UT were characterised by a fairly even surface with just a few discontinuities (Figure 4-27).

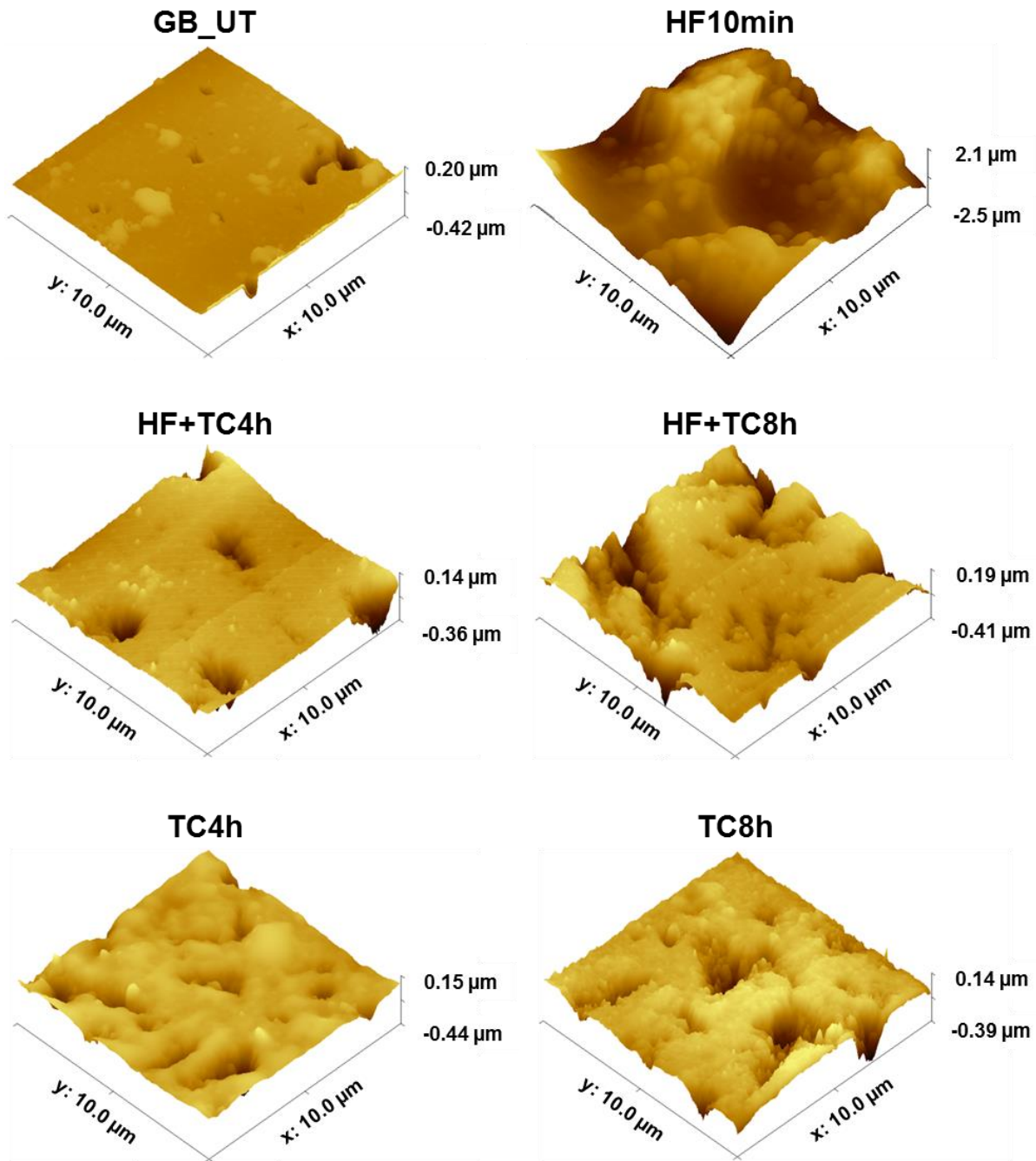


Figure 4-27 Representative micrographs of GB surfaces visualised via AFM

This is also supported by a low R_{rms} value of 21.2 ± 7.4 nm (Figure 4-28). Milling with TC for four hours increased the surface roughness to 46.0 ± 8.3 nm (TC4h), while an eight hour treatment enhanced the R_{rms} value further to 64.2 ± 9.3 nm (TC8h). It can

be derived from Figure 4-27 that the density of surface irregularities was increased compared to TC4h during the extended milling. Taking the micrographs from Figure 4-27 into account, HF10min exhibited a drastically increased R_{rms} value of 697 ± 488 nm due to the respective frequency and depth of extended asperities located on the scan area.

It needs to be emphasised that the R_{rms} does not reflect the frequency of occurrence of surface roughness (equation 12). Instead, it provides information about the level of asperities. If AFM micrographs are additionally taken into account, the extended milling time protocol did only increase the occurrence of surface roughness area-wise, but also the depth of asperities.

Due to the experimental setup, it was not possible to quantify roughness of HF+TC4h and HF+TC8h across the whole surface as sensitivity of the cantilever could solely be adjusted to micron or submicron irregularities. This limitation of AFM is widely accepted and has been acknowledged in literature [82]. Therefore it was decided to focus investigations on regions on the carrier surface where no evident alteration through HF had taken place. These findings correspond well to the R_{rms} values of TC4h and TC8h (Figure 4-28).

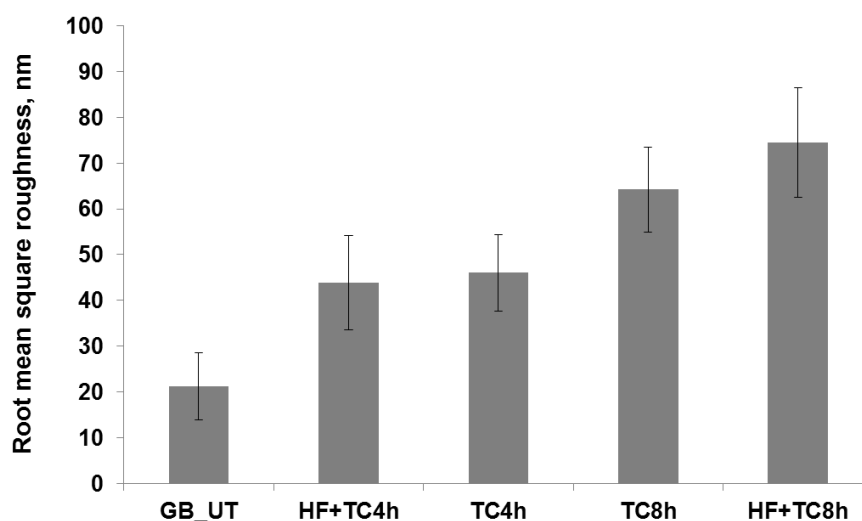


Figure 4-28 R_{rms} (+StD) values of GB_UT and modified GBs representing the extent of nano scale roughness. Results of HF10min have been excluded to increase clarity (n=75)

4.3.1.1 Particle Size and Shape

After modification, GBs were checked for particle size and shape to ensure comparability of these properties. In addition, a different batch of GB_UT was utilised for this study making a re-measurement of the starting material necessary. Considering the PSDs, alteration of surface topography resulted only in a slight decrease in particle diameter regardless of the modification technique (Figure 4-29 (top)). Particle shape was altered to a small extent as well, as sphericity was increased during HF treatment and/or milling with TC (Figure 4-29 (bottom)).

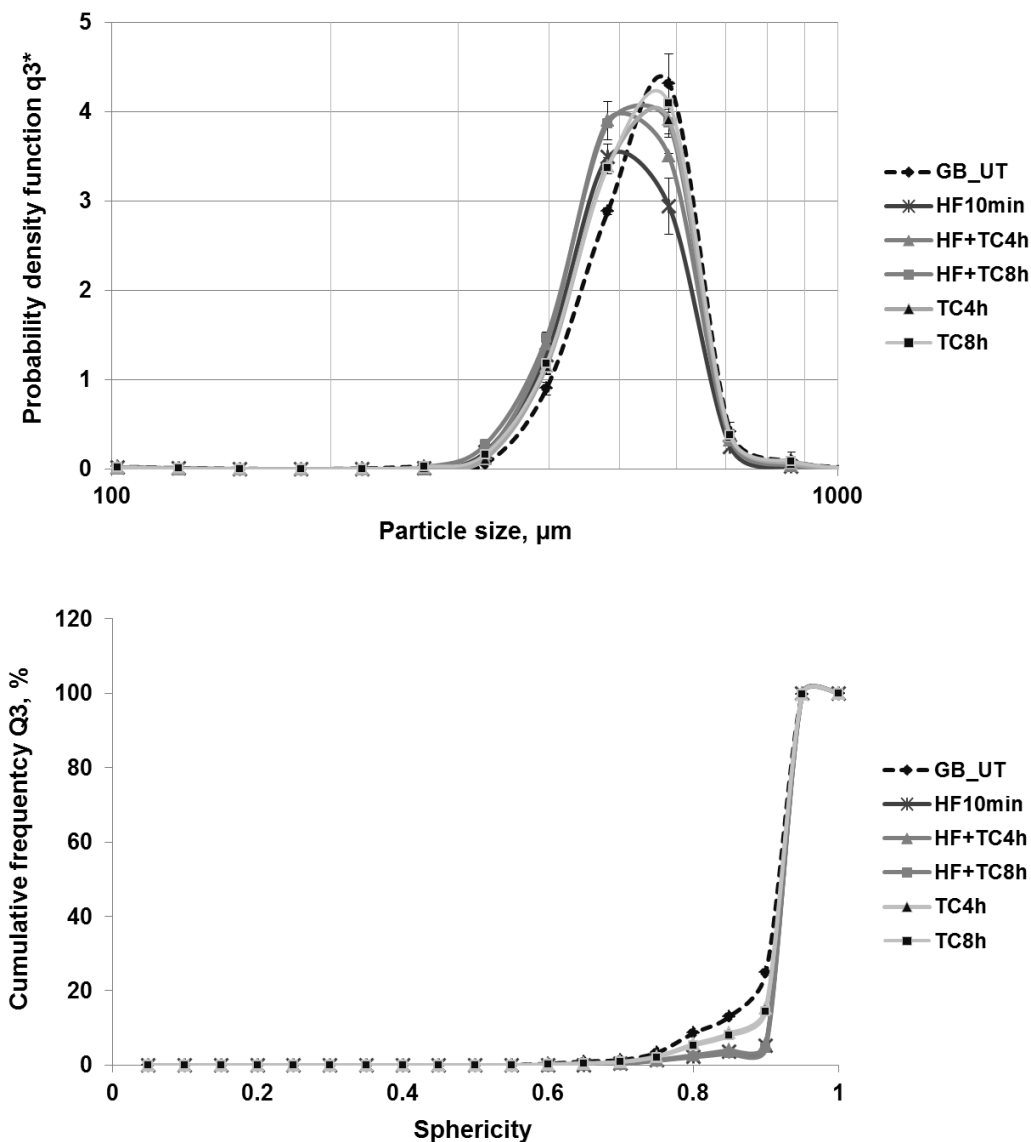


Figure 4-29 PSDs (+StD) with logarithmic scaling on the x-axis (top) and particle sphericities (bottom) of GB_UT and surface-modified GBs (n=3)

Marginal changes in PSD can be linked to the processes occurring during the actual modifications. HF is known to etch glass and therefore slight decreases in GB diameter would be expected. Furthermore, ball milling of GBs with TC does not only induce roughness but also abrades the surface to some extent. Besides, both techniques potentially erase irregularities present on the carrier particles leading to an overall increased sphericity. It needs to be acknowledged that neither modification significantly influenced the overall shape or particle size when comparing x_{50} values or mean sphericities. As mentioned earlier, this was defined as fundamental requirement to a suitable surface modification technique.

4.3.1.2 Powder Rheometry

Surface alteration influenced flowability as seen in BFE measurements (Figure 4-30). Here, BFEs ranging from 123.3 mJ up to 208.7 mJ were obtained. Milling with TC for 4 hours led to a substantial decrease in BFE compared to GB_UT, whereas an 8 hour treatment time increased it again. The highest BFE was observed for HF10min.

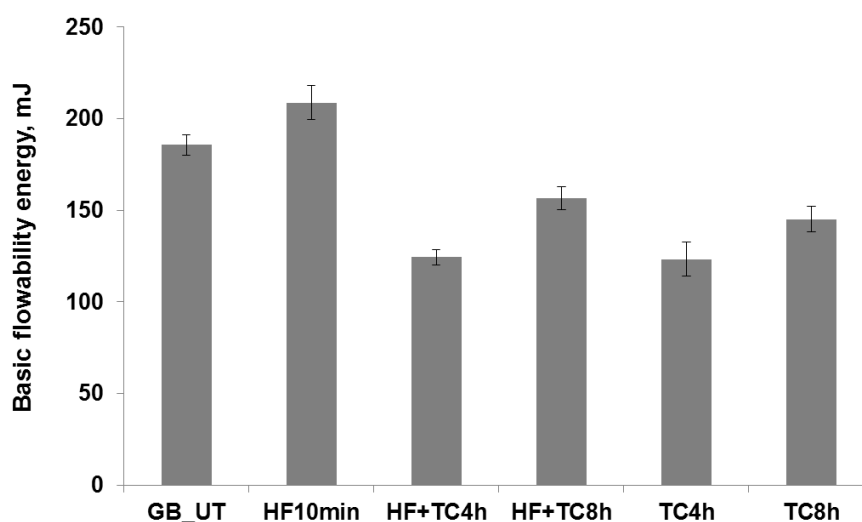


Figure 4-30 BFEs (+StD) of untreated and modified GBs (n=7)

In general, it is assumed that a low BFE, with few exceptions, indicates enhanced flowability [177]. Therefore, an increase in BFE caused by roughness on micro-scale (HF10min) illustrates deteriorated flow properties. Although surface cavities are not large enough to induce intensive mechanical interlocking, they potentially lead to extended interaction between the particles. Consequently, higher forces need to be

applied to establish the particular flow pattern in this setup. On the contrary, a significantly lower energy needed to move the blade through the samples during the downward traverse was experienced for GBs milled with TC (TC4h, TC8h). This can be attributed to the reduction of ridges present on the surface of GB_UT through the milling process. However, the extended milling time led to rougher particles diminishing flowability again.

Another applied technique in this context was the wall friction test, as it allowed the examination of interactions between carrier and inhaler wall material. Figure 4-31 gives measured WFAs in the range of 10.0° to 12.7° for the different GBs indicating a slight increase for GBs with nano-scale roughness on the surface (TC4h, TC8h). Additionally, incubation with HF enhanced the WFA further.

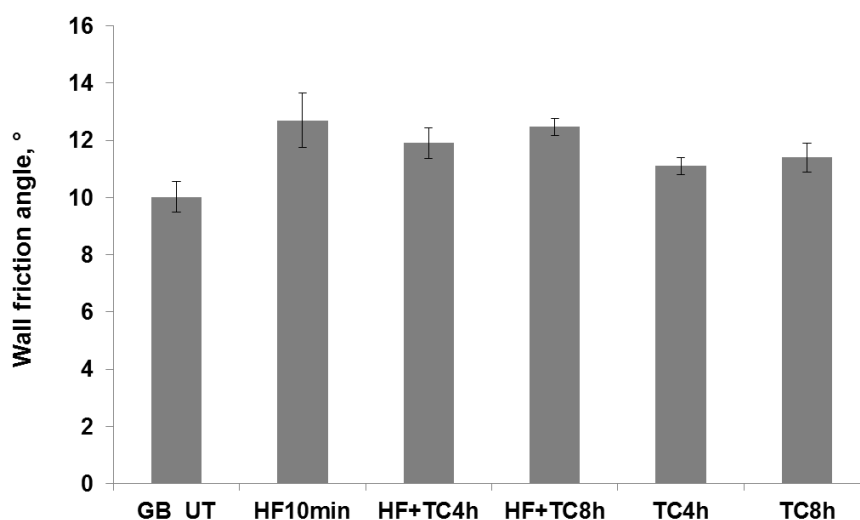


Figure 4-31 WFAs (+StD) of different GBs on wall material of the Modular Inhaler (n=7)

In summary, the introduction of surface roughness, regardless of its scale, had an enhancing effect on frictional forces between carrier and wall material. This corresponds well previous studies where the WFA could be correlated to surface roughness in a positive manner [178].

4.3.2 Influence on True Surface Coverage

This study employed two APIs, namely BUD and FF in spray-dried quality. TSCs were evaluated to examine the impact of surface modifications on effective drug loading at different CSCs. In general, an effective surface coverage of 100 % could not be

reached (Figure 4-32). Moreover, the TSC was always lower than the corresponding CSC. This is true for both APIs and all types of GBs. It also becomes clear that a nearly linear relationship between theoretical and effective drug loading was obtained. This illustrates a distinct correlation between the API quantity originally weighed in and the true fraction attached to the total GB surface.

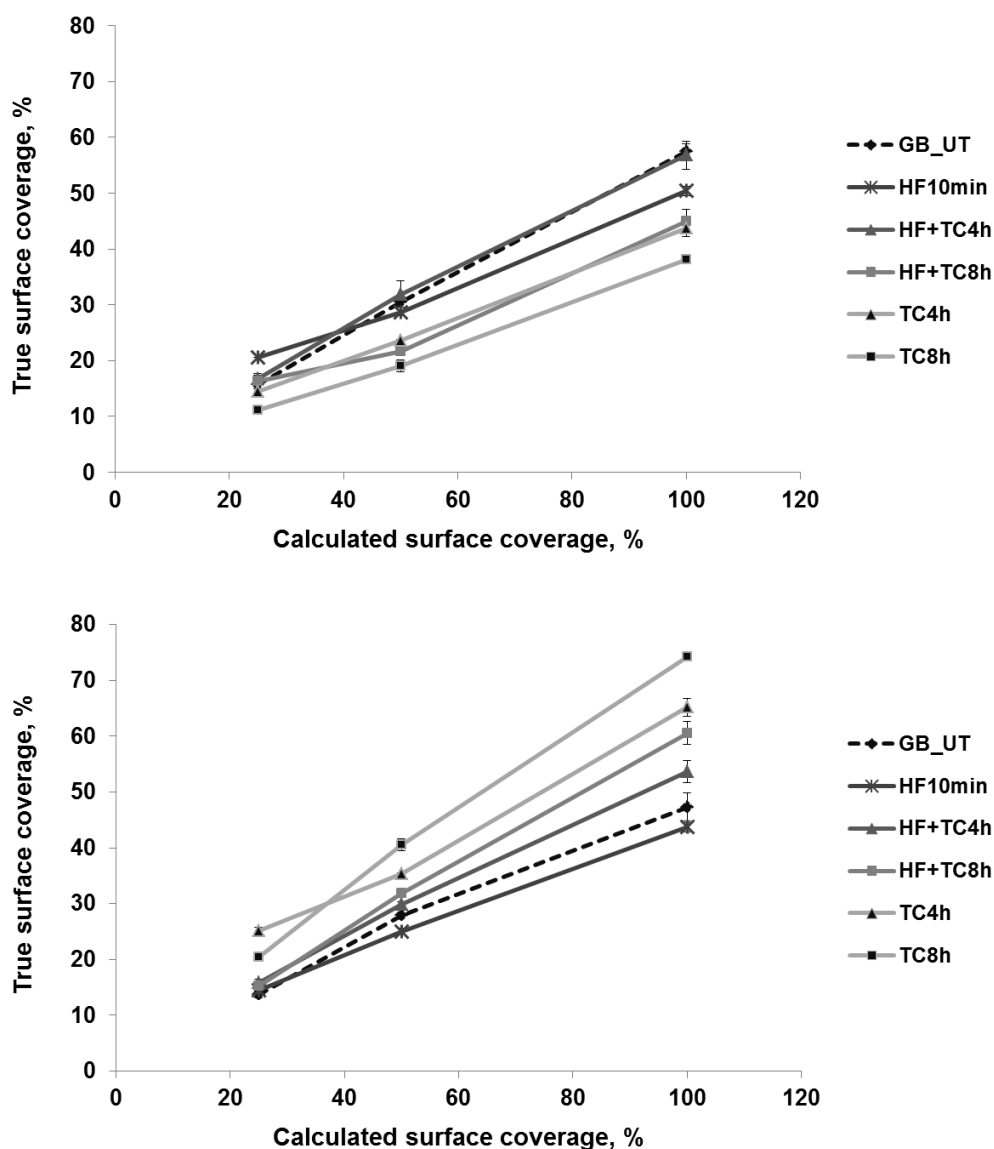


Figure 4-32 Correlation between CSCs and the corresponding TSCs (+StD) for interactive mixtures containing GBs and FF (top) and BUD (bottom) (n=10)

Figure 4-32 (top) shows results for FF, where highest overall resulting TSCs were exhibited by the blend containing GB_UT at 57.5 ± 1.3 %, 30.5 ± 0.9 % and 14.9 ± 1.7 % for 100 %, 50 % and 25 % CSC, respectively. TC4h displayed a substantial decrease in terms of effective drug loading while an extension of milling time

to 8 hours led to further reduction of TSC to $38.1 \pm 1.5 \%$, $19.0 \pm 0.7\%$ and $11.1 \pm 0.4 \%$ for 100 %, 50 % and 25 % CSC, respectively. Blends containing BUD exhibited contrary results (Figure 4-32 (bottom)). Highest TSCs were observed when using GBs which had been subjected to TC milling. Again, a milling time of 8 hours showed the more distinctive effect with TSCs of $74.3 \pm 0.8 \%$, $40.5 \pm 1.3 \%$ and $20.4 \pm 0.2 \%$. The application of a milling step increased the drug loading in general which becomes evident when comparing results for HF10min, HF+TC4h and HF+TC8h. An extended milling protocol amplified this effect as well. For the most part, the overall tendencies described above were found for all three different coverage rates but are most prominent for the highest CSC of 100 %.

As already pointed out, results presented lower TSC compared to the corresponding CSC in any case. This was again due a substantial proportion of API being adhered to the inner walls of the mixing vessel after blending (see section 4.2.2). The degree of drug recovery from the mixing vessel was determined to be dependent on the respective modification. For FF, the highest drug loading was reached on GB_UT. This was due to the physico-chemical properties of drug and carrier. For the latter, free silanol groups bring hydrophilicity to the surface. FF is also rather hydrophilic compared to BUD. In consequence, interaction between carrier and FF will be conveyed by hydrogen bonds to a certain extent leading to comparably high AFs for GB_UT and the API. Grinding with TC introduced submicron surface roughness as confirmed by AFM. Thus, a reduction of contact area between carrier and API is expected (Figure 4-33). Here, less contact area ultimately led to weaker binding of FF to the GB surface causing to the lowest TSCs for TC4h and TC8h.



Figure 4-33 Schematic illustration of a plain untreated GB surface (left) and a surface subjected to TC milling (right) occupied with spray-dried API particles

In theory, BUD should bind to the hydrophilic GB surface to a limited extent on account of a minor potential for interaction (mainly van-der-Waals forces) relative to FF. This was proven by lower TSCs for blends containing GB_UT and BUD compared to those with GB_UT and FF and additionally by comparing blends with HF10min and

BUD to those with HF10min and FF. In the case of BUD, roughness on nano-scale led to an enhanced effective drug loading. It is suggested that the hydrophobic drug particles are more likely to bind to the hydrophilic GB surface, if contact area is reduced. But this only holds true in the presence of repulsive forces between carrier and API. Although the net charge of components in interactive mixtures has not been tested with the present setup, a study performed by Elajnaf et al. supports the theory [179]. That study investigated, inter alia, the effect of blending on the electrostatic charge of carrier and API. Here, interactive blends of salbutamol sulphate and carrier lactose were employed showing that both components got charged negatively during tumble blending in a stainless steel mixing container. This was ascribed to electron transfer from the container material inducing negative net charge of carrier and API particles which ultimately triggered repulsive forces between the two. Furthermore, electron-acceptor (γ^+) and electron-donor (γ^-) parameters were examined for various container materials by contact angle measurements with different liquids [180]. These materials included not only different metals, but also glass. It was discovered that γ^-/γ^+ was four times higher for stainless steel than for glass, indicating a high probability for electron transfer from the mixing vessel to GBs. Applying this theory to the present study, both carrier and API should get charged negatively during blending. This would indicate the existence of repulsive forces conclusively explaining highest TSCs for TC8h.

It can be taken from Figure 4-32 that BUD exhibited higher overall TSCs compared to FF which might seem incomprehensible as far as chemical properties of the APIs are considered. Nevertheless, observations made during the optimisation of blending conditions might provide a plausible rationale. Preparing homogeneous blends containing BUD required solely a blending time of 30 min at 20 rpm. In contrast, a blending protocol of 35 min at 20 rpm followed by 5 min at 30 rpm had to be applied to ensure sufficient drug loading and adequate homogeneity when using FF. This implies that the ratio of cohesive to adhesive forces is higher for FF causing the formation of agglomerates which are not attached to the carrier surface.

4.3.3 Impaction Analysis

Figure 4-34 (top) displays respirable fractions of interactive mixtures containing GB_UT and modified GBs blended with FF. For each type of GB, three different CSCs were investigated. In general, a distinctive trend concerning the effect of drug loading on aerodynamic performance analogous to that in section 4.2.3 was identified. The respirable fraction was improved when increasing the CSC. This is true for each blend under investigation and applies to both APIs.

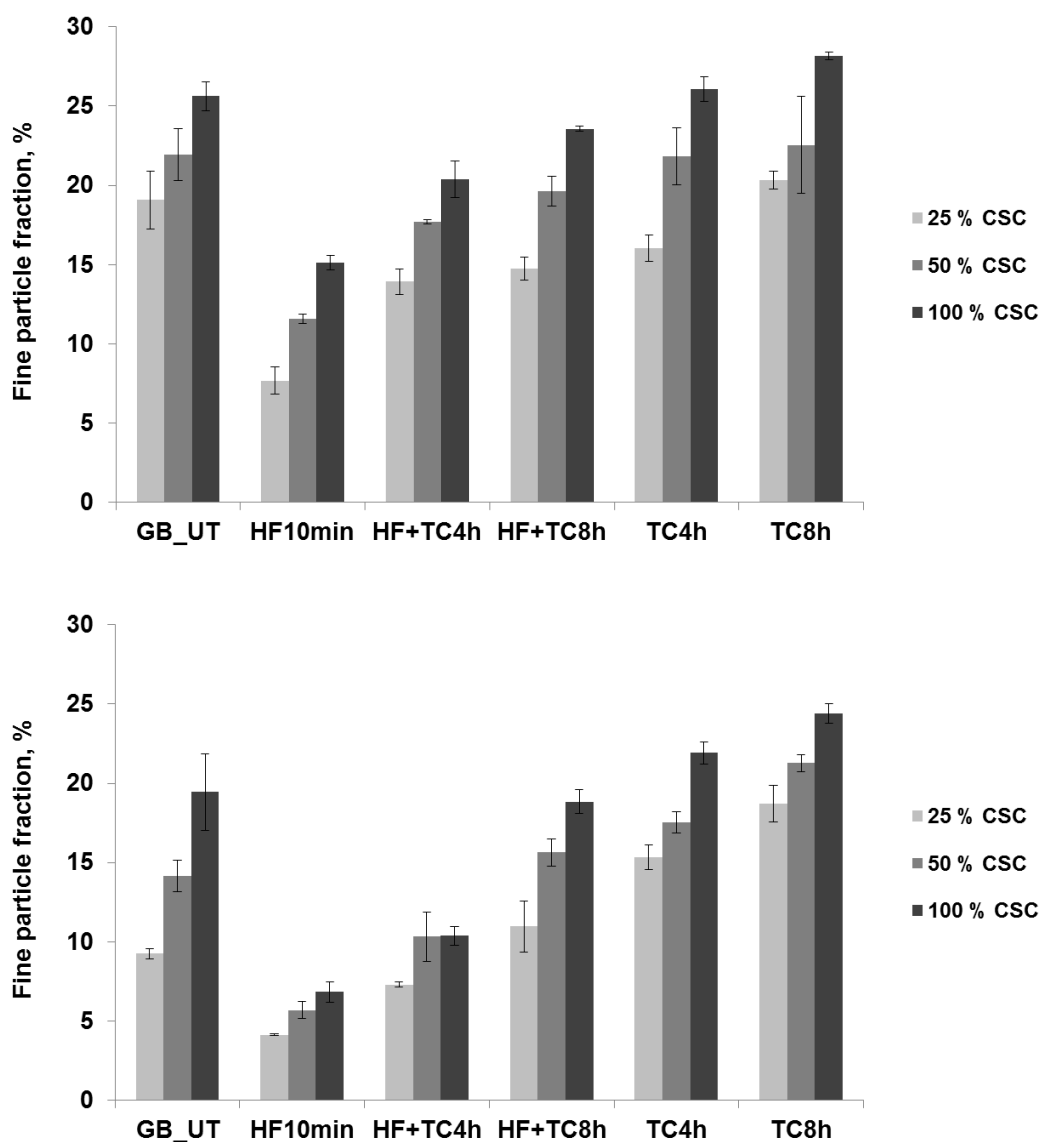


Figure 4-34 FPFs (+StD) of blends containing different GBs and FF (top) or BUD (bottom) for CSCs of 100 %, 50 % and 25 % (n=3)

When evaluating the impact of surface modifications, a significant decrease in FPF through the introduction of micron-sized roughness becomes apparent. For FF, res-

pirable fraction decreased from 25.6 ± 0.9 % for GB_UT to 15.1 ± 0.5 % for HF10min (100 % CSC). Through the addition of a milling step with TC, respirable fractions could be increased again almost to the level of GB_UT as seen for HF+TC8h. The enhancing effect on respirable fraction is further displayed by major FPFs exhibited by TC4h (26.1 ± 0.8 %) and TC8h (28.2 ± 0.2 %). Trends described in this section also hold true for BUD. However, absolute values of FPFs differed to a substantial extent from those obtained when using FF. Respirable fractions of BUD were experienced to be lower in any case (Figure 4-34 (bottom)).

Again, the FPF was normalized to a fictive TSC of 30 % for each type of GB to directly compare the different blends as described in section 4.2.3. When evaluating the resulting FPFs of FF and BUD, it becomes clear that trends shown above are still existent (Figure 4-35). However, results can now be compared in a direct way regardless of differing TSCs.

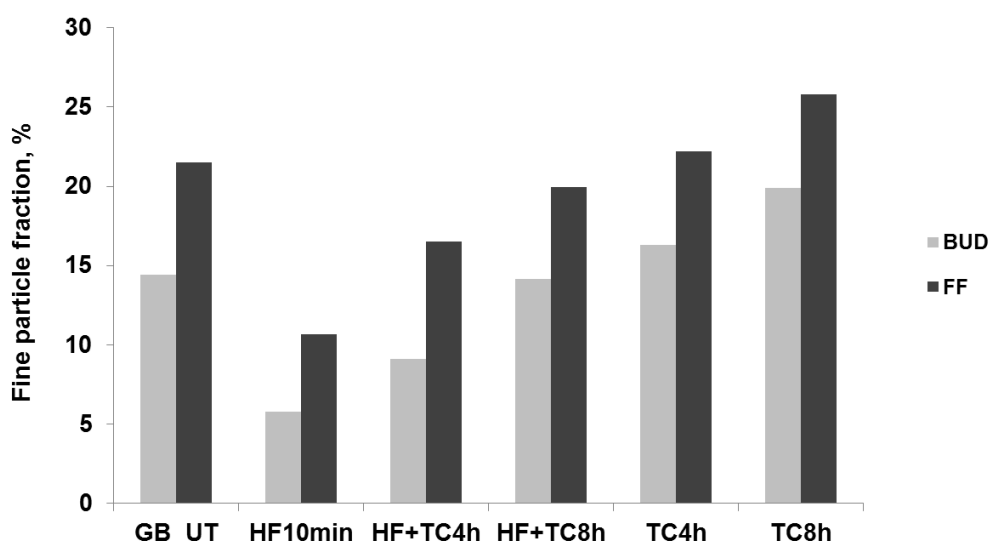


Figure 4-35 Resulting FPFs at 30 % TSC for untreated and modified GBs blended with FF (black bars) or BUD (grey bars)

A significant decrease in respirable fraction was observed in the presence of deep cavities (μm range) for both APIs and SEM pictures provide a conclusive explanation for this. After blending, API particles had accumulated in those discontinuities (Figure 4-36 (left)). This observation has been ascribed to an enhanced potential for adhesive forces in those regions [181]. In addition, API particles located in those active sites potentially find shelter from the airstream during inhalation which causes a persisting attachment onto the carrier surface. In the course of a recent revision of the active

sites theory, it was proposed to define the activity of surface areas by their ability to shelter API particles from removal forces during inhalation directly linking drug dispersion to site activity [182]. In case of the Cyclohaler, those removal forces are mainly based on drag and lift process, while inertial impaction only plays a minor role for this device. Moreover, it was confirmed by examination of GBs taken from the preseparator after inhalation routine. Figure 4-36 (right) shows indentations remaining occupied with a certain amount of drug. Even though a high flow rate of 100 L/min was applied, the kinetic energy of the air stream was evidently not high enough to detach the API causing a drastic decrease in respirable fraction. The same trend was existent when comparing FPFs of blends containing HF+TC4h or HF+TC8h to those containing TC4 or TC8h, respectively.

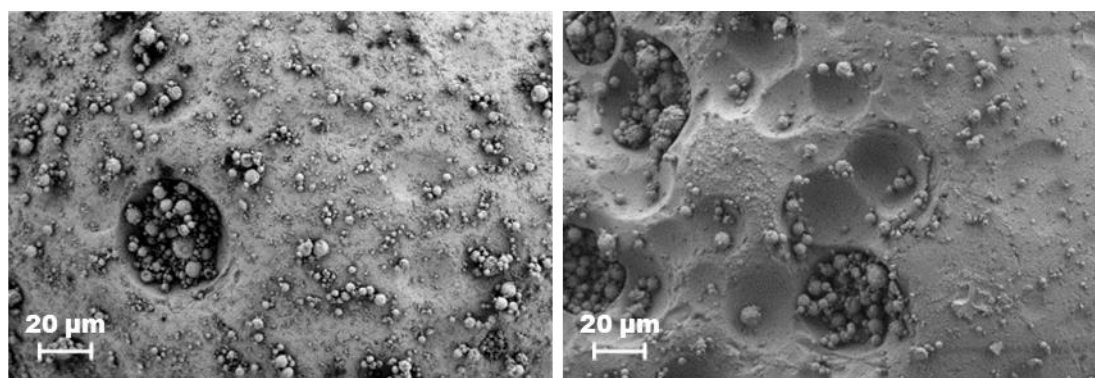


Figure 4-36 SEM micrographs of the interactive mixture containing HF10min and BUD at 50 % CSC before (left) and after inhalation (right)

Consistent observations were made by Littringer et al., where mannitol carrier particles with large indentations of up to 50 µm in diameter were obtained through spray drying by adjusting process parameters [57]. They also experienced an accumulation of drug particles in those cavities leading to a lowered respirable fraction. In contrast, Dickhoff et al. found a beneficial effect of the presence of cavities on aerodynamic performance as they potentially protect drug particles from press-on forces created during the blending process [183]. It was acknowledged, however, that this potentially favourable effect might solely be relevant for inhalation devices where drug detachment is triggered by inertial forces, e.g. Novolizer or Turbuhaler [84]. When using the Cyclohaler, where the dispersion principle is based on drag and lift forces, this is not expected as entrapped drug particles remain largely unaffected by those forces [181]. Hence, presented results for the impact of micron-scale roughness are primarily ap-

plicable to inhalation devices that induce drug redispersion by mechanisms similar to the Cyclohaler, e.g. the Diskus.

The presence of nano-scale roughness induced an increase in FPF, which is true for FF as well as BUD (Figure 4-35). Presumably, these submicron irregularities reduced the contact area between carrier and API and consequently diminished the potential for interaction between the two. This led to lower adhesive forces ultimately facilitating drug detachment to enhance the FPF. Again, the extended milling time showed an even more pronounced effect as superior FPFs were achieved when using TC8h. The obtained results are in good agreement with earlier findings by Kawashima et al., where a decrease in aerodynamic performance was determined for lactose particles with a smoothed surface [184]. This was ascribed to an increase in contact area leading to stronger van-der-Waals attractive forces. Despite obvious differences in chemical characteristics of FF and BUD, the same trends were observed as far as respirable fractions are concerned. A recent study carried out within the DFG priority program "PiKo" examined the effect of sub-micron surface roughness which was introduced inter alia by plasma etching using salbutamol sulphate as API [81]. Obtained results showed a positive correlation between roughness and FPF. These findings imply that a decrease in contact area created through nano-scale roughness promotes drug detachment regardless of chemical properties of the API.

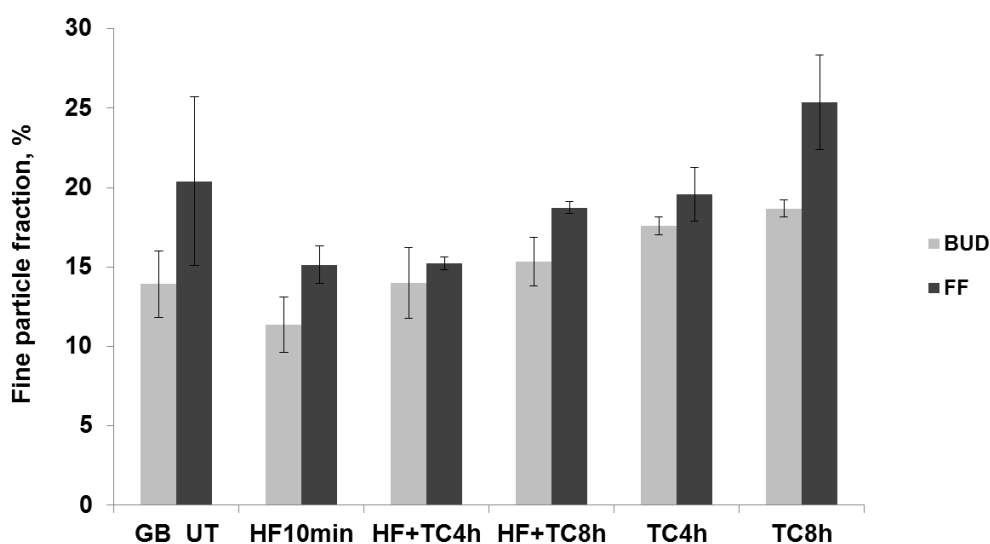


Figure 4-37 FPFs (+StD) for untreated and modified GBs blended with FF micro (black bars) or BUD micro (grey bars) (n=3)

Additionally, trials were carried out utilising the APIs in micronised quality. In the course of this, blends were prepared with an API to carrier ratio of 1:100 (m/m) as the irregular shape of the particles did not allow calculations concerning surface coverages. A drug content of 1 % can also be considered as a common concentration in blends for inhalation. FF micro exhibited respirable fraction in the range of $15.1 \pm 1.2 \%$ to $25.4 \pm 3.0 \%$. For its hydrophobic counterpart (BUD), FPFs between $11.4 \pm 1.7 \%$ and $18.7 \pm 0.5 \%$ were obtained (Figure 4-37).

Here, GB treatment with HF again diminished the FPF whereas the introduction of nano-scale roughness facilitated drug detachment. This is true for both APIs. It also becomes apparent that the impact of micro-scale roughness was less pronounced for micronised drugs compared to the spray-dried quality. This implies a limited capacity of the indentations to withhold those drug particles during inhalation. Interestingly, higher overall FPFs were obtained for spray-dried compared to micronised APIs despite lower mean particle sizes of the latter (Figure 4-38). These results may be linked to an improved aerodynamic behaviour of spray-dried particles due to, e.g. tailored spherical shape and lower density.

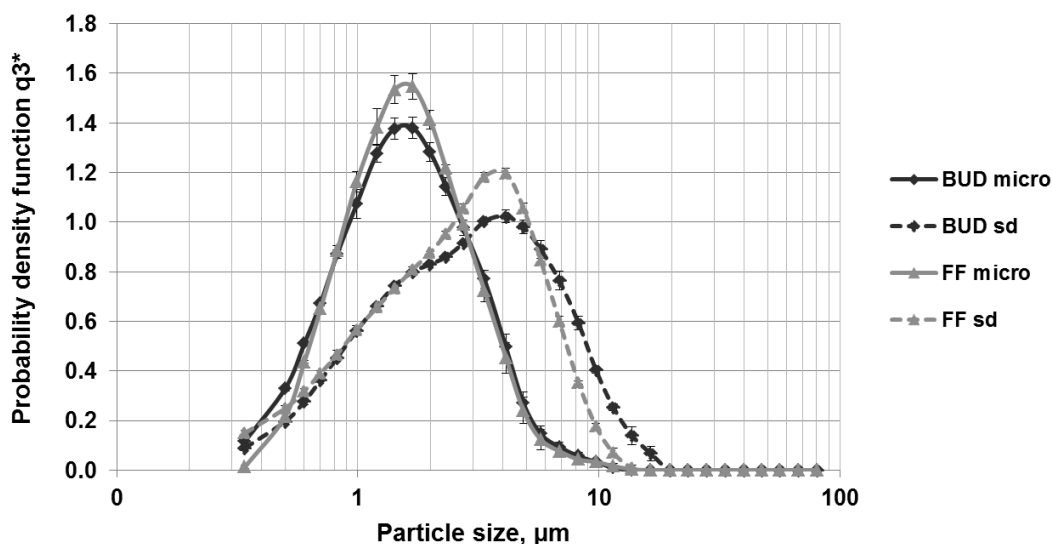


Figure 4-38 PSDs with logarithmic scaling on the x-axis of BUD and FF in micronised and spray-dried quality

To conclude, the presence of nano-scale roughness was favourable for an efficient drug detachment, while larger indentations hindered drug detachment subsequently reducing the aerodynamic performance. As shown in the present chapter, this is gen-

erally valid despite extensively varying morphological and chemical properties of the drug particles.

However, as the blends differed in TSC, the amount of active delivered to the lungs expressed as FPD also has to be taken into account. This is because not only the fraction of API but also the total dose is of interest for pulmonary drug delivery. To do so, results gained for spray-dried APIs were evaluated again.

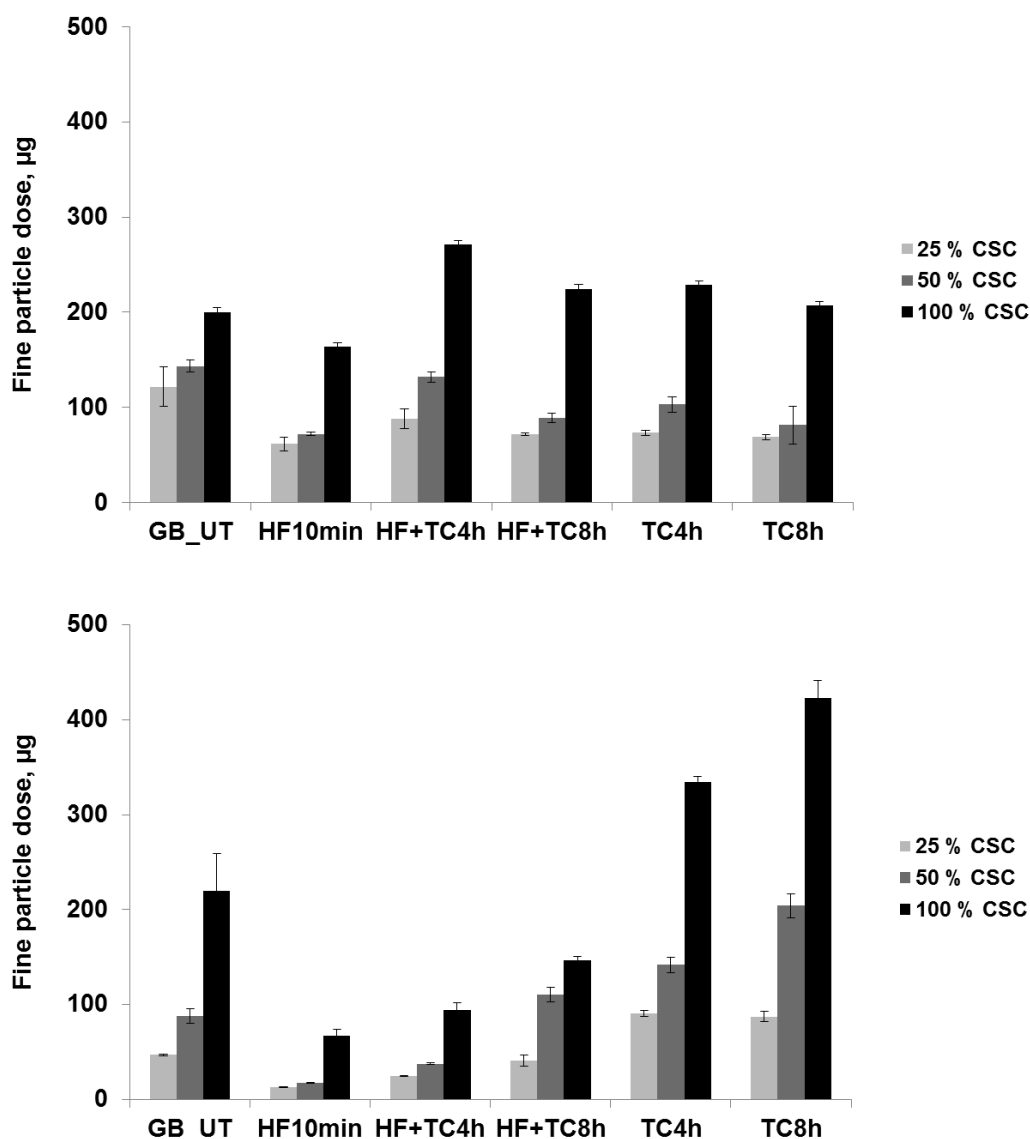


Figure 4-39 FPDs (+StD) of blends containing different GBs and FF (top) or BUD (bottom) for different CSCs of 100 %, 50 % and 25 % (n=3)

As seen in Figure 4-39 (top) which displays FPDs of blends containing FF, some trends described earlier for the FPF are still existent but less pronounced. Albeit a decrease in respirable dose for HF10min ($163.9 \pm 3.7 \mu\text{g}$ for 100 % CSC) compared

to GB_UT ($199.8 \pm 5.2 \mu\text{g}$ for 100 % CSC), HF+TC8h, TC4h and TC8h presented comparable FPDs. Highest doses were found for HF+TC4h. As far as BUD is concerned, distinctive tendencies regarding the effect of surface modification on the FPD were observed (Figure 4-39 (bottom)). Corresponding to FPFs, the amount of fine particles was decreased through HF treatment to $67.36 \pm 6.5 \mu\text{g}$ (100 % CSC) while milling with TC led to an almost two-fold increase up to $423.1 \pm 18.0 \mu\text{g}$ compared to $220.1 \pm 40.0 \mu\text{g}$ for GB_UT.

The FPD represents the total dose of API theoretically delivered to the lower airways and therefore can be seen as the result of the interplay between FPF and TSC. For FF, TC milling led to a substantial decrease in TSC (section 4.2.2) while respirable fraction was enhanced by that modification resulting in only medium FPDs. Lower respirable doses due to small FPFs were observed when applying HF treatment while it had a negligible effect on TSC. This is also true for BUD. Here, however, introduction of nano-scale roughness significantly increased the TSC. This modification had a positive effect on the FPF leading to drastically increased FPDs for TC4h and TC8h as well.

4.3.4 Adhesion Forces

The AF between two particles is equivalent in magnitude to the force which is required for their detachment or separation. Different measuring setups have been introduced in the past years to investigate those forces including centrifugation, vibration and impact separation [185,186]. But these techniques only allow indirect determination of AFs as they measure the amount of particles which get detached under certain conditions. AFM, however, monitors the detachment of a single particle from another one providing precise measures of AFs. These investigations helped to further enlighten the relationship between interparticle interactions and drug detachment.

It can be taken from Figure 4-40 that HF treatment did not alter AFs between carrier and API, e.g. seen for GB_UT at $111.3 \pm 30.5 \text{ nN}$ and HF10min at $114.7 \pm 38.9 \text{ nN}$. Milling with TC for 4 hours significantly decreased AFs (HF+TC4h and TC4h). The extended milling protocol led to further decrease illustrated for TC8h ($26.18 \pm 9.7 \text{ nN}$).

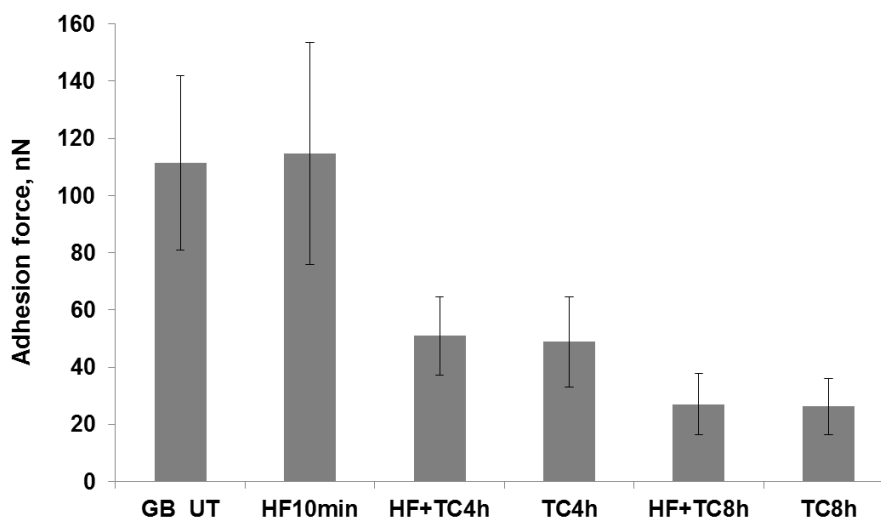


Figure 4-40 Adhesion forces (+StD) between GB_UT or modified GBs and BUD sd (n=75)

Interestingly, the effect of HF treatment was negligible in any case. It can be concluded that no enhanced interactive forces prevail in the cavities in contrast to assumptions by de Boer et al. [181]. Therefore, those forces were not accountable for drug entrapment on the carrier surface in this setup. Instead, the present findings emphasise that the diminished respirable fractions were dependent on the ability of larger indentions to physically shelter the drug particles located inside from the airstream. However, the assumption of TC treatment leading to diminished contact area between carrier and API could be verified. Reduced adhesive forces can conclusively be related to an enhanced aerodynamic performance of the respective blends.

4.4 The Importance of Inhaler Geometry

Up to this point, focus has been put on the DPI formulation to explain aerodynamic performance by carrier surface characteristics. In this chapter, the role of the inhalation device will be examined. The overall aim was the identification of inhaler parts with a significant impact on dispersion, deagglomeration and consequently on drug delivery efficiency. This was implemented with DoE approaches utilising the Modular Inhaler system (section 3.1.6.2). Different dimensioning of inhaler parts were defined as the respective factors within the experimental design. FPF, device retention (DR) and specific device resistance (SDR) were set as responses to be investigated. For comprehensive examination, two APIs, namely BUD micro and IB micro, were used each to form interactive mixtures with GB_UT.

GBs are merely intended as a model carrier system. Beyond that, they exhibit widely different material characteristics compared to conventional carriers (Table 4-4). Thus, the present study should also point out differences and similarities in the aerodynamic behaviour of blends containing either GBs or lactose. In order to do so, obtained results were directly compared to those from Friebel [87], hereafter referred to as the *earlier study*. In that, different inhaler combinations have been examined using α -lactose monohydrate as carrier.

Blends were prepared according to [87] with a fixed drug content of 1.0 %. This enabled a comparison of results using BUD micro and IB micro but replacing lactose by GB. Nevertheless, the setup of the study had to be adjusted due to GB properties as discussed in the following.

Table 4-4 Characteristic properties of GBs in comparison to commonly used lactoses for inhalation [187–189]

Property	Lactohale [®] 100	Lactohale [®] 200	SiLibeads [®] Type S
Particle size, μm	120 – 145 (x_{50})	50 – 100 (x_{50})	400 – 600 (size range)
Poured density, g/L	690	650	2500
Tapped density, g/L	840	950	2500
Particle shape	Irregular	Irregular	Spherical

4.4.1 Design of Experiments

In the present experimental designs, a fractional factorial design (section 3.2.1) was applied to determine the practical relevance of device components for aerodynamic behaviour of the interactive mixture. For the upper part of the inhaler, different cross sectional areas (CSAs) of the mouthpiece were employed. Impact of the dimensioning of grid, i.e. stanchions width and free grid area, was of interest as well. Finally, dimensioning of the bottom part was investigated, where CSA of the air inlet and height of the deagglomeration chamber were varied (Table 4-5). Device retention was defined as the combined fractions of API remaining in the device and the capsules after inhalation. The influence of the dimensioning on respirable fraction and DR of BUD and IB were systematically examined within these DoEs. In addition, the SDR was determined for each inhaler part combination to get information about the air flow velocity within the device. Firstly, results were visually displayed in so-called contour plots to provide an overview of the range of the different responses. Secondly, the extent to which each significant factor affected the different responses was shown in coefficient plots.

Table 4-5 Dimensioning of the upper part, grid and bottom part of the inhaler in sizes small (S), medium (M) and large (L)

Dimensioning	S	M	L
Mouthpiece, CSA, mm ²	7.06	21.30	35.54
Grid, Free grid area, mm ²	20.71	35.76	50.80
Grid, Stanchions width, mm	7.06	21.30	35.54
Air inlet, CSA, mm ²	11.82	17.70	23.57
Deagglomeration chamber, Height, mm	7.00	8.00	9.00

4.4.2 Influence on Aerodynamic Performance

Figure 4-41 visualises the effect of the different inhaler parts on the FPF of BUD, whereby values in the range of $14.1 \pm 1.3 \%$ to $31.4 \pm 2.1 \%$ were obtained. The dimensioning of all three components showed a significant effect on the FPF.

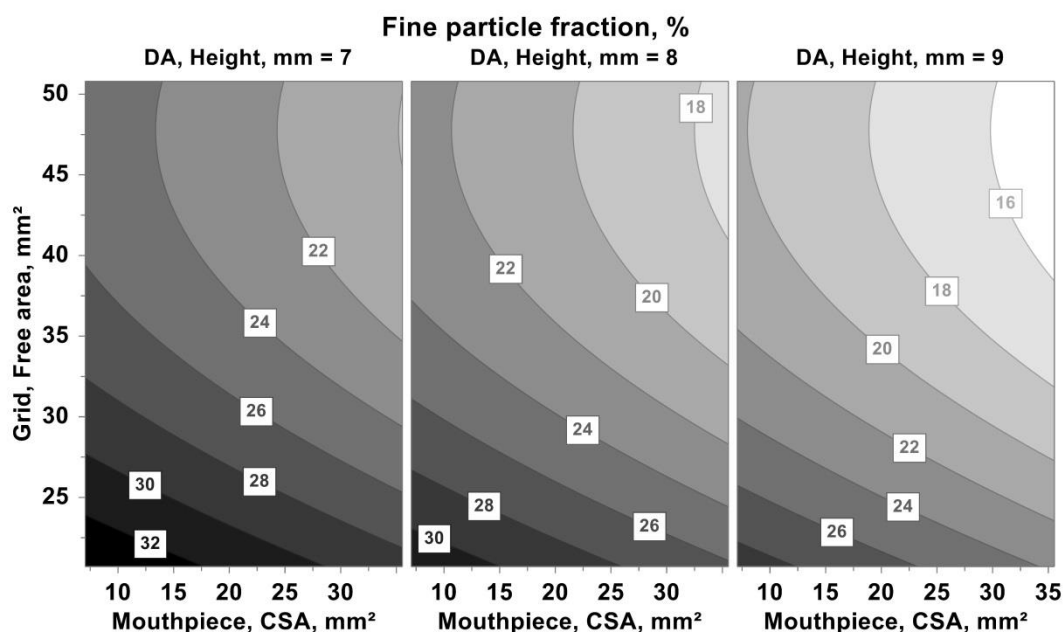


Figure 4-41 4D Contour plot of the FPF for BUD as a response of the factors mouthpiece CSA on the x-axis and grid (represented by the free grid area) on the y-axis. Results are given for the three different bottom parts represented by deagglomeration chamber height of 7, 8 and 9 mm; DA=Deagglomeration chamber

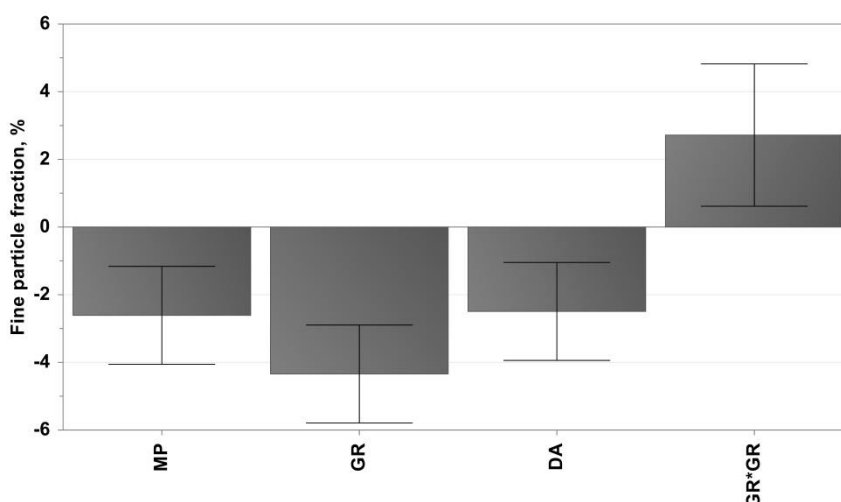


Figure 4-42 Illustration of the significant effects of different inhaler parts on the FPF for BUD (coefficients scaled and centred). Gained values display the change in FPF, if the respective factor is changed by one level; MP=Mouthpiece, GR=Grid, DA=Deagglomeration chamber

Increasing the dimensioning of each inhaler part was unfavourable for the aerodynamic performance. Accordingly, highest FPF was exhibited by the device composed of a small upper and bottom part as well as a small grid (Modular_S), while lowest FPF was experienced for overall large dimensioning (Modular_L). Additionally, a positive quadratic correlation of the grid became apparent (Figure 4-42).

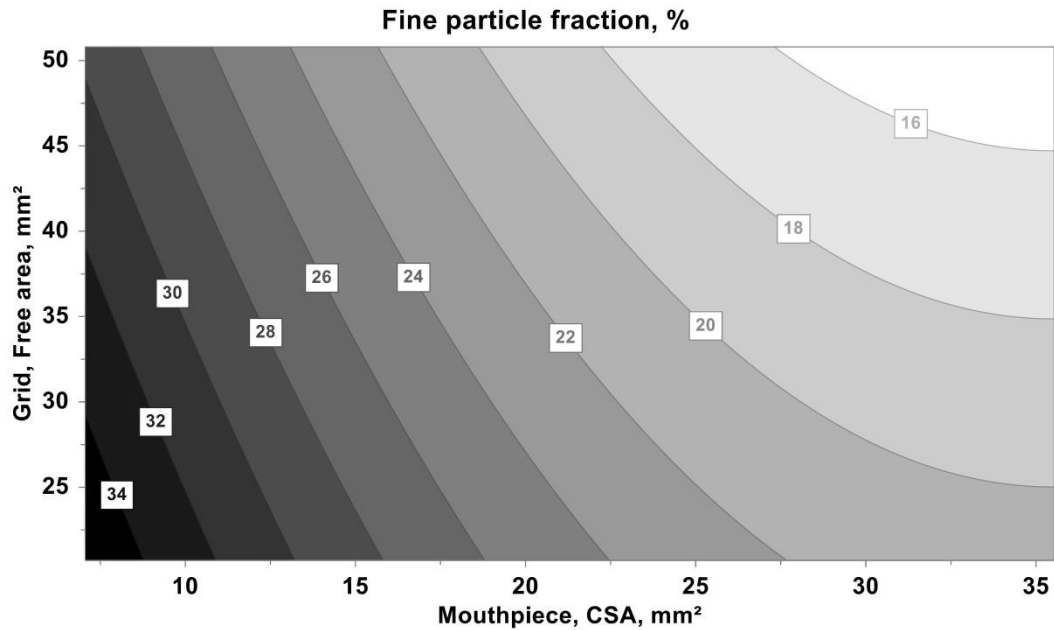


Figure 4-43 Contour plot of the FPF for IB as a response of the factors mouthpiece on the x-axis and grid (represented by the free grid area) on the y-axis

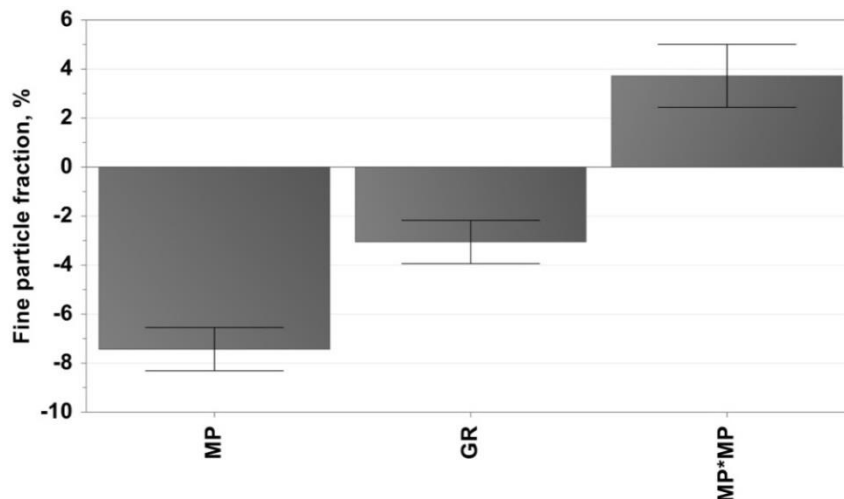


Figure 4-44 Illustration of the significant effects of different inhaler parts on the FPF for IB (coefficients scaled and centred). Gained values display the change in FPF, if the respective factor is changed by one level; MP=Mouthpiece, GR=Grid, DA=Deagglomeration chamber

Dispersion behaviour of blends containing IB was governed by the dimensioning of MP and grid leading to FPFs between $14.7 \pm 0.3 \%$ and $35.2 \pm 1.7 \%$ (Figure 4-43). Again, increasing the dimensioning of the respective inhaler parts influenced the respirable fraction in a negative way. In addition, a quadratic correlation (positive) to the mouthpiece occurred (Figure 4-44).

The negative effect of an increased CSA of the mouthpiece can be ascribed to its impact on the air stream velocity. In the present setup, a fixed flow rate of 60 L/min was applied to ensure sufficient entrainment of high density GB particles. At a constant flow, resistance of the inhalation device gets reduced when increasing the mouthpiece diameter. This leads to a decelerated air stream. This can be derived from equation 17 which is applied to approximately determine the velocity (V) within a specific inhaler part as a function of flow rate (Q). It is also supported by Computational Fluid Dynamic analysis presented by Coates et al., where a significantly lower exit velocity was determined for an increase in MP diameter of the inhalation device [190]. Consequently, less kinetic energy is transferred to the interactive mixture which lowers the effectiveness of drug redispersion. As a result, aerodynamic performance is reduced independently of API.

$$V_{inhaler\ part} = \frac{Q \cdot 1000}{CSA_{inhaler\ part} \cdot 60} \quad \text{equation 17}$$

In the *earlier study*, an opposite effect was documented. A large mouthpiece was favourable for an enhanced aerodynamic performance. This might seem contradictory at first sight, but is entirely coherent when experimental conditions are considered. The present study featured a consistent flow rate leading to varying pressure drops and thus different air stream velocities in the device for the different combinations of inhaler parts. The *earlier study* implemented the opposite approach, setting a constant pressure drop of 4 kPa, defined by the Ph. Eur. as standard conditions. This resulted in varying flow rates and thus a constant air stream velocity [106]. It had been possible to apply this setup there due to the fundamental differences in carrier characteristics. Density and particle size were both much lower for lactose compared to GBs. By increasing the mouthpiece diameter, inhaler resistance was lowered. As a consequence, a higher flow rate was needed to maintain the 4 kPa pressure drop

which raised the kinetic energy of the airstream and the level of turbulence. This triggered superior drug detachment.

A small grid was needed to achieve higher respirable fractions for both APIs. It is assumed that a smaller free grid space decelerates emptying of the capsule chamber. By that, the kinetic energy of the airstream was applied to the interactive mixture for the whole duration of the inhalation manoeuvre. This enhanced deagglomeration of interactive mixtures to ultimately increase the respirable fraction. This corresponds to findings from the *earlier study* and indicates that a slow and controlled discharge of the deagglomeration chamber is desirable regardless of carrier properties.

For the hydrophobic BUD, the bottom part (air inlet and deagglomeration chamber) significantly influenced respirable fraction. Tightening the air inlet and lowering the deagglomeration chamber enhanced the aerodynamic performance. On the one hand, this is also due to an increased air stream velocity at constant flow rate through a reduction of CSA of the air inlet. On the other hand, a smaller deagglomeration chamber decreased the distance particles had to be lifted to leave the inhaler. The latter factor is certainly negligible for conventional carriers with a relatively low specific weight, but is relevant for high density GBs. Interestingly, the choice of the bottom part did not affect the respirable fraction of IB. It can be concluded that BUD needs to exit the inhaler persisting on the carrier to ensure proper drug detachment and dispersion. IB, however, is already dispersed within the DA and is consequently not dependent on leaving the inhalation device while still being adhered to the carrier. On the contrary, the *earlier study* stated a positive effect for BUD and a negative effect for IB. Taking these findings into account, present results hint at different deagglomeration and dispersion behaviour of the two APIs.

4.4.3 Influence on Device Retention

For BUD, an extension of grid or an increase in the dimensioning of bottom part reduced or increased the fraction of API remaining in device and capsules, respectively. Hereby, DRs between $6.5 \pm 1.8 \%$ and $32.0 \pm 2.5 \%$ were reached (Figure 4-45). A quadratic effect of the air inlet/deagglomeration chamber was found as well (Figure 4-46).

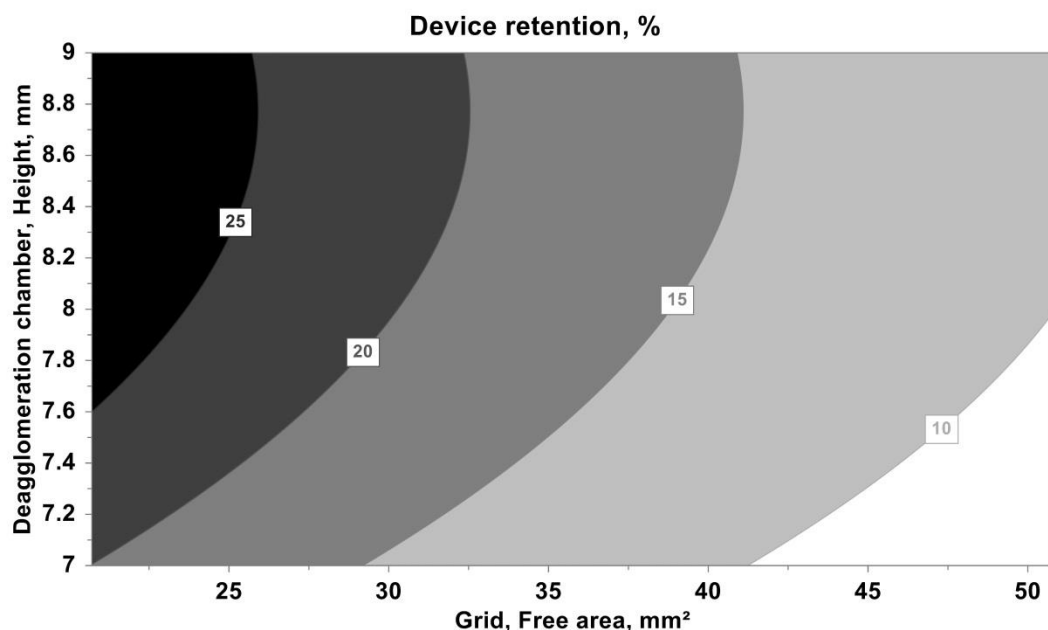


Figure 4-45 Contour plot of the DR for BUD as a response of the factors grid (represented by the free grid area) on the x-axis and the bottom part (represented as height of the deagglomeration chamber) on the y-axis

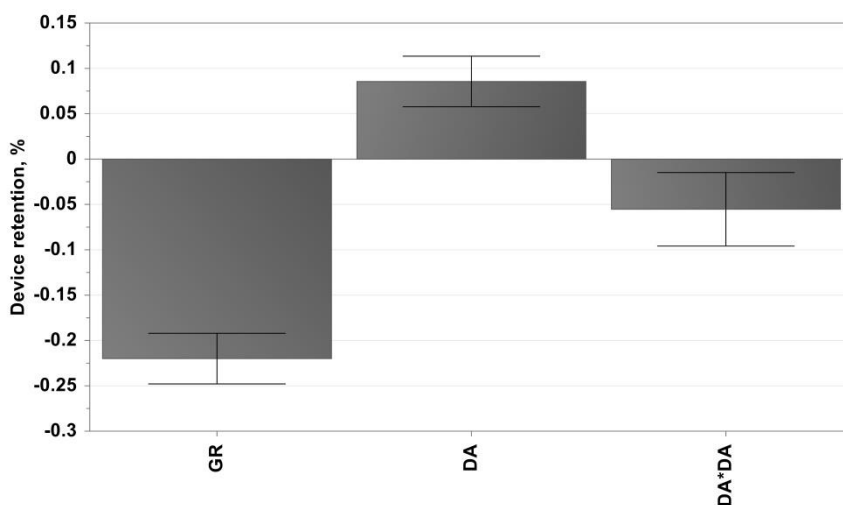


Figure 4-46 Illustration of the significant effects of different inhaler parts on the FPF for BUD (coefficients scaled and centred). Gained values display the change in DR, if the respective factor is changed by one level; MP=Mouthpiece, GR=Grid, DA=Deagglomeration chamber

An increase in DR of the hydrophilic IB was observed when using a large-dimensioned grid (Figure 4-47), along with a quadratic correlation and an interaction between grid and air inlet/deagglomeration chamber (Figure 4-48). IB showed DRs in the range of $2.3 \pm 0.3 \%$ – $21.5 \pm 3.8 \%$. In contrast to BUD, the bottom part did not

have a significant impact on the DR. The choice of the mouthpiece on the remaining API fraction was found to be negligible for both APIs.

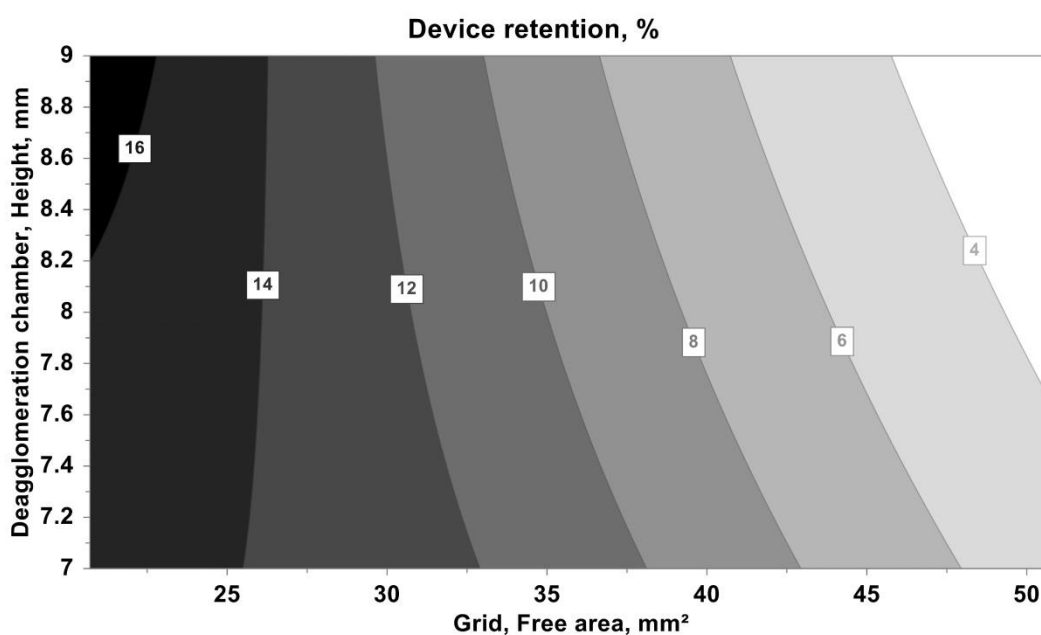


Figure 4-47 Contour plot of the DR for IB as a response of the factors grid (represented by the free grid area) on the x-axis and bottom part (represented as height of the deagglomeration chamber) on the y-axis

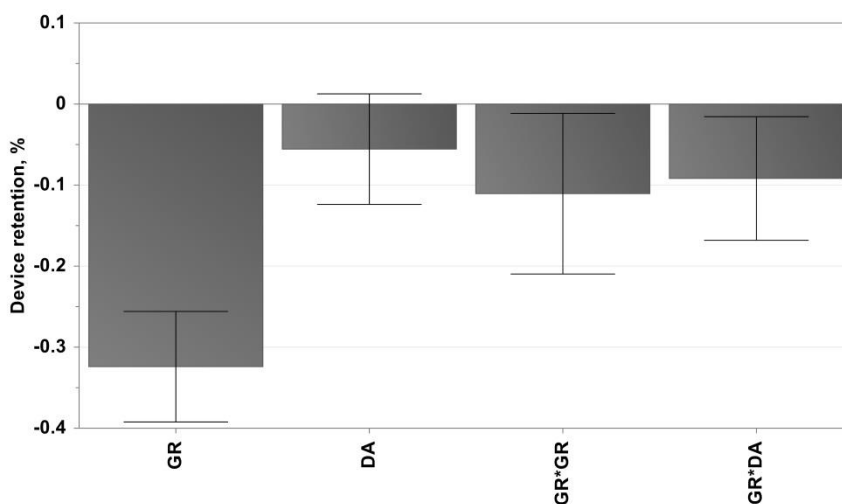


Figure 4-48 Illustration of the significant effects of different inhaled parts on the FPF for IB (coefficients scaled and centred). Gained values display the change in DR, if the respective factor is changed by one level; MP=Mouthpiece, GR=Grid, DA=Deagglomeration chamber

Microscopic examination revealed openings with a diameter of ~ 0.6 mm present in the small grid. Consequently, GBs potentially clog this grid leading to an insufficient emptying of the DA, whereas a larger free grid space allows the interactive mixture to

leave the chamber fast and (almost) entirely. This applies to both APIs regardless of their chemical properties. The varying effects of the bottom on DR of the two drugs were rather complex to interpret. As already pointed out, BUD needs to leave the chamber adhered to the GBs for a sufficient detachment during inhalation. A large-dimensioned bottom part generally provides an extended height of the deagglomeration chamber which leads to an extended distance that the interactive mixture has to be lifted to exit the inhaler. An expanded air inlet reduces the air stream velocity. Therefore, the more interactive mixture is retained by the inhaler, the more BUD will be withheld at the same time. Therefore, the dimensioning of the bottom part significantly influences BUD drug retention.

For IB, the choice of upper and bottom part did not have a significant effect on DR. This is because an adequate dispersion and deagglomeration is facilitated even at lower air velocities and if the GBs are retained in the deagglomeration chamber. This ultimately results in an independence of the amount of drug remaining in the device from the dimensioning of the bottom part.

4.4.4 Influence on Specific Device Resistance

In addition, the SDR was investigated which is a suitable parameter to compare inhalation devices in respect to their resistance. The dimensioning of the upper and bottom part significantly influenced the SDR leading to values between 0.032 and 0.064 kPa^{0.5}*min/L (Figure 4-49). In addition, an interactive effect of mouthpiece and air inlet/deagglomeration chamber was observed (Figure 4-50).

The impact of upper and bottom part of the inhaler on SDR can be ascribed to a subsequent change in air flow characteristics within the device. If cross sectional area of air inlet and mouthpiece are increased this results in an unimpeded air flow through the device. In contrast, tightening of respective parts increased the resistance. It can also be taken from Figure 4-50 that CSA of the mouthpiece governed the SDR to a larger extent. This is due to major differences in the dimensioning of the upper part, where one level equalled a gain in area of 14.24 mm² in contrast to the air inlet (gain of 5.88 mm²).

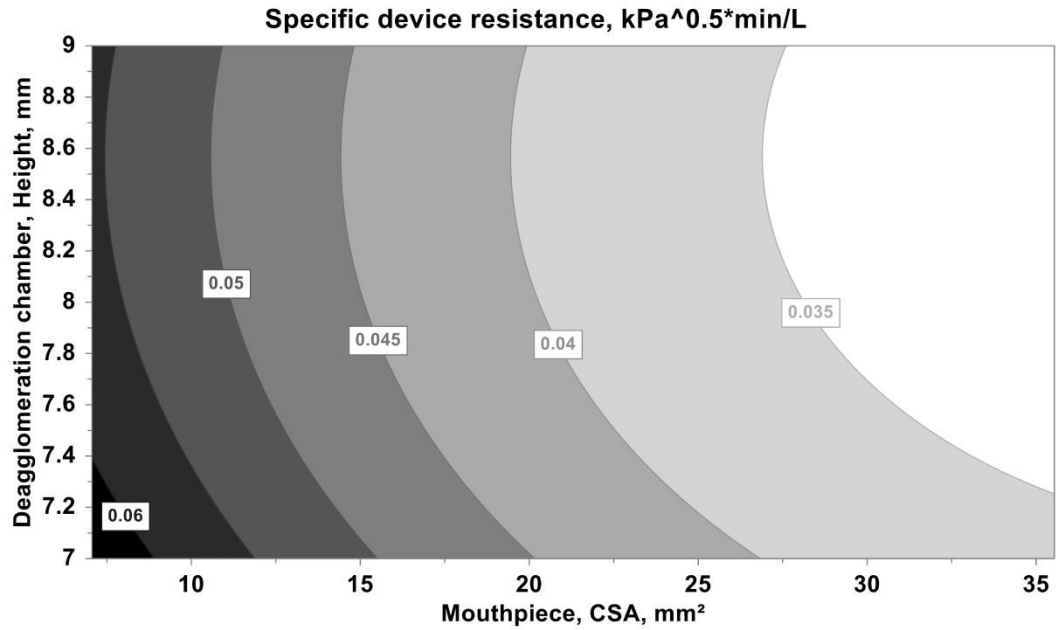


Figure 4-49 Contour plot of the SDR as a response of the factors mouthpiece (represented by the CSA) on the x-axis and the bottom part (represented as height of the deagglomeration chamber) on the y-axis

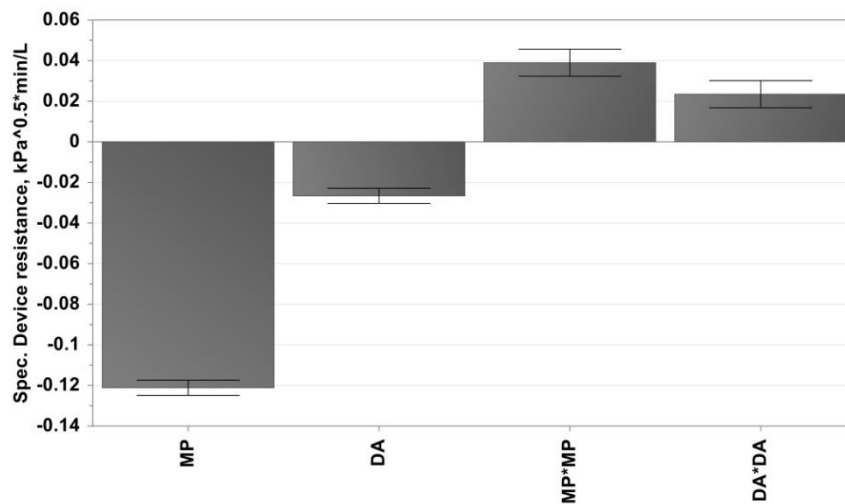


Figure 4-50 Illustration of the significant effects of different inhaled parts on the SDR (coefficients scaled and centred). Gained values display the change in SDR, if the respective factor is changed by one level; MP=Mouthpiece, GR=Grid, DA=Deagglomeration chamber

4.5 The Importance of API Properties

Following investigations concerning the importance of inhaler geometry and carrier properties, the effect of the second component in an interactive mixture, namely the API, on aerodynamic behaviour will be examined in this chapter. To do so, NGI trials were conducted employing IB in micronised and BUD in micronised as well as spray-dried quality. Their respective PSDs can be taken from Figure 4-51. Based on findings from section 4.4, three different Modular Inhaler combinations such as all small (Modular_S), all medium (Modular_M) or all large (Modular_L) dimensioned parts were selected. The commercially available Cyclohaler was utilised as comparison in the present setup.

Potentially varying dispersion and detachment behaviours have already been proposed for different APIs. To gain a deeper understanding of this process, deposition profiles based on impaction data were utilised to display the fraction of API located on each stage of the NGI in addition to the resulting FPFs.

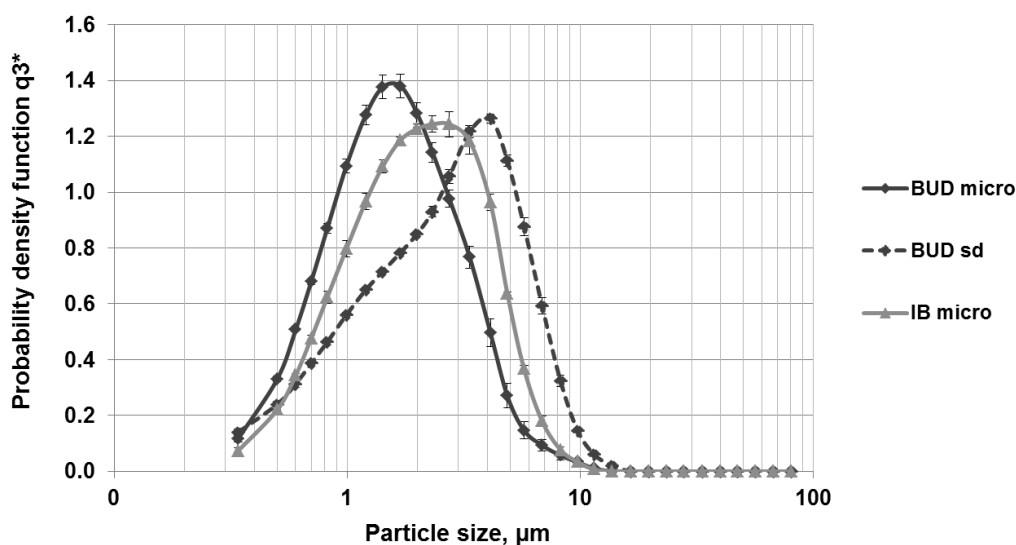


Figure 4-51 PSDs (+StD) with logarithmic scaling on the x-axis of BUD in micronised and spray-dried quality and IB micro (n=3)

4.5.1 Micronised versus Spray Dried Budesonide

Deposition profiles of BUD micro (top) and BUD sd (bottom) when using different inhalation devices are depicted in Figure 4-52. Here, fractions of API recovered from the device, induction port and preseparator as well as from stages of the NGI are dis-

played. For both API qualities, the DR decreased with increasing dimensioning of the Modular Inhaler from 18.3 ± 1.4 % to 9.0 ± 3.2 % (micro) and from 24.2 ± 3.4 % to 8.7 ± 1.9 % (sd). An intermediate retention can be ascribed to the Cyclohaler (despite an extended standard deviation).

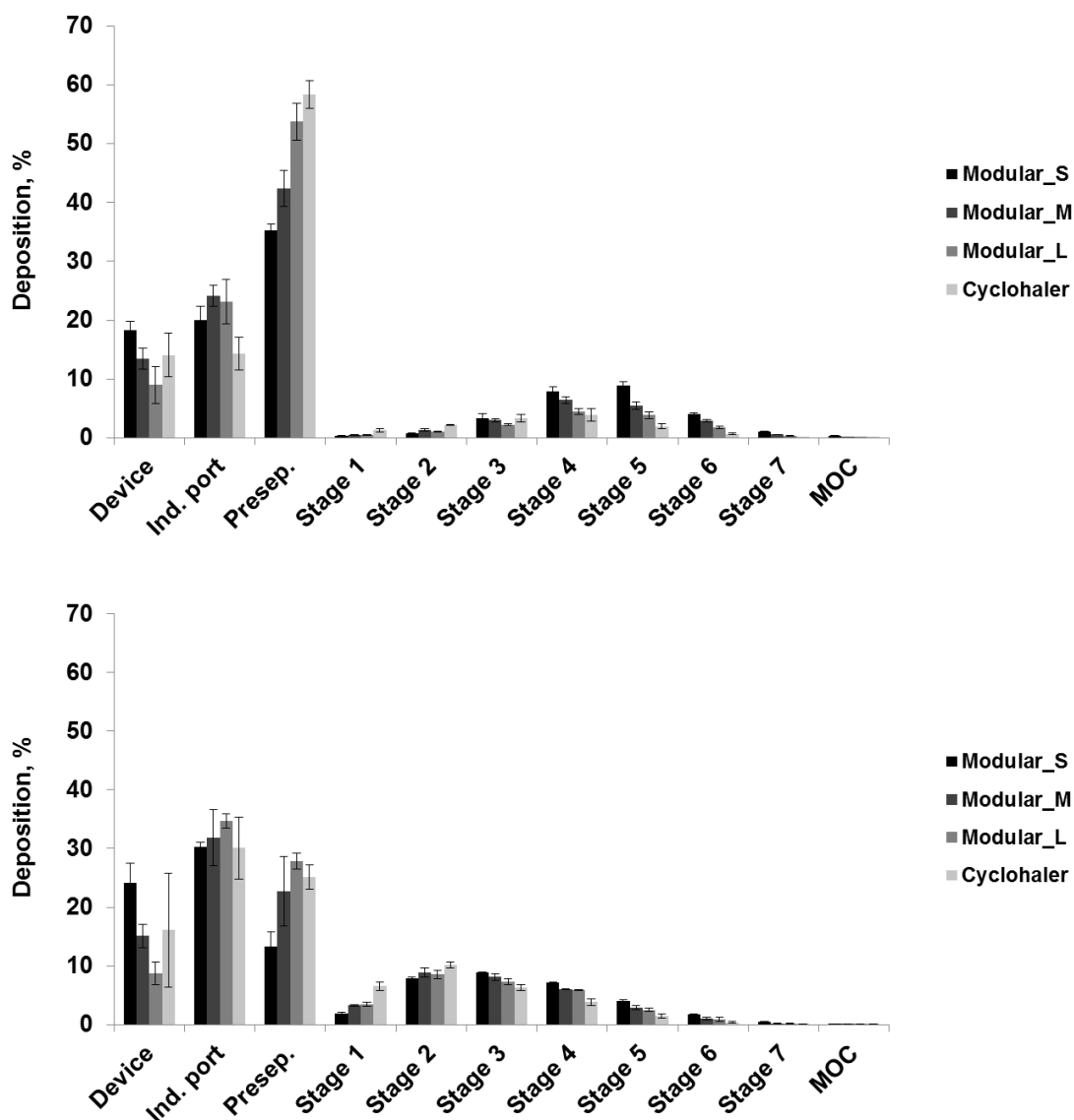


Figure 4-52 NGI deposition profiles (+StD) of BUD micro (top) and BUD sd (bottom) from different device settings (n=3)

Within the preseparator fractions a clear correlation to inhaler dimensioning was observed. API deposition increased from Modular_S up to Modular_L. This trend was most prominent for micronised material (35.2 ± 1.0 % to 53.8 ± 3.1 %). In general, BUD micro exhibited higher overall fractions in the preseparator compared to BUD sd. Overall increased fractions in the induction port were exhibited by BUD micro ranging

from 30.1 ± 5.3 % (Cyclohaler) to 34.7 ± 1.2 % (Modular_L). As far as deposition on the stages is considered, BUD in spray-dried and micronised quality showed very different results. BUD micro displayed a distribution with a maximum on stages 4 and 5. Highest overall fractions of BUD sd were found on stages 2 and 3.

As expected, maximum DR was observed for Modular_S decreasing over Modular_M to L. This is linked to, inter alia, the reduced free grid area which hindered and decelerated emptying of the chamber in the Modular_S. Comparable fractions found in Modular_M and Cyclohaler can conclusively be related to their similar grid structure as single openings were determined as ~ 1.6 mm and ~ 1.7 mm in diameter, respectively. The observation that most GBs were deposited in the preseparator explains higher fractions of micronised BUD in this compartment. This is due to a substantial proportion of drug still being attached to the carrier after inhalation manoeuvre and indicates the presence of extended AFs between micronised drug and carrier. Firstly, these might arise from carrier particles applying inertial and frictional forces on drug particles during blending [191]. Enhancement of these so-called press-on forces have been described to trigger an intimate contact between carrier and API and also to force a deformation of particles [192]. Even though blends containing BUD micro were blended for a shorter time compared to spray-dried quality (20 min vs. 30 min), the intensity was higher in the first case (30 rpm vs. 20 rpm). Since the total energy input during blending shows a quadratic relation to mixing speed but increases only linearly with the time, major press-on forces are applied to the micronised drug during blending [193]. Moreover, BUD micro and GBs present a different contact area compared to the spray dried counterpart (Figure 4-53).



Figure 4-53 Schematic illustration of plain untreated GB surfaces occupied with spherical spray-dried (left) and irregular shaped micronised drug particles (right)

Irregular, rather cuboid-shaped particles provide more contact area for interaction with the carrier surface. In contrast, spherical particles have fewer contact points leading to less potential for interaction [108]. In addition, AFs arising from external press-on forces will be limited if contact area is low [193]. Therefore, detachment of micronised

particles is impeded compared to the spray-dried drug to ultimately reduce the aerodynamic performance.

Since the SD process resulted in larger particles ($x_{50}=2.7\ \mu\text{m}$) compared to micronised quality ($x_{50}=1.6\ \mu\text{m}$), extended deposition of BUD sd in the induction port cannot be justified by differing size of particles. Instead, higher cohesive forces present in the spray-dried material might be accountable. This is supported by observations made during handling of the spray-dried powder. It appeared rather sticky compared to the micronised drug. In consequence, the tendency of forming agglomerates is significantly higher for BUD sd. This is generally in contrast to other research, where only minor agglomerate strength was found for spherical particles compared to angular- or irregular-shaped ones [194]. It has been acknowledged, however, that extended cohesive forces might be present in spray-dried material [195]. This was proposed to be due to residual solvent to enhance capillary forces. As those agglomerates are mostly deposited in the throat area according to their increased size, deposition in the induction port rises significantly. This is in accordance with a comparatively high deposition of BUD sd on NGI stage 1 which has a defined cut-off diameter of $8.06\ \mu\text{m}$ at a flow rate of $60\ \text{L/min}$ [196]. Although no clear correlation between inhaler dimensioning and induction port fraction could be established, Modular_S led to the lowest deposition in this compartment. On the one hand, this was due to the dimensioning of the air-ducting parts as discussed above. On the other hand, the smaller grid facilitated drug deagglomeration.

Different deposition profiles on the stages can be linked to varying particles sizes and PSDs. The micronised API was mainly deposited on Stages 4 and 5 with a cut-off diameter of $1.66\ \mu\text{m}$ and $0.94\ \mu\text{m}$, respectively (at $60\ \text{L/min}$). This reflects the PSD and the x_{50} ($1.6\ \mu\text{m}$) of BUD micro very well. It can be assumed that the API fraction which was detached from the carrier was also sufficiently deagglomerated. In contrast, most BUD sd was recovered from stage 2 with cut-off diameter of $4.46\ \mu\text{m}$. The spray-dried material showed a higher x_{50} value of $2.7\ \mu\text{m}$. Nevertheless, it substantiates the suggestion that higher cohesive forces are present for BUD sd. This potentially causes the persistence of drug agglomerates that impact on earlier stages of the NGI during inhalation.

Figure 4-54 displays FPFs resulting from the corresponding deposition profiles. Regardless of the API quality, Modular_S proved to have the best aerodynamic performance (FPF = 31.4 ± 2.1 % for BUD micro and 32.4 ± 1.7 % for BUD sd). Extending the dimensioning of inhaler parts reduced the FPF to 14.1 ± 1.3 % (BUD micro) and 21.1 ± 0.9 % (BUD sd). The Cyclohaler performed comparatively poor which is true for both API qualities.

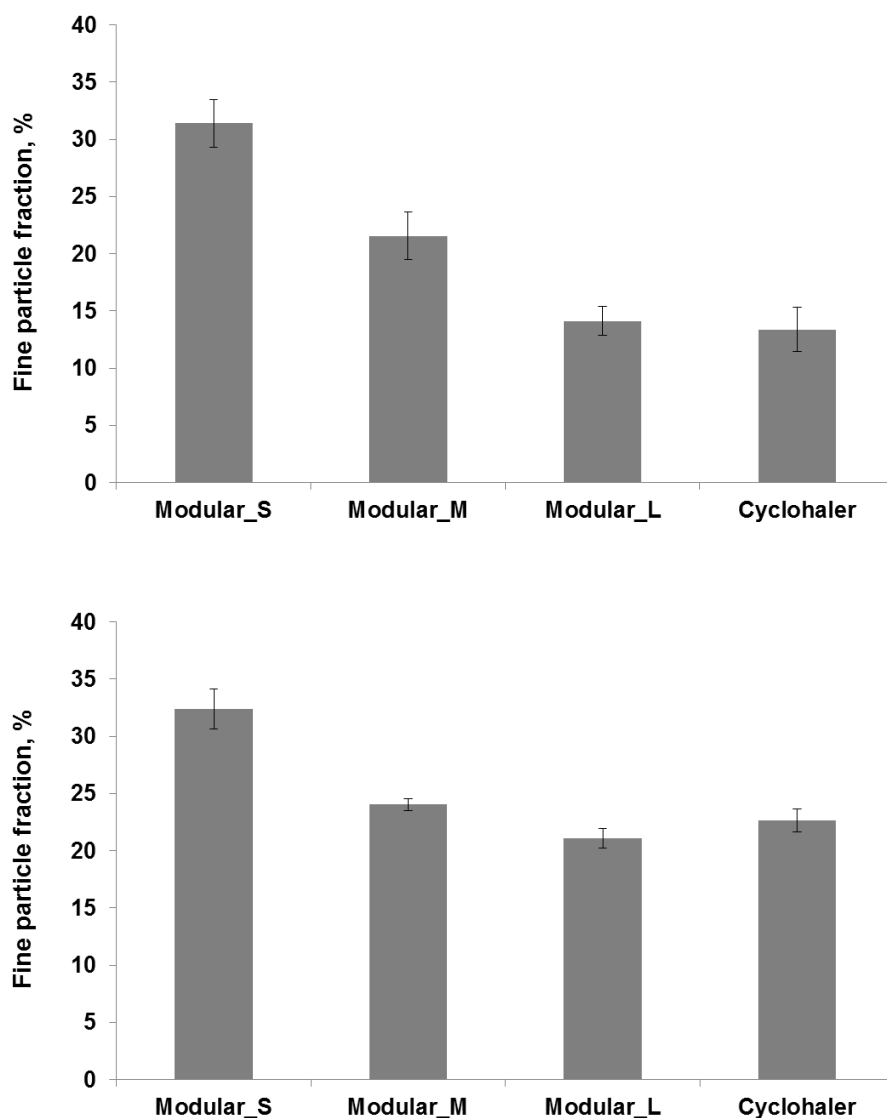


Figure 4-54 FPFs (+StD) of blends containing BUD micro (top) or BUD sd (bottom) for different inhalers (n=3)

Respirable fractions gained from the Modular Inhalers can be interpreted with the help of findings from section 4.4.2, where a small dimensioning of the respective inhaler parts was favourable in any case. This results from an extended airflow within the in-

haler due to a tight air inlet and mouthpiece. Additionally, the low level of deagglomeration chamber and the small grid trigger proper drug dispersion and detachment from the carrier. Differences in respirable fractions were more pronounced for the micronised drug. It is assumed that the different ability of the devices to disperse the interactive mixtures has a stronger impact in the presence of comparatively higher AFs between GBs and BUD micro. As a consequence, the choice of a suitable inhalation device becomes even more important, when extensive AFs prevail in the powder blend. In contrast, BUD sd was found to get properly detached even when using the less efficient Modular_L. However an overall better performance was achieved by using the Modular Inhaler system compared to the Cyclohaler.

4.5.2 Budesonide versus Ipratropium Bromide Micronised

In addition to material quality, the effect of chemical properties of the drug was examined. To do so, two different APIs, BUD and IB were employed for this study. Interactive mixtures were prepared accordingly with GB_UT.

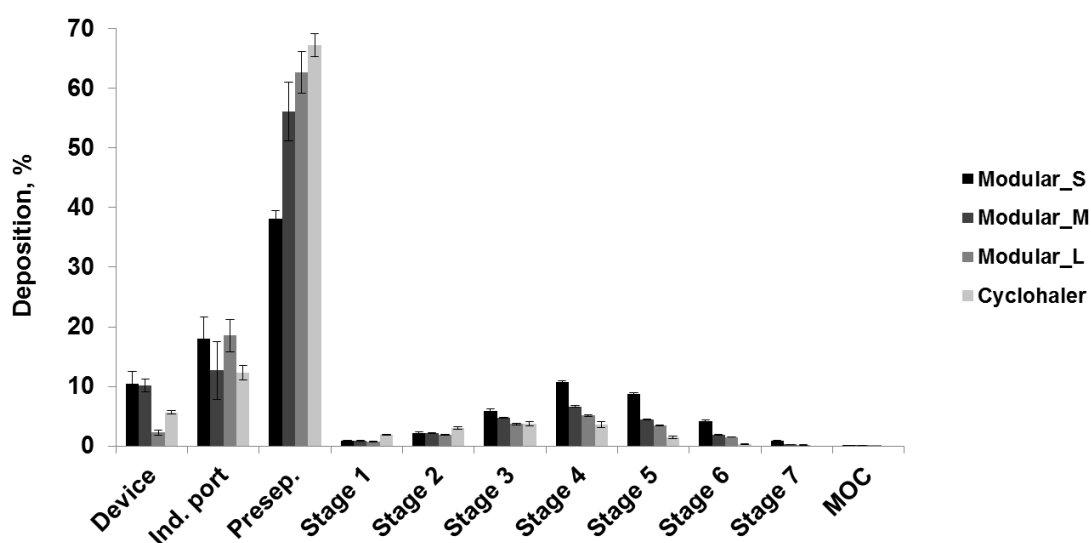


Figure 4-55 Deposition profiles of IB micro regarding device and different NGI compartments

In general, IB was retained to a lower extent within the device compared to BUD (Figure 4-55), but highest (10.4 ± 2.2 %) and lowest (2.2 ± 0.5 %) DRs were also gained from Modular_S and Modular_L, respectively. Fewer overall amount of drug was found in the induction port ranging from 12.3 ± 1.3 % to 18.0 ± 3.6 %. Fractions

recovered from the preseparator were found to be between 38.1 ± 1.4 % and 67.2 ± 1.9 %. Looking at NGI stages, most API was recovered from stages 4 (3.6 ± 0.5 % – 10.7 ± 0.3 %) and 5 (1.5 ± 0.2 % – 8.7 ± 0.2 %). On stages 3 to 7, most API was found for Modular_S, whereas Cyclohaler triggered highest deposition on stages 1 and 2.

The overall lower DR compared to BUD can be accounted to the chemical characteristics of GBs and IB. Due to their hydrophilic nature, extended attractive forces are present between the two. It is assumed that this leads to a reduced drug detachment during processing of the interactive mixture (capsule filling). Consequently, a smaller amount of API is recovered from the device and inserted capsules. Higher overall fractions of IB in the preseparator can conclusively be explained that way as well. Extended attractive forces increase the potential for a persisting adhesion of the API during inhalation. Therefore, the airstream detached less IB from the carrier. Different deposition profiles on the NGI stages for IB and BUD are due to differing PSDs of the two drugs (Figure 4-51). Lowest deposition on stages 1 and 2 as well as highest deposition on stages 3 – 7 observed for Modular_S also display an enhanced dispersion. In contrast, the stage deposition exhibited by the Cyclohaler display the opposing trend compared to Modular_S. This indicates a rather poor aerodynamic performance of the Cyclohaler.

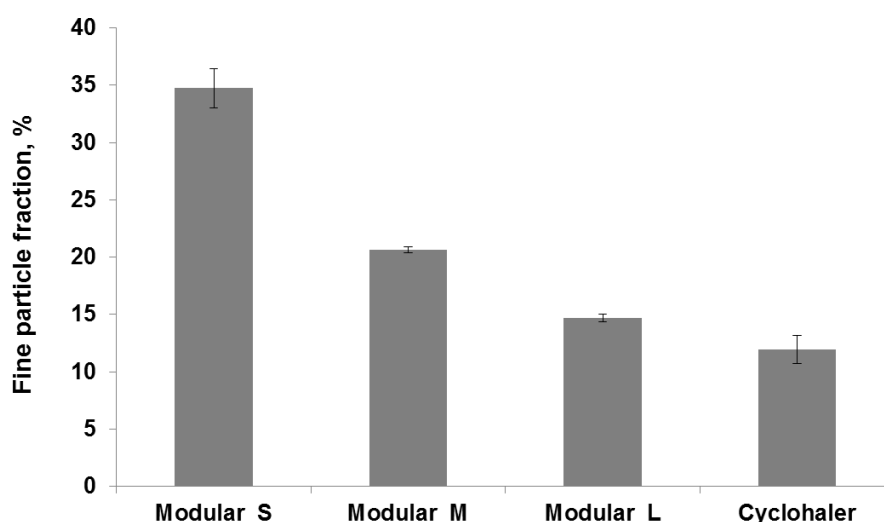


Figure 4-56 FPFs of blends containing IB micro for different inhalers

Figure 4-56 shows fine particle fractions as the result of using various inhalation devices under investigation. A clear trend was observed concerning the Modular Inhaler system, where a downsizing of the inhaler dimensioning enhanced the FPF from 14.7 ± 0.3 % (Modular_L) to 34.7 ± 1.7 % (Modular_S). The Cyclohaler presented a low value of 12.0 ± 1.2 %.

Taking findings obtained from hydrophobic BUD into account demonstrates that both APIs show a similar aerodynamic performance for the respective modular inhaler combination. It can be concluded that the overall effect of device dimensioning is widely the same for different drugs, regardless of their chemical properties. Moreover, when using GBs as carrier, the device should generally have a small dimensioning to increase the resistance and consequently the air stream velocity within the device to ensure proper drug detachment.

5 Overall Conclusion and Future Perspectives

The present work highlights the importance of carrier surface properties on interparticle interactions in DPI formulations. It is shown that these interactions play a key role for a successful pulmonary drug delivery and also determine the effective drug load and thus, have to be taken into consideration. Moreover, the choice of inhaler, or more precisely, its conception is critical as air flow velocity within the device and also dispersion principle govern the aerodynamic performance.

The first part of this thesis clearly revealed that spray drying was a suitable technique to produce drug powders with the desired material properties (PSD, shape). Here, process parameters have to be chosen thoughtfully to control particle size and also maintain an efficient process. This was material dependent, thus this evaluation needs to be done for each API. Nonetheless, the study shows that it is possible to set particle properties for a wide range of materials.

To systematically investigate the impact of carrier surface characteristics on interparticle interactions, GBs were utilised as a model carrier system. The chemical properties of the carrier significantly influenced the FPF of the hydrophobic model drug (BUD), while this effect became less prominent for the more hydrophilic model APIs (FF, TB). It also became evident that the FPD needs to be considered as well when evaluating the aerodynamic performance. This was because carrier surface modification did not only affect the FPF but also impacted the effective drug loading (TSC). As already suggested, the control of adhesive forces, e.g. by lowering of van-der-Waals forces, is of great importance in that context. Even though major adhesion potentially increases blend homogeneity and drug load, it reduces the probability for drug detachment and ultimately drug delivery efficiency. It can be derived from the present investigation that surface chemistry of the carrier is especially important for formulations with more hydrophobic drugs like corticosteroids. Here, it determines not only the effective drug load, but also the overall aerodynamic performance.

The alteration of surface topography proved to determine the aerodynamic performance as well. Although the introduction of nano-scale roughness showed to negatively influence the TSC, it increased the overall aerodynamic performance of

the API (FPF and FPD). This was regardless of chemical nature of the drug. Decreased AFs between carrier and API were measured by AFM and could be identified as the major cause for this. Indentations on micro scale, however, should be avoided for an optimal drug delivery since they can shelter API particles from drag and lift forces during inhalation. This is particularly important when using inhalation devices which rely on those forces for drug detachment and deagglomeration, e.g. the Cyclohaler. Indentations can shelter API particles from those forces during inhalation. Inertial impaction, however, affects all particles the same way, regardless of their position leading to a negligible effect of larger carrier discontinuities for devices such as the Novolizer. These findings especially apply to round-shaped drug particles. When using drugs of angular or needle-like shape its orientation on the carrier becomes of importance as well. This might induce other interactions, e.g. mechanical interlocking.

The third part demonstrated the importance of the device conception on drug delivery. A systematic investigation on the influence of the dimensioning of essential inhaler parts in comparison with an earlier study clearly demonstrated the interplay between formulation and device. While an overall small dimensioning was widely favourable for GBs, large-dimensioned inhaler parts showed improved aerodynamic performance for blends containing lactose. Predicting the performance of a specifically designed device is very difficult since this will be also highly dependent on material properties of the carrier and also the dispersion behaviour of the API. Therefore, a general formula for the “perfect” device cannot be provided but rather has to be always seen in combination with the respective formulation. Nevertheless, the present study drew important conclusions from the comparison of two carriers with extensively different properties and might therefore contribute to the design of future inhalation devices.

Future research should focus on implementing introduced surface modifications to a conventional carrier and compare obtained results to the present findings. Initially, this would comprise the establishment of suitable modification techniques.

6 Summary

The design of formulations intended for inhalation is a major challenge since many different factors need consideration in order to guarantee major drug delivery. This becomes especially important in dry powder inhalation. Balanced interparticle interactions between carrier and API are key factors for an optimal aerodynamic performance. In addition, the inhalation device is also of great importance. Its conception and dimensioning determine flow of the airstream within the device and dispersion principle.

Therefore, the focus in the present thesis is put on the investigation of factors, which influence interparticle interactions. This should enable a deeper understanding of them and their impact on the behaviour of the powder blend. Ultimately, findings shall facilitate the development of new dry powder inhaler formulations and the choice of the suitable device for an optimal drug delivery. For this, glass beads (GBs) were chosen as a model carrier system to selectively alter their surface.

Initially, drug powders were manufactured via spray drying. To cover a wide range of active pharmaceutical ingredients (APIs), hydrophobic budesonide (BUD), formoterol fumarate (FF) and hydrophilic tiotropium bromide (TB) were selected. The influence of process parameters on material properties was examined within experimental designs. By that, it was possible to produce particles in the desired size range of 1 to 5 μm and also optimise the spray drying process in terms of resulting product yield.

In order to investigate the impact of chemical surface properties of the carrier, these were altered by a targeted silanisation of the GB surface with different agents. This led to an enhanced hydrophobicity displayed by an increase in contact angle from 24.0 ° to 86.1 °. This modification also influenced the dispersive part of the surface energy (28.0 – 61.4 mJ/m^2) as shown by inverse gas chromatography measurements. A positive correlation between hydrophobicity and effective drug loading was shown for the hydrophobic BUD. Impaction analysis using the Next Generation Pharmaceutical Impactor, however, showed that the fine particle fraction (FPF) was reduced from 19.5 % to 11.2 %. This was due to increased AFs between carrier and API. This highlights the necessity to control these adhesive forces by, inter alia, alter-

ation of carrier surface chemistry. Moreover, a dependency on the dispersive surface energy was found. Further experiments demonstrated that the correlation of drug loading and FPF to carrier surface chemistry was less pronounced or even insignificant with increased hydrophilicity of the API.

Furthermore, the influence of carrier surface roughness was investigated for BUD and FF. The incubation with hydrofluoric acid and/or ball milling with tungsten carbide successfully altered topographical parameters, i.e. introduced roughness on micro- and/or nano-scale to the GB surface. This was examined via scanning electron and atomic force microscopy. The modifications proved to influence the effective drug loading. Moreover, they had a major impact on the aerodynamic performance as micron-sized indentations drastically reduced the FPF. This could be linked to their ability to shelter drug particles from the airstream during inhalation. Nano-scale roughness on the other hand led to a significant increase of the FPF up to 28.2 % (FF). These trends were also existent when using BUD. This clearly demonstrated the general validity of these findings regardless of chemical properties of the API.

The importance of a capsule-based inhalation device was examined as well. Here, an experimental design was applied to identify important inhaler parts and the impact of their dimensioning. The air-ducting parts as well as the grid (separating capsule chamber and mouthpiece) significantly altered the FPF of the investigated drugs BUD and ipratropium bromide between 14.3 % to 31.4 % and 14.7 % to 35.2 %, respectively. It was concluded that in case of GBs, an overall small dimensioning of the device leading to a high velocity of air is favourable for an optimal drug delivery. In addition, API properties such as crystallinity, shape and size also had a significant effect on aerodynamic performance since they triggered varying cohesive and adhesive forces as well as a different contact area.

This thesis presents the systematic investigation on the effect of carrier surface properties on the aerodynamic performance and therefore contributes substantially to a deeper comprehension of interparticle interactions between carrier and API. Additionally, the importance of the inhalation device, or more precisely its dimensioning, could be demonstrated. Present findings also showed that the efficient drug delivery is highly dependent on the interplay between device and formulation.

7 Summary (German)

Das Formulierungsdesign für inhalative Zubereitungen stellt eine große Herausforderung dar, da eine Reihe von Faktoren beachtet werden muss, um einen optimalen Transport des Wirkstoffes in die Lunge sicherzustellen. Allerdings kommt einer optimierten Formulierung gerade bei der Trockenpulverinhalation eine besondere Bedeutung zu. Die Balance der interpartikulären Wechselwirkungen zwischen Arzneistoff und Träger ist hier entscheidend für eine effektive Wirkstoffdeposition. Ferner spielt auch der Inhalator selbst eine besondere Rolle. Dessen Aufbau und Dimensionierung bestimmen den Luftfluss im Inneren sowie das Dispergierprinzip.

Aus diesem Grund liegt der Fokus der vorliegenden Arbeit auf der Untersuchung von Faktoren, die die interpartikulären Wechselwirkungen beeinflussen. Hierbei soll ein tieferes Verständnis dieser Faktoren und deren Einfluss auf das Verhalten der Pulvermischungen erhalten werden, um letztendlich die Entwicklung neuer Formulierungen für die Trockenpulverinhalation und die Wahl des passenden Inhalators vereinfachen. Hierfür wurden Glaskugeln (GBs) als Modellträgersystem ausgewählt und deren Oberfläche gezielt modifiziert.

Zunächst wurden geeignete Wirkstoffpulver über Sprühtrocknung hergestellt. Um ein breites Wirkungsspektrum mit unterschiedlichen chemischen Eigenschaften zu untersuchen, wurden Budesonid, Formoterolfumarat und Tiotropiumbromid ausgewählt. Im Rahmen eines experimentellen Versuchsplans wurde der Einfluss der Prozessparameter der Sprühtrocknung auf Materialeigenschaften des Produkts untersucht. So konnten hierbei Partikel mit der erwünschten Größe von 1 bis 5 μm hergestellt werden. Außerdem konnte die Prozessausbeute optimiert werden.

Um den Effekt der chemischen Oberflächeneigenschaften des Trägers zu untersuchen, wurde eine unterschiedliche Beschaffenheit der Oberfläche durch eine gezielte Silanisierung mit unterschiedlichen Agenzien herbeigeführt. Dies verringerte die Hydrophilie, was durch einen Anstieg des gemessenen Kontaktwinkels von 24.0 ° auf bis zu 86.1 ° bestätigt wurde. Untersuchungen mittels inverser Gaschromatographie zeigten, dass gleichzeitig auch die dispersive Oberflächenenergie verändert wurde (28,0 – 61,4 mJ/m^2). Für das hydrophobe Budesonid konnte eine positive Korrelation der Hydrophobizität zur effektiven Oberflächenbeladung des Trägers gezeigt

werden. Impaktionsversuche mit dem Next Generation Pharmaceutical Impactor zeigten allerdings, dass die inhalierbare Fraktion (FPF) durch diesen Prozess von 19,5 % auf 11,2 % gesenkt wurde. Es konnte mithilfe der Rasterkraftmikroskopie gezeigt werden, dass dies das Resultat steigender Adhäsionskräfte zwischen Träger und Wirkstoff war. Dies verdeutlicht, welche große Bedeutung diesen adhäsiven Kräften zukommt, und dass sie, zum Beispiel über eine Modifizierung der Oberflächenchemie des Trägers, verändert werden sollten um eine optimale Wirkstoffdeposition zu erhalten. Im weiteren Verlauf zeigte sich aber eine abnehmende Signifikanz dieser Korrelationen mit steigender Hydrophilie des Wirkstoffes.

Des Weiteren wurde der Effekt einer veränderten Oberflächenrauheit für zwei unterschiedliche Wirkstoffe (Budesonid, Formoterol) genau untersucht. Die hierfür eingesetzten Techniken (Inkubation mit Flusssäure, Mahlung mit Wolframcarbid) führten zu einer erfolgreichen Einführung von Mikro- und/oder Nanorauheit auf der Oberfläche. Dies wurde mithilfe der Rasterelektronen- und Rasterkraftmikroskopie verdeutlicht. Diese Modifikationen hatten einen signifikanten Einfluss auf die Wirkstoffbeladung des Trägers. Darüber hinaus reduzierten die Mikrorauheiten die inhalierbare Fraktion deutlich, was deren Fähigkeit, die Wirkstoffpartikel vor dem Luftstrom zu schützen, zugeschrieben werden konnte. Nanorauheit führte hingegen zu einer deutlichen Steigerung der FPF bis zu 28.2 % (für Formoterol). Diese Trends konnten auch für Budesonid gezeigt werden, was deren Allgemeingültigkeit unabhängig von den chemischen Eigenschaften des Wirkstoffes deutlich macht.

Im weiteren Verlauf dieser Arbeit wurde auch die Bedeutung des Inhalators (kapselbasiert) untersucht. Im Rahmen eines experimentellen Versuchsplans wurde hier der Einfluss der Dimensionierung verschiedener Bauteile geprüft und direkt mit früheren Untersuchungen verglichen, in denen Laktose als Träger verwendet wurde. Die luftführenden Bauteile sowie der Gittereinsatz, der die Deagglomerationskammer vom Mundstück trennt, zeigten deutliche Effekte auf die FPF der untersuchten Wirkstoffe Budesonid und Ipratropiumbromid, die von 14,3 % bis 31,4 % bzw. 14,7 % bis 35,2 % reichte. Dabei wurde deutlich, dass im Falle der GBs eine kleine Dimensionierung aller untersuchten Bauteile vorteilhaft für eine optimale Deposition des Wirkstoffs in der Lunge ist. Dies wurde einer erhöhten Geschwindigkeit des Luftstroms im Inhalator zugeschrieben. Des Weiteren zeigten Untersuchungen bezüglich der Materialeigenschaften (Kristallinität, Partikelform und -größe), dass auch diese einen deutlichen

Einfluss auf das aerodynamische Verhalten der Mischung zeigten. Dies wurde durch ein unterschiedliches Maß an Kohäsions- und Adhäsionskräften und durch unterschiedlich große Kontaktflächen bedingt.

Die vorliegende Arbeit trägt mit der systematischen Untersuchung der Effekte unterschiedlicher Eigenschaften der Trägeroberfläche auf das aerodynamische Verhalten der Mischung wesentlich zu einem tiefgreifenden Verständnis der interpartikulären Wechselwirkungen zwischen Arzneistoff und Träger bei. Des Weiteren konnte die Bedeutung des Inhalators bzw. dessen Dimensionierung für eine optimale Wirkstoffdeposition in der Lunge verdeutlicht werden. Hierbei zeigte sich aber auch, dass die Effektivität, mit der der Wirkstoff in die Lunge gebracht wird, deutlich von einem Zusammenspiel von Inhalator und Formulierung abhängt.

8 Appendix

8.1 HPLC Methods

8.1.1 Budesonide

Mobile phase:	25 % ddH ₂ O 75 % Methanol
Column:	LiChroCART [®] 125-4, LiChrospher [®] 100 RP-18 (5 µm) with precolumn
Flow rate:	1.0 mL/min
Wavelength:	248 nm
Injection volume:	100 µL
Oven temperature	25°C

Samples were dissolved in ddH₂O:methanol 25 %:75 % (V/V)

8.1.2 Formoterol Fumarate

Mobile phase:	45 % buffering system (2.34 g/L sodium octansulfonate and 1.38 g/L NaH ₂ PO ₄ •H ₂ O, pH adjusted to 3.2 with ortho-phosphoric acid 85 %) 40 % methanol 15 % acetonitrile
Column:	LiChroCART 125-4, LiChrospher RP select B (5 µm) with precolumn

Flow rate: 1.2 mL/min

Wavelength: 214 nm

Injection volume: 100 μ L

Oven temperature 25°C

Samples were dissolved in $\text{d}_d\text{H}_2\text{O}$:methanol:acetonitrile 45 %:40 %:15 % (V/V)

8.1.3 Ipratropium Bromide

Mobile phase: 71 % buffering system (1.42 g/L sodium heptanesulfonate, pH adjusted to 3.3 with ortho-phosphoric acid 85 %)
29 % acetonitrile

Column: LiChroCART[®] 125-4, LiChrospher[®] 100 CN (5 μ m) with precolumn

Flow rate: 1.2 mL/min

Wavelength: 220 nm

Injection volume: 100 μ L

Oven temperature 25°C

Samples were dissolved in $\text{d}_d\text{H}_2\text{O}$

8.1.4 Tiotropium Bromide

Mobile phase: 71 % buffering system (1.42 g/L sodium heptane-sulfonate, pH adjusted to 3.2 with ortho-phosphoric acid 85 %)
29 % acetonitrile

Column: LiChroCART[®] 125-4, LiChrospher[®] 100 CN (5 µm) with precolumn

Flow rate: 1.2 mL/min

Wavelength: 239 nm

Injection volume: 100 µL

Oven temperature 25°C

Samples were dissolved in d_4H_2O

8.2 Materials

Acetone	Sigma-Aldrich, Inc., St. Louis, USA
Acetonitrile	Sigma-Aldrich, Inc., St. Louis, USA
Brij [®] 35	Carl Roth GmbH & Co. KG, Karlsruhe, Germany
Budesonide	Minakem SAS, Dunkerque, France
Decane	Sigma Aldrich
d_dH_2O	freshly produced with Finn Aqua 75, San-Asalo-Sohlberg Corp., Helsinki, Finland
Ethanol	Merck KGaA, Darmstadt, Germany
Formoterol fumarate	Vamsi Labs Ltd., Maharashtra, India
Glass beads (SiLibeads [®])	Sigmund Lindner GmbH, Warmensteinbach, Germany
Glycerol	Merck KGaA, Darmstadt, Germany
Helium 5.0	Linde AG, Munich, Germany
Heptan	Merck KGaA, Darmstadt, Germany
Hexane	Sigma-Aldrich, Inc., St. Louis, USA
Hydrofluoric acid 38 %	Merck KGaA, Darmstadt, Germany
Hydrogen 5.0	Linde AG, Munich, Germany
Ipratropium bromide	Boehringer Ingelheim Pharma AG & Co. KG
Methanol	Merck KGaA, Darmstadt, Germany
Methylene chloride	AppliChem GmbH, Gatersleben, Germany
Nitrogen 5.0	Linde AG, Munich, Germany
Nonane	Sigma-Aldrich, Inc., St. Louis, USA

Octane	Sigma-Aldrich, Inc., St. Louis, USA
o-Phosphoric acid	Merck KGaA, Darmstadt, Germany
Sodium heptansulphonate	Carl Roth GmbH & Co. KG, Karlsruhe, Germany
Sodium octansulphonate	Arcos Organics, Geel, Belgium
Tiotropium bromide	Hangzhou Hyper Chemicals Ltd., Zhejiang, China
Tungsten carbide	Wolfram Bergbau und Huetten AG, St. Martin i.S., Austria

8.3 Abbreviations

AFM	Atomic force microscopy
API	Active pharmaceutical ingredient
APSD	Aerodynamic particle size distribution
BFE	Basic flowability energy
BUD	Budesonide
CAB	Cohesive-adhesive balance
CDPMS	Chloro(methyl)diphenylsilane
COPD	Chronic obstructive pulmonary disease
CSR	Cross sectional area
DD	Delivered dose
DR	Device retention
ddH ₂ O	Double distilled H ₂ O
DGF	Drying gas flow
DoE	Design of experiments
DPI	Dry powder inhaler
DR	Device retention
DVS	Dynamic vapour sorption
ED	Emitted dose
FC	Feed concentration
FF	Formoterol fumarate
FPD	Fine particle dose
FPF	Fine particle fraction

FPTS	Trimethoxy(3,3,3-trifluoropropyl)silane
FR	Feed rate, %
GB	Glass bead
HF	Hydrofluoric acid
HPLC	High performance liquid chromatography
IB	Ipratropium bromide
ICS	Inhaled corticosteroids
iGC	Inverse gas chromatography
LAMA	Long-acting muscarinic antagonist
micro	Micronised
MMAD	Mass median aerodynamic diameter
NGI	Next Generation Pharmaceutical Impactor
pMDI	Pressurised metered-dose inhaler
PSD	Particle size distribution
RD	Recovered dose
rH	Relative humidity
rpm	Rounds per minute
R_{rms}	Root mean square of surface roughness
rStD	Relative standard deviation
SD	Spray drying
sd	spray-dried
SDR	Specific device resistance
SEM	Scanning electron microscopy

SGF	Spray gas flow, L/h
StD	Standard deviation
TB	Tiotropium bromide
TC	Tungsten carbide
T_{inlet}	Inlet temperature °C
TPCS	Chlorotiphenylsilane
WFA	Wall friction angle
XRPD	X-ray powder diffraction

8.4 Formula Symbols

c_x	Coefficient
γ_s^d	Dispersive surface energy, mJ/m ²
d	Diameter
D	Diffusion coefficient
f_n	Factor level
g	Gravitational acceleration, m/s ²
η	Viscosity, Pa*s
k	Boltzmann's constant, J/K
m	Mass, kg
n/n_m	Surface occupancy
p_a	Air density, kg/m ³
P_{EQPC}	Perimeter of the equivalent circle, m
P_{real}	Real perimeter, m
p_p	Particle density, kg/m ³
p_0	H ₂ O density, kg/m ³
Q	Air flow, m/s
Q^2	Indicator for future prediction precision
$Q3$	Cummulative volume-based distribution, %
$q3^*$	Probability density function
R^2	Indicator for model significance
SA	Surface area, m ²

Sph	Sphericity
Stk	Stokes' number
V	Velocity, m/s
V_{ts}	Terminal settling velocity, m/s
X	Shape factor
x_{10}	10 % quantile of the PSD
x_{50}	Median of the PSD
x_{90}	90 % quantile of the PSD
y	Response to the respective factors

8.5 Overview of Experimental Designs

8.5.1 Spray Drying of Budesonide (section 4.1.1)

Exp. No.	Run Order	Inlet Temperature, °C	Feed rate, %	Feed concentration, %
1	15	80	6	4
2	5	120	6	4
3	13	80	10	4
4	9	120	10	4
5	10	80	6	10
6	14	120	6	10
7	3	80	10	10
8	6	120	10	10
9	16	80	8	7
10	18	120	8	7
11	4	100	6	7
12	19	100	10	7
13	1	100	8	4
14	17	100	8	10
15	12	100	8	7
16	11	100	8	7
17	7	100	8	7
18	2	100	8	7
19	8	100	8	7

8.5.2 Spray Drying of Formoterol Fumarate (section 4.1.2)

Exp. No.	Run Order	Feed rate, %	Spray gas flow, L/h	Feed concentration, %
1	18	4	334	2.5
2	11	8	334	2.5
3	17	4	334	7.5
4	2	8	334	7.5
5	6	4	426	2.5
6	9	8	426	2.5
7	7	4	426	7.5
8	13	8	426	7.5
9	15	4	380	5
10	19	8	380	5
11	3	6	380	2.5
12	8	6	380	7.5
13	16	6	334	5
14	10	6	426	5
15	4	6	380	5
16	1	6	380	5
17	12	6	380	5
18	5	6	380	5
19	14	6	380	5

8.5.3 Spray Drying of Tiotropium Bromide (section 4.1.3)

Exp. No.	Run Order	Inlet temperature, °C	Spray gas flow, L/h	Feed concentration, %
1	9	120	380	2
2	14	120	380	4
3	11	120	496	2
4	7	120	496	4
5	15	150	380	2
6	16	150	380	4
7	19	150	496	2
8	8	150	496	4
9	12	135	438	2
10	10	135	438	4
11	2	135	380	3
12	6	135	496	3
13	4	120	438	3
14	3	150	438	3
15	1	135	438	3
16	17	135	438	3
17	18	135	438	3
18	5	135	438	3
19	13	135	438	3

8.5.4 The Importance of Inhaler Geometry (section 4.4.1)

Exp. No.	Run Order	Mouthpiece, Cross sectional area, mm ²	Grid, Free grid area, mm	Deagglomeration chamber, Height, mm
1	19	7.06	20.71	7
2	2	35.54	20.71	7
3	16	7.06	50.80	7
4	3	35.54	50.80	7
5	5	7.06	20.71	9
6	6	35.54	20.71	9
7	7	7.06	50.80	9
8	11	35.54	50.80	9
9	9	7.06	35.76	8
10	10	35.54	35.76	8
11	4	21.30	20.71	8
12	15	21.30	50.80	8
13	8	21.30	35.76	7
14	13	21.30	35.76	9
15	14	21.30	35.76	8
16	12	21.30	35.76	8
17	1	21.30	35.76	8
18	18	21.30	35.76	8
19	17	21.30	35.76	8

9 References

- [1] J.L. Rau, The Inhalation of Drugs: Advantages and Problems, *Respiratory Care* 50 (2005) 367–382.
- [2] D.-D. Pham, E. Fattal, N. Tsapis, Pulmonary drug delivery systems for tuberculosis treatment, *International Journal of Pharmaceutics* 478 (2015) 517–529.
- [3] S. Onoue, S. Yamada, Pirfenidone in respirable powder form for the treatment of pulmonary fibrosis: a safer alternative to the current oral delivery system?, *Therapeutic delivery* 4 (2013) 887–889.
- [4] G. Thiringer, N. Svedmyr, Comparison of infused and inhaled terbutaline in patients with asthma, *Scand J Respir Dis.* 57 (1976) 17–24.
- [5] Q.T. Zhou, S.S.Y. Leung, P. Tang, T. Parumasivam, Z.H. Loh, H.-K. Chan, Inhaled formulations and pulmonary drug delivery systems for respiratory infections, *Advanced drug delivery reviews* 85 (2015) 83–99.
- [6] P.C. Lip Kwok, H.-K. Chan, Pulmonary Delivery of Peptides and Proteins, in: C. van der Walle (Ed.), *Peptide and Protein Delivery*, Elsevier Science, San Diego, CA, USA, 2011, pp. 23–46.
- [7] L. Garcia-Contreras, H.D.C. Smyth, Liquid-Spray or Dry-Powder Systems for Inhaled Delivery of Peptide and Proteins?, *American Journal of Drug Delivery* 3 (2005) 29–45.
- [8] D.A. Wall, Pulmonary Absorption of Peptides and Proteins, *Drug Delivery* 2 (2008) 1–20.
- [9] P.C.L. Kwok, H.-K. Chan, Pulmonary drug delivery, *Therapeutic delivery* 4 (2013) 877–878.
- [10] H. Chrystyn, Is total particle dose more important than particle distribution?, *Respiratory Medicine* 91 (1997) 17–19.
- [11] I. Ashurt, A. Malton, D. Prime, B. Sumbly, Latest advances in the development of dry powder inhalers, *Pharm Sci Technol Today* 3 (2000) 246–256.
- [12] Y. Kawashima, M. Imai, H. Takeuchi, H. Yamamoto, K. Kamiya, T. Hino, Improved flowability and compactibility of spherically agglomerated crystals of ascorbic acid for direct tableting designed by spherical crystallization process, *Powder Technology* 130 (2003) 283–289.

- [13] F. Podczeck, The relationship between physical properties of lactose monohydrate and the aerodynamic behaviour of adhered drug particles, *International Journal of Pharmaceutics* 160 (1998) 119–130.
- [14] J. Shur, B. Saluja, S. Lee, J. Tibbatts, R. Price, Effect of Device Design and Formulation on the In Vitro Comparability for Multi-Unit Dose Dry Powder Inhalers, *The AAPS journal* 17 (2015) 1105–1116.
- [15] A. Patwa, A. Shah, Anatomy and physiology of respiratory system relevant to anaesthesia, *Indian journal of anaesthesia* 59 (2015) 533–541.
- [16] E.R. Weibel, Geometry and dimensions of airways of conductive and transitory zones. In: *Morphometry of the Human Lung*, in: *Morphometry of the Human Lung* Berlin, Heidelberg: Springer; 1963., pp. 110–135.
- [17] G. Thews, P. Vaupel, E. Mutschler (Eds.), *Anatomie, Physiologie und Pathophysiologie des Menschen*. 5., völlig neu bearb. und erw. Aufl. Stuttgart: Wissenschaftl. Verlagsges, 1999.
- [18] K. Aktories, U. Förstermann, F. Hofmann, K. Starke, *Allgemeine und spezielle Pharmakologie und Toxikologie: Begründet von W. Forth, D. Henschler, W. Rummel; gebundene Ausgabe*, Elsevier Science, 2009.
- [19] W.F. Tonnis, G.F. Kersten, H.W. Frijlink, W.L.J. Hinrichs, A.H. de Boer, J.-P. Amorij, Pulmonary vaccine delivery: A realistic approach?, *Journal of aerosol medicine and pulmonary drug delivery* 25 (2012) 249–260.
- [20] D. Edwards, J. Hanes, G. Caponetti, J. Hrkach, A. Ben-Jebria, Eskew, M.: Mintzes, J., D. Deaver, N. Lotan, R. Langer, Large Porous Particles for Pulmonary Drug Delivery, *Science* (1997) 1868–1872.
- [21] M.S. Hassan, R.W.M. Lau, Effect of particle shape on dry particle inhalation: Study of flowability, aerosolization, and deposition properties, *AAPS PharmSciTech* 10 (2009) 1252–1262.
- [22] T.C. Carvalho, J.I. Peters, R.O. Williams, Influence of particle size on regional lung deposition--what evidence is there?, *International Journal of Pharmaceutics* 406 (2011) 1–10.
- [23] T. Peng, S. Lin, B. Niu, X. Wang, Y. Huang, X. Zhang, G. Li, X. Pan, C. Wu, Influence of physical properties of carrier on the performance of dry powder inhalers, *Acta pharmaceutica Sinica. B* 6 (2016) 308–318.

-
- [24] S.L. Lee, W.P. Adams, B.V. Li, D.P. Conner, B.A. Chowdhury, L.X. Yu, In vitro considerations to support bioequivalence of locally acting drugs in dry powder inhalers for lung diseases, *The AAPS journal* 11 (2009) 414–423.
- [25] S. Newman, G. Woodman, S.W. Clarke, Deposition of carbenicillin aerosols in cystic fibrosis: effects of nebuliser system and breathing pattern, *Thorax* 43 (188) 318–322.
- [26] W. Kamin, F. Erdnüss, I. Krämer, Inhalation solutions--which ones may be mixed? Physico-chemical compatibility of drug solutions in nebulizers--update 2013, *Journal of cystic fibrosis official journal of the European Cystic Fibrosis Society* 13 (2014) 243–250.
- [27] H. Steckel, F. Eskandar, Factors affecting aerosol performance during nebulization with jet and ultrasonic nebulizers, *European Journal of Pharmaceutical Sciences* 19 (2003) 443–455.
- [28] S.W. Stein, C.G. Thiel, The History of Therapeutic Aerosols: A Chronological Review, *Journal of aerosol medicine and pulmonary drug delivery* 30 (2017) 20–41.
- [29] D. Traini, P. Rogueda, P. Young, R. Price, Surface energy and interparticle forces correlations in model pMDI formulations, *Pharmaceutical research* 22 (2005) 816–825.
- [30] B. Khassawneh, M. Al-Ali, K. Alzoubi, M. Batarseh, S. Al-Safi, A. Sharara, M. Alnasr, Handling of inhaler device in actual pulmonary practise: metered-dose inhaler versus dry powder inhaler, *Respiratory Care* 53 (2008) 324–328.
- [31] B. Kilgore, K. Al Katranji, M. Woodall, M. Shepherd, S.L. Flesher, Improving Resident Knowledge of Spacers, *Clinical pediatrics* 55 (2016) 1050–1053.
- [32] A. Berlinski, B. Cooper, Oronasal and Tracheostomy Delivery of Soft Mist and Pressurized Metered-Dose Inhalers With Valved Holding Chamber, *Respiratory Care* 61 (2016) 913–919.
- [33] W. Kamin, M. Frank, S. Kattenbeck, P. Moroni-Zentgraf, H. Wachtel, S. Zielen, A Handling Study to Assess Use of the Respimat(®) Soft Mist™ Inhaler in Children Under 5 Years Old, *Journal of aerosol medicine and pulmonary drug delivery* 28 (2015) 372–381.
- [34] A. Elajnaf, P. Carter, G. Rowley, The effect of relative humidity on electrostatic charge decay of drugs and excipient used in dry powder inhaler formulation, *Drug Development and Industrial Pharmacy* 33 (2007) 967–974.
-

- [35] L. Li, S. Sun, T. Parumasivam, J.A. Denman, T. Gengenbach, P. Tang, S. Mao, H.-K. Chan, L-Leucine as an excipient against moisture on in vitro aerosolization performances of highly hygroscopic spray-dried powders, *European Journal of Pharmaceutics and Biopharmaceutics* 102 (2016) 132–141.
- [36] S. Onoue, N. Hashimoto, S. Yamada, Dry powder inhalation systems for pulmonary delivery of therapeutic peptides and proteins, *Expert Opinion on Therapeutic Patents* 18 (2008) 429–442.
- [37] S.A. Meenach, Y.J. Kim, K.J. Kauffman, N. Kanthamneni, E.M. Bachelder, K.M. Ainslie, Synthesis, optimization, and characterization of camptothecin-loaded acetalated dextran porous microparticles for pulmonary delivery, *Molecular pharmaceutics* 9 (2012) 290–298.
- [38] S. Alipour, H. Montaseri, M. Tafaghodi, Inhalable, large porous PLGA microparticles loaded with paclitaxel: Preparation, in vitro and in vivo characterization, *Journal of microencapsulation* 32 (2015) 661–668.
- [39] T. Nakate, H. Yoshida, A. Ohike, Y. Tokunaga, R. Ibuki, Y. Kawashima, Formulation development of inhalation powders for FK888 using the E-haler to improve the inhalation performance at a high dose, and its absorption in healthy volunteers, *European Journal of Pharmaceutics and Biopharmaceutics* 59 (2005) 25–33.
- [40] S. Hiendrawan, B. Verianyah, Tjandrawinata, R., A bottom-up process approach for micronization of Ibuprofen, *Journal of Chemical and Pharmaceutical Research* 7 (2015) 708–715.
- [41] H. Steckel, L. Pichert, B.W. Müller, Influence of process parameters in the ASES process on particle properties of budesonide for pulmonary delivery, *European Journal of Pharmaceutics and Biopharmaceutics* 57 (2004) 507–512.
- [42] V. Joshi, S. Dwivedi, G. Ward, Increase in the Specific Surface Area of Budesonide During Storage Postmicronization, *Pharmaceutical research* 19 (2002) 7–12.
- [43] R. Westmeier, H. Steckel, Combination particles containing salmeterol xinafoate and fluticasone propionate: Formulation and aerodynamic assessment, *Journal of pharmaceutical sciences* 97 (2008) 2299–2310.
- [44] H. Steckel, J. Thies, B.W. Mueller, Micronizing of steroids for pulmonary delivery by supercritical carbon dioxide, *International Journal of Pharmaceutics* 152 (1997) 99–110.

-
- [45] J.G. Weers, D.P. Miller, Formulation Design of Dry Powders for Inhalation, *Journal of pharmaceutical sciences* 104 (2015) 3259–3288.
- [46] L. Tajber, D.O. Corrigan, O.I. Corrigan, A.M. Healy, Spray drying of budesonide, formoterol fumarate and their composites--I. Physicochemical characterisation, *International Journal of Pharmaceutics* 367 (2009) 79–85.
- [47] C. Parlati, P. Colombo, F. Buttini, P.M. Young, H. Adi, A.J. Ammit, D. Traini, Pulmonary spray dried powders of tobramycin containing sodium stearate to improve aerosolization efficiency, *Pharmaceutical research* 26 (2009) 1084–1092.
- [48] H. Steckel, H.G. Brandes, A novel spray-drying technique to produce low density particles for pulmonary delivery, *International Journal of Pharmaceutics* 278 (2004) 187–195.
- [49] A.H.L. Chow, H.H.Y. Tong, P. Chattopadhyay, B.Y. Shekunov, Particle engineering for pulmonary drug delivery, *Pharmaceutical research* 24 (2007) 411–437.
- [50] Y.-F. Maa, P.-A. Nguyen, T. Sweeney, S. Shire, C. Hsu, Protein Inhalation Powders: Spray Drying vs Spray Freeze Drying, *Pharmaceutical research* 16 (1999) 249–254.
- [51] H. Larhrib, X.M. Zeng, G.P. Martin, C. Marriott, J. Pritchard, The use of different grades of lactose as a carrier for aerosolised salbutamol sulphate, *International Journal of Pharmaceutics* 191 (1999) 1–14.
- [52] H. Steckel, N. Bolzen, Alternative sugars as potential carriers for dry powder inhalations, *International Journal of Pharmaceutics* 270 (2004) 297–306.
- [53] S. Li, T.W. Patapoff, D. Overcashier, C. Hsu, T.H. Nguyen, R.T. Borchardt, Effects of reducing sugars on the chemical stability of human relaxin in the lyophilized state, *Journal of pharmaceutical sciences* 85 (1996) 873–877.
- [54] G. Saint-Lorant, P. Leterme, A. Gayot, M.P. Flament, Influence of carrier on the performance of dry powder inhalers, *International Journal of Pharmaceutics* 334 (2007) 85–91.
- [55] S. Tee, C. Marriott, X. Zeng, G. Martin, The use of different sugars as fine and coarse carriers for aerosolised salbutamol sulphate, *International Journal of Pharmaceutics* 208 (2000) 111–123.
- [56] S.J. Nolan, J. Thornton, C.S. Murray, T. Dwyer, Inhaled Mannitol (Bronchitol) for Cystic Fibrosis, *Paediatric respiratory reviews* 18 (2016) 52–54.
- [57] E.M. Littringer, A. Mescher, H. Schroettner, L. Achelis, P. Walzel, N.A. Urbanetz, Spray dried mannitol carrier particles with tailored surface properties--the influ-
-

- ence of carrier surface roughness and shape, *European Journal of Pharmaceutics and Biopharmaceutics* 82 (2012) 194–204.
- [58] P. Harjunen, T. Lankinen, H. Salonen, V. Lehto, K. Järvinen, Effects of carriers and storage of formulation on the lung deposition of a hydrophobic and hydrophilic drug from a DPI, *International Journal of Pharmaceutics* 263 (2003) 151–163.
- [59] J. Ooi, D. Traini, S. Hoe, W. Wong, P.M. Young, Does carrier size matter? A fundamental study of drug aerosolisation from carrier based dry powder inhalation systems, *International Journal of Pharmaceutics* 413 (2011) 1–9.
- [60] W. Kaiyaly, On the effects of blending, physicochemical properties, and their interactions on the performance of carrier-based dry powders for inhalation - A review, *Advances in colloid and interface science* 235 (2016) 70–89.
- [61] M.M.d. Villiers, Description of the kinetics of the deagglomeration of drug particle agglomerates during powder mixing, *International Journal of Pharmaceutics* 151 (1997) 1–6.
- [62] K. Thalberg, E. Berg, M. Fransson, Modeling dispersion of dry powders for inhalation. The concepts of total fines, cohesive energy and interaction parameters, *International Journal of Pharmaceutics* 427 (2012) 224–233.
- [63] S. Mangal, F. Meiser, G. Tan, T. Gengenbach, D.A.V. Morton, I. Larson, Applying surface energy derived cohesive-adhesive balance model in predicting the mixing, flow and compaction behaviour of interactive mixtures, *European Journal of Pharmaceutics and Biopharmaceutics* 104 (2016) 110–116.
- [64] V.N.P. Le, T.H. Hoang Thi, E. Robins, M.P. Flament, Dry powder inhalers: study of the parameters influencing adhesion and dispersion of fluticasone propionate, *AAPS PharmSciTech* 13 (2012) 477–484.
- [65] P. Begat, D.A.V. Morton, J. Staniforth, R. Price, The Cohesive-Adhesive Balances in Dry Powder Inhaler Formulations II: Influence on Fine Particle Delivery Characteristics, *Pharmaceutical research* 21 (2004) 1826–1833.
- [66] M.D. Jones, H. Harris, J.C. Hooton, J. Shur, G.S. King, C.A. Mathoulin, K. Nichol, T.L. Smith, M.L. Dawson, A.R. Ferrie, R. Price, An investigation into the relationship between carrier-based dry powder inhalation performance and formulation cohesive-adhesive force balances, *European Journal of Pharmaceutics and Biopharmaceutics* 69 (2008) 496–507.

-
- [67] P. Begat, R. Price, H. Harris, D.A. Morton, J.N. Staniforth, The Influence of Force Control Agents on the Cohesive-Adhesive Balance in Dry Powder Inhaler Formulations, *KONA* 23 (2005) 109–121.
- [68] M.J. Telko, A.J. Hickey, Dry Powder Inhaler Formulation, *Respiratory Care* 50 (2005) 1209–1227.
- [69] P.M. Young, R. Price, M.J. Tobyn, M. Buttrum, F. Dey, The influence of relative humidity on the cohesion properties of micronized drugs used in inhalation therapy, *Journal of pharmaceutical sciences* 93 (2004) 753–761.
- [70] R. Price, P. Young, S. Edge, J. Staniforth, The influence of relative humidity on particulate interactions in carrier-based dry powder inhaler formulations, *International Journal of Pharmaceutics* 246 (2002) 47–59.
- [71] S. Das, I. Larson, P. Young, P. Stewart, Influence of storage relative humidity on the dispersion of salmeterol xinafoate powders for inhalation, *Journal of pharmaceutical sciences* 98 (2009) 1015–1027.
- [72] S. Karner, M. Maier, E. Littringer, N.A. Urbanetz, Surface roughness effects on the tribo-charging and mixing homogeneity of adhesive mixtures used in dry powder inhalers, *Powder Technology* 264 (2014) 544–549.
- [73] R. Scherließ, Aerosole Lecture Script Department of Pharmaceutics and Biopharmaceutics, Kiel University (2016).
- [74] H. Steckel, B.W. Mueller, In vitro evaluation of dry powder inhalers II: Influence of carrier particle size and concentration on in vitro deposition, *International Journal of Pharmaceutics* 154 (1997) 31–37.
- [75] W. Kaialy, A. Alhalaweh, S.P. Velaga, A. Nokhodchi, Influence of lactose carrier particle size on the aerosol performance of budesonide from a dry powder inhaler, *Powder Technology* 227 (2012) 74–85.
- [76] W. Kaialy, T. Hussain, A. Alhalaweh, A. Nokhodchi, Towards a more desirable dry powder inhaler formulation: Large spray-dried mannitol microspheres outperform small microspheres, *Pharmaceutical research* 31 (2014) 60–76.
- [77] H. Larhrib, G.P. Martin, C. Marriott, D. Prime, The influence of carrier and drug morphology on drug delivery from dry powder formulations, *International Journal of Pharmaceutics* 257 (2003) 283–296.
- [78] X.M. Zeng, G.P. Martin, C. Marriott, J. Pritchard, The influence of carrier morphology on drug delivery by dry powder inhalers, *International Journal of Pharmaceutics* 200 (2000) 93–106.
-

- [79] R.S. Dhumal, S.V. Biradar, A.R. Paradkar, P. York, Particle engineering using sonocrystallization: Salbutamol sulphate for pulmonary delivery, *International Journal of Pharmaceutics* 368 (2009) 129–137.
- [80] L.W. Chan, L.T. Lim, P.W. Heng, Immobilization of fine particles on lactose carrier by precision coating and its effect on the performance of dry powder formulations, *Journal of pharmaceutical sciences* 92 (2003) 975–984.
- [81] S. Zellnitz, H. Schroettner, N.A. Urbanetz, Influence of surface characteristics of modified glass beads as model carriers in dry powder inhalers (DPIs) on the aerosolization performance, *Drug Development and Industrial Pharmacy* 41 (2015) 1710–1717.
- [82] M.-P. Flament, P. Leterme, A. Gayot, The influence of carrier roughness on adhesion, content uniformity and the in vitro deposition of terbutaline sulphate from dry powder inhalers, *International Journal of Pharmaceutics* 275 (2004) 201–209.
- [83] D. Traini, P.M. Young, F. Thielmann, M. Acharya, The influence of lactose pseudopolymorphic form on salbutamol sulfate-lactose interactions in DPI formulations, *Drug Development and Industrial Pharmacy* 34 (2008) 992–1001.
- [84] A.H. de Boer, P. Hagedoorn, D. Gjaltema, J. Goedee, H.W. Frijlink, Air classifier technology (ACT) in dry powder inhalation Part 4. Performance of air classifier technology in the Novolizer® multi-dose dry powder inhaler, *International Journal of Pharmaceutics* 310 (2006) 72–80.
- [85] Y. Cui, S. Schmalfuß, S. Zellnitz, M. Sommerfeld, N. Urbanetz, Towards the optimisation and adaptation of dry powder inhalers, *International Journal of Pharmaceutics* 470 (2014) 120–132.
- [86] A.H. de Boer, P. Hagedoorn, D. Gjaltema, J. Goedee, H.W. Frijlink, Air classifier technology (ACT) in dry powder inhalation Part 3. Design and development of an air classifier family for the Novolizer® multi-dose dry powder inhaler, *International Journal of Pharmaceutics* 310 (2006) 70–82.
- [87] C. Friebel, Rationale Entwicklung eines Inhalationssystems, Dissertation (2010).
- [88] Drugbank, Budesonide, 2017, <https://www.drugbank.ca/drugs/DB01222>.
- [89] Drugbank, Formoterol, 2017, <https://www.drugbank.ca/drugs/DB00983>.
- [90] Drugbank, Ipratropium bromide, 2017, <https://www.drugbank.ca/drugs/DB00332>.
- [91] Drugbank, Tiotropium, 2017, <https://www.drugbank.ca/drugs/DB01409>.

-
- [92] S.R. Naikwade, A.N. Bajaj, P. Gurav, M.M. Gatne, P. Singh Soni, Development of budesonide microparticles using spray-drying technology for pulmonary administration: design, characterization, in vitro evaluation, and in vivo efficacy study, *AAPS PharmSciTech* 10 (2009) 993–1012.
- [93] L. Thorsson, O. Borga, S. Edsbäcker, Systemic availability of budesonide after nasal administration of three different formulations: pressurized aerosol, aqueous pump spray, and powder, *Br J Clin Pharmacol.* (1999) 619–624.
- [94] P.J. Barnes, *Anti-inflammatory Actions of Glucocorticoids: Molecular Mechanisms.*
- [95] R. Buhl, D. Berdel, C.-P. Criege, A. Gillissen, P. Kardos, C. Kroegel, W. Leupold, H. Lindemann, H. Magnussen, D. Nowak, D. Pfeiffer-Kascha, K. Rabe, M. Rolke, G. Schultze-Werninghaus, H. Sitter, D. Ukena, C. Vogelmeier, T. Welte, R. Wetzengel, H. Worth, *Leitlinie zur Diagnostik und Therapie von Patienten mit Asthma -- Herausgegeben von der Deutschen Atemwegsliga und der Deutschen Gesellschaft für Pneumologie und Beatmungsmedizin e. V.*, *Pneumologie (Stuttgart, Germany)* 60 (2006) 139–177.
- [96] H. Lemoine, C. Overlack, A. Köhl, H. Worth, D. Reinhardt, Formoterol, fenoterol, and salbutamol as partial agonists for relaxation of maximally contracted guinea pig tracheae: comparison of relaxation with receptor binding, *Lung* 170 (1992) 163–180.
- [97] M. Cazzola, J. Ora, A. Di Paolo, E. Puxeddu, L. Calzetta, P. Rogliani, Onset of action of budesonide/formoterol Spiromax((R)) compared with budesonide/formoterol Turbuhaler((R)) in patients with COPD, *Pulmonary pharmacology & therapeutics* 39 (2016) 48–53.
- [98] S. Ejiofor, A.M. Turner, *Pharmacotherapies for COPD*, *Clinical medicine insights. Circulatory, respiratory and pulmonary medicine* 7 (2013) 17–34.
- [99] T.R. MacGregor, R. ZuWallack, V. Rubano, M.A. Castles, H. Dewberry, M. Ghafouri, C.C. Wood, Efficiency of Ipratropium Bromide and Albuterol Deposition in the Lung Delivered via a Soft Mist Inhaler or Chlorofluorocarbon Metered-Dose Inhaler, *Clinical and translational science* 9 (2016) 105–113.
- [100] N. Zhong, H.S. Moon, K.H. Lee, A.A. Mahayiddin, W. Boonsawat, M.G.D. Isidro, C. Bai, A. Mueller, N. Metzdorf, A. Anzueto, TIOtroprium Safety and Performance In Respimat (TIOSPIR): Analysis of Asian cohort of COPD patients, *Respirology* 21 (2016) 1397–1403.
-

- [101] H.A.M. Kerstjens, B. Disse, W. Schroder-Babo, T.A. Bantje, M. Gahlemann, R. Sigmund, M. Engel, J.A. van Noord, Tiotropium improves lung function in patients with severe uncontrolled asthma: A randomized controlled trial, *The Journal of allergy and clinical immunology* 128 (2011) 308–314.
- [102] Sigmund Lindner GmbH, Product Data Sheet SiLibeads Type S (2017).
- [103] G.A.C.M. Spierings, Wet chemical etching of silicate glasses in hydrofluoric acid based solutions, *J Mater Sci* 28 (1993) 6261–6273.
- [104] M. Tao, Y. Jin, N. Gu, L. Huang, A method to control the fabrication of etched optical fiber probes with nanometric tips, *J. Opt.* 12 (2010) 1–5.
- [105] G. Pitcairn, A scintigraphic study to evaluate the deposition patterns of a novel anti-asthma drug inhaled from the Cyclohaler dry powder inhaler, *Advanced drug delivery reviews* 26 (1997) 59–67.
- [106] European Directorate for the Quality of Medicines & Healthcare, European Pharmacopeia (Ph. Eur. 8.8): Ph. Eur. 2.9.18 Zubereitungen zur -Inhalation: -Aerodynamische Beurteilung feiner -Teilchen, Deutscher Apotheker Verlag (2016).
- [107] W. Kleppmann, *Produkte und Prozesse optimieren*, Carl Hanser Verlag, Wien, 2009.
- [108] H. Steckel, H.G. Brandes, A novel spray-drying technique to produce low density particles for pulmonary delivery, *International Journal of Pharmaceutics* 278 (2004) 187–195.
- [109] L. Tajber, D.O. Corrigan, O.I. Corrigan, A.M. Healy, Spray drying of budesonide, formoterol fumarate and their composites--I. Physicochemical characterisation, *International Journal of Pharmaceutics* 367 (2009) 79–85.
- [110] R. Vehring, *Pharmaceutical Particle Engineering via Spray Drying*, *Pharm Res* 25 (2008) 999–1022.
- [111] N. Chew, H.K. Chan, Effect of Powder Polydispersity on Aerosol Generation, *J Pharm Phamaceut Sci* 5 (2002) 162–168.
- [112] K. Johnson, Preparation of peptide and protein powders for inhalation, *Advanced drug delivery reviews* 26 (1997) 3–15.
- [113] M. Irngartinger, V. Camuglia, M. Damm, J. GOEDE, H.W. Frijlink, Pulmonary delivery of therapeutic peptides via dry powder inhalation: effects of micronisation and manufacturing, *European Journal of Pharmaceutical Sciences* 58 (2004) 7–14.

-
- [114] D.O. Corrigan, O.I. Corrigan, A.M. Healy, Physicochemical and in vitro deposition properties of salbutamol sulphate/ipratropium bromide and salbutamol sulphate/excipient spray dried mixtures for use in dry powder inhalers, *International Journal of Pharmaceutics* 322 (2006) 22–30.
- [115] C.F. Burmeister, A. Kwade, Process engineering with planetary ball mills, *Chemical Society reviews* 42 (2013) 7660–7667.
- [116] Willy A. Bachofen AG Maschinenfabrik, EN Turbula Leaflet, http://www.wab.ch/fileadmin/redaktion/downloads/prospekt/FR_Turbula_Donnees_techniques.pdf.
- [117] C. Bosquillon, C. Lombry, V. Preat, R. Vanbever, Comparison of particle sizing techniques in the case of inhalation dry powders, *Journal of pharmaceutical sciences* 90 (2001) 2032–2041.
- [118] S. Nazzal, I. Smalyukh, O. Lavrentovich, A. Mansoor, Preparation and in vitro characterisation of a eutectic based semisolid self-nanoemulsified drug delivery system (SNEDDS) of ubiquinone: mechanism and progress of emulsion formation, *International Journal of Pharmaceutics* 235 (2002) 247–265.
- [119] H. Sagehorn, J. List, T. Wiegand, R. Weichert, T. Wriedt, Characterization of Airborne Fibers via Fraunhofer Theory: Examination of the Validity of Fraunhofer Theory Using the Exact Scattering Theory MMP, *Particle & Particle Systems Characterisation* 18 (2001) 55–63.
- [120] M. von Ardenne, Das Elektronen-Rastermikroskop, *Z. Physik* 109 (1938) 553–572.
- [121] J.C. Hooton, C.S. German, M.C. Davies, C.J. Roberts, A comparison of morphology and surface energy characteristics of sulfathiazole polymorphs based upon single particle studies, *European Journal of Pharmaceutical Sciences* 28 (2006) 315–324.
- [122] C.B. Packhaeuser, K. Lahnstein, J. Sitterberg, T. Schmehl, T. Gessler, U. Bakowsky, W. Seeger, T. Kissel, Stabilization of aerosolizable nano-carriers by freeze-drying, *Pharmaceutical research* 26 (2009) 129–138.
- [123] J.W. Kwek, I.U. Vakarelski, W.K. Ng, J.Y. Heng, R.B. Tan, Novel parallel plate condenser for single particle electrostatic force measurements in atomic force microscope, *Colloids and Surfaces A: Physicochemical and Engineering Aspects* 385 (2011) 206–212.

- [124] M. Bunker, M. Davies, C. Roberts, Towards screening of inhalation formulations: measuring interactions with atomic force microscopy, *Expert opinion on drug delivery* 2 (2005) 613–624.
- [125] P. Klapetek, D. Nečas, C. Anderson, Gwyddion user guide, gwyddion.net/download/user-guide/gwyddion-user-guide-en.pdf, accessed 16 May 2017.
- [126] W.F. Heinz, J.H. Hoh, Spatially resolved force spectroscopy of biological surfaces using the atomic force microscope, *Trends in Biotechnology* 17 (1999) 143–150.
- [127] H.-J. Butt, B. Cappella, M. Kappl, Force measurements with the atomic force microscope: Technique, interpretation and applications, *Surface Science Reports* 59 (2005) 1–152.
- [128] F. Karakas, B. Hassas, Effect of surface roughness on interaction of particles in flotation, *Physicochemical Problems of Mineral Processing* 52 (2016) 18–34.
- [129] European Directorate for the Quality of Medicines & Healthcare, *European Pharmacopeia (Ph. Eur. 8.8): Ph. Eur. 2.9.23 Bestimmung der Dichte von Feststoffen mit Hilfe von Gaspyknometern* Deutscher Apotheker Verlag.
- [130] A. Saleki-Gerhardt, G. Zografi, Non-Isothermal and Isothermal Crystallization of Sucrose from the Amorphous State, *Pharmaceutical research* 11 (1994) 1166–1173.
- [131] A. Columbano, G. Buckton, P. Wikeley, A study of the crystallisation of amorphous salbutamol sulphate using water vapour sorption and near infrared spectroscopy, *International Journal of Pharmaceutics* 237 (2002) 171–178.
- [132] S. Ali, J. Heng, A.A. Nikolaev, K.E. Waters, Introducing inverse gas chromatography as a method of determining the surface heterogeneity of minerals for flotation, *Powder Technology* 249 (2013) 373–377.
- [133] S. Mohammadi-Jam, K.E. Waters, Inverse gas chromatography applications: a review, *Advances in colloid and interface science* 212 (2014) 21–44.
- [134] I.M. Grimsey, J.C. Feeley, P. York, Analysis of the surface energy of pharmaceutical powders by inverse gas chromatography, *Journal of pharmaceutical sciences* 91 (2002) 571–583.
- [135] R. Ho, M. Naderi, J.Y.Y. Heng, D.R. Williams, F. Thielmann, P. Bouza, A.R. Keith, G. Thiele, D.J. Burnett, Effect of milling on particle shape and surface en-

- ergy heterogeneity of needle-shaped crystals, *Pharmaceutical research* 29 (2012) 2806–2816.
- [136] P.P. Yla-Maihaniemi, J.Y.Y. Heng, F. Thielmann, D.R. Williams, Inverse gas chromatographic method for measuring the dispersive surface energy distribution for particulates, *Langmuir the ACS journal of surfaces and colloids* 24 (2008) 9551–9557.
- [137] J.Y.S. Tay, C.V. Liew, P.W.S. Heng, *Powder Flow Testing: Judicious Choice of Test Methods*, AAPS PharmSciTech (2016).
- [138] G. Léonard, N. Abatzoglou, Stress distribution in lubricated vs unlubricated pharmaceutical powder columns and their container walls during translational and torsional shear testing, *Powder Technology* 203 (2010) 534–547.
- [139] Søren Vinter Søgaard, Characterization of powder properties using a powder rheometer, Presented on: The 2nd Electronic Conference on Pharmaceutical sciences (2012).
- [140] V.A. Marple, D.L. Roberts, F.J. Romay, N.C. Miller, K.G. Truman, M. van Oort, B. Olsson, M.J. Holroyd, J.P. Mitchell, D. Hochrainer, Next generation pharmaceutical impactor (a new impactor for pharmaceutical inhaler testing). Part I: Design, *Journal of aerosol medicine the official journal of the International Society for Aerosols in Medicine* 16 (2003) 283–299.
- [141] P. Sheth, S.W. Stein, P.B. Myrdal, Factors influencing aerodynamic particle size distribution of suspension pressurized metered dose inhalers, *AAPS PharmSciTech* 16 (2015) 192–201.
- [142] De Boer, Inhalation characteristics and their effects on in vitro drug delivery from dry powder inhalers Part 1. Inhalation characteristics, work of breathing and volunteers' preference in dependence of the inhaler resistance.
- [143] M. Sacchetti, M. van Oort, Spray-drying and supercritical fluid particle generation techniques, in: In: Hickey, A.J. (Ed.), *Inhalation Aerosols, Physical and Biological Basis for Therapy*, vol. 94. Marcel Dekker, New York, NY, pp. 337–384.
- [144] C. Bosquillon, C. Lombry, V. Pr at, R. Vanbever, Influence of formulation excipients and physical characteristics of inhalation dry powders on their aerosolization performance, *Journal of Controlled Release* 70 (2001) 329–339.
- [145] A. Chawla, K. Taylor, J.M. Newton, M. Johnson, Production of spray dried salbutamol sulphate for use in dry powder aerosol formulation, *International Journal of Pharmaceutics* 108 (1994) 233–240.

- [146] N. Chew, H.K. Chan, Effect of powder polydispersity on aerosol generation, *J Pharm Biopharmaceut Sci* 5 (2002) 162–168.
- [147] S. Naikwade, Preparation and In Vitro Evaluation of Budesonide Spray Dried Microparticles for Pulmonary Delivery, *Sci. Pharm.* 77 (2009) 419–441.
- [148] K. Mosén, K. Bäckström, K. Thalberg, T. Schaefer, H.G. Kristensen, A. Axelson, Particle Formation and Capture During Spray Drying of Inhalable Particles, *Pharmaceutical Development and Technology* 9 (2005) 409–417.
- [149] E.M. Littringer, S. Zellnitz, K. Hammernik, V. Adamer, H. Friedl, N.A. Urbanetz, Spray Drying of Aqueous Salbutamol Sulfate Solutions Using the Nano Spray Dryer B-90: The Impact of Process Parameters on Particle Size, *Drying Technology* 31 (2013) 1346–1353.
- [150] K. Alexander, C. Judson King, Factors governing surface morphology of spray-dried amorphous substances, *Drying Technology* 3 (2007) 321–348.
- [151] P. Harjunen, V.-P. Lehto, J. Väliisaari, T. Lankinen, P. Paronen, K. Järvinen, Effects of ethanol to water ratio in feed solution on the crystallinity of spray-dried lactose, *Drug Development and Industrial Pharmacy* 28 (2002) 949–955.
- [152] Y. Fang, S. Rogers, C. Selomulya, X.D. Chen, Functionality of milk protein concentrate: Effect of spray drying temperature, *Biochemical Engineering Journal* 62 (2012) 101–105.
- [153] M.I.U. Islam, T.A.G. Langrish, The Effect of Different Atomizing Gases and Drying Media on the Crystallization Behavior of Spray-Dried Powders, *Drying Technology* 28 (2010) 1035–1043.
- [154] J. Broadhead, S.K. Edmond Rouan, C.T. Rhodes, The spray drying of pharmaceuticals, *Drug Development and Industrial Pharmacy* 18 (2008) 1169–1206.
- [155] T. Müller, R. Krehl, J. Schiewe, C. Weiler, H. Steckel, Influence of small amorphous amounts in hydrophilic and hydrophobic APIs on storage stability of dry powder inhalation products, *European Journal of Pharmaceutics and Biopharmaceutics* 92 (2015) 130–138.
- [156] K. Iida, Y. Hayakawa, H. Okamoto, K. Danjo, H. Luenberger, Influence of Storage Humidity on the in Vitro Inhalation Properties of Salbutamol Sulfate Dry Powder with Surface Covered Lactose Carrier, *Chem. Pharm. Bull.* 52 (2004) 444–446.

-
- [157] J. Vollenbroek, G.A. Hebbink, S. Ziffels, H. Steckel, Determination of low levels of amorphous content in inhalation grade lactose by moisture sorption isotherms, *International Journal of Pharmaceutics* 395 (2010) 62–70.
- [158] B.C. Hancock, G. Zografi, Characteristics and significance of the amorphous state in pharmaceutical systems, *Journal of pharmaceutical sciences* 86 (1997) 1–12.
- [159] Y. Guo, E. Shalaev, S. Smith, Physical stability of pharmaceutical formulations: Solid-state characterization of amorphous dispersions, *TrAC Trends in Analytical Chemistry* 49 (2013) 137–144.
- [160] T. Müller, J. Schiewe, R. Smal, C. Weiler, M. Wolkenhauer, H. Steckel, Measurement of low amounts of amorphous content in hydrophobic active pharmaceutical ingredients with dynamic organic vapor sorption, *European Journal of Pharmaceutics and Biopharmaceutics* 92 (2015) 102–111.
- [161] P. Tong, G. Zografi, Effects of water vapor absorption on the physical and chemical stability of amorphous sodium indomethacin, *AAPS PharmSciTech* 5 (2004) e26.
- [162] M.G. Cares-Pacheco, R. Calvet, G. Vaca-Medina, A. Rouilly, F. Espitalier, Inverse Gas Chromatography a tool to follow physicochemical modifications of pharmaceutical solids: crystal habit and particles size surface effects, *International Journal of Pharmaceutics* (2015).
- [163] S.A. Wildman, G.M. Crippen, Prediction of Physicochemical Parameters by Atomic Contributions, *J. Chem. Inf. Comput. Sci.* 39 (1999) 868–873.
- [164] A. Taglietti, C.R. Arciola, A. D'Agostino, G. Dacarro, L. Montanaro, D. Campoccia, L. Cucca, M. Vercellino, A. Poggi, P. Pallavicini, L. Visai, Antibiofilm activity of a monolayer of silver nanoparticles anchored to an amino-silanized glass surface, *Biomaterials* 35 (2014) 1779–1788.
- [165] J.Y.Y. Heng, D.F. Pearse, F. Thielmann, T. Lampke, A. Bismarck, Methods to determine surface energies of natural fibres: A review, *Composite Interfaces* 14 (2007) 581–604.
- [166] F. Thielmann, Introduction into the characterisation of porous materials by inverse gas chromatography, *Journal of Chromatography A* 1037 (2004) 115–123.
- [167] F. Thielmann, D.J. Burnett, J.Y.Y. Heng, Determination of the surface energy distributions of different processed lactose, *Drug Development and Industrial Pharmacy* 33 (2007) 1240–1253.
-

- [168] E. Guenette, A. Barrett, D. Kraus, R. Brody, L. Harding, G. Magee, Understanding the effect of lactose particle size on the properties of DPI formulations using experimental design, *International Journal of Pharmaceutics* 380 (2009) 80–88.
- [169] A.M. Boshhiha, N.A. Urbanetz, Influence of carrier surface fines on dry powder inhalation formulations, *Drug Development and Industrial Pharmacy* 35 (2009) 904–916.
- [170] B.H.J. Dickhoff, Adhesive mixtures for powder inhalation: The effect of carrier (surface and bulk) properties, carrier payload and mixing conditions on the performance of adhesive mixtures for inhalation s.n. (2006).
- [171] J.A. Hersey, Ordered mixing: A new concept in powder mixing practice, *Powder Technology* 11 (1975) 41–44.
- [172] J.N. Staniforth, Performance-Modifying Influences in Dry Powder Inhalation Systems, *Aerosol Science and Technology* 22 (1995) 346–353.
- [173] P.M. Young, O. Wood, J. Ooi, D. Traini, The influence of drug loading on formulation structure and aerosol performance in carrier based dry powder inhalers, *International Journal of Pharmaceutics* 416 (2011) 129–135.
- [174] D. El-Sabawi, S. Edge, R. Price, P.M. Young, Continued Investigation Into the Influence of Loaded Dose on the Performance of Dry Powder Inhalers: Surface Smoothing Effects, *Drug Development and Industrial Pharmacy* 32 (2008) 1135–1138.
- [175] F. Podczeck, Adhesion forces in interactive powder mixtures of a micronized drug and carrier particles of various particle size distributions, *Journal of Adhesion Science and Technology* 12 (1998) 1323–1339.
- [176] P.M. Young, S. Edge, D. Traini, M.D. Jones, R. Price, D. El-Sabawi, C. Urry, C. Smith, The influence of dose on the performance of dry powder inhalation systems, *Int J Pharm* 296 (2005) 26–33.
- [177] E. Cordts, Advanced powder characterisation techniques for inhalation powder mixtures (2014).
- [178] Freeman Technology Limited, An Investigation into the Wall Friction Angle of a Range of Low Friction Materials Used in the Manufacture of Pharmaceutical Processing Equipment.
- [179] A. Elajnaf, P. Carter, G. Rowley, Electrostatic characterisation of inhaled powders: Effect of contact surface and relative humidity, *European journal of phar-*

- maceutical sciences official journal of the European Federation for Pharmaceutical Sciences 29 (2006) 375–384.
- [180] H. Adi, P.C.L. Kwok, J. Crapper, P.M. Young, D. Traini, H.-K. Chan, Does electrostatic charge affect powder aerosolisation?, *Journal of pharmaceutical sciences* 99 (2010) 2455–2461.
- [181] A.H. de Boer, P. Hagedoorn, D. Gjaltema, J. Goede, K. Kussndrager, H.W. Frijlink, Air classifier technology (ACT) in dry powder inhalation Part 2. The effect of lactose carrier surface properties on the drug-to-carrier interaction in adhesive mixtures for inhalation, *International Journal of Pharmaceutics* 260 (2003) 201–216.
- [182] F. Grasmeyer, H.W. Frijlink, A.H. de Boer, A proposed definition of the 'activity' of surface sites on lactose carriers for dry powder inhalation, *European journal of pharmaceutical sciences official journal of the European Federation for Pharmaceutical Sciences* 56 (2014) 102–104.
- [183] B. Dickhoff, A.H. de Boer, D. Lambregts, H.W. Frijlink, The effect of carrier surface and bulk properties on drug particle detachment from crystalline lactose carrier particles during inhalation, as function of carrier payload and mixing time, *European Journal of Pharmaceutics and Biopharmaceutics* 56 (2003) 291–302.
- [184] Y. Kawashima, T. Serigano, T. Hino, H. Yamamoto, H. Takeuchi, Effect of surface morphology of carrier lactose on dry powder inhalation property of pranlukast hydrate, *International Journal of Pharmaceutics* 172 (1998) 179–188.
- [185] Y. Shimada, M. Sunada, M. Mizuno, Y. Yonezawa, H. Sunada, M. Yokosuka, H. Kimura, H. Takebayashi, Measurement of the adhesive force of fine particles on tablet surfaces and method of their removal, *Drug Development and Industrial Pharmacy* 26 (2000) 149–158.
- [186] F. Podczek, J. Michael Newton, Development of an Ultracentrifuge Technique To Determine the Adhesion and Friction Properties between Particles and Surfaces, *Journal of pharmaceutical sciences* 84 (1995) 1067–1071.
- [187] DFE Pharma, <http://www.dfepharma.de/de-de/excipients/inhalation-lactose/lactohale-100.aspx>.
- [188] DFE Pharma, <http://www.dfepharma.de/de-de/excipients/inhalation-lactose/lactohale-200.aspx>.
- [189] Sigmund Lindner GmbH, Product Data Sheet SiLibeads Typ S, Microglas.

- [190] M.S. Coates, H.-K. Chan, D.F. Fletcher, H. Chiou, Influence of mouthpiece geometry on the aerosol delivery performance of a dry powder inhaler, *Pharmaceutical research* 24 (2007) 1450–1456.
- [191] B.H.J. Dickhoff, A.H. de Boer, D. Lambregts, H.W. Frijlink, The interaction between carrier rugosity and carrier payload, and its effect on drug particle redispersion from adhesive mixtures during inhalation, *European Journal of Pharmaceutics and Biopharmaceutics* 59 (2005) 197–205.
- [192] F. Podczeck, Assessment of the mode of adherence and the deformation characteristics of micronized particles, *International Journal of Pharmaceutics* 145 (1996) 65–76.
- [193] P. Selvam, H.D.C. Smyth, Effect of Press-on Forces on Drug Adhesion in Dry Powder Inhaler Formulations, *Journal of Adhesion Science and Technology* 25 (2012) 1659–1670.
- [194] M.D. Louey, M. van Oort, A.J. Hickey, Aerosol Dispersion of Respirable Particles in Narrow Size Distributions Produced by Jet-Milling and Spray-Drying Techniques, *Pharm Res* 21 (2004) 1200–1206.
- [195] S.E. Papadakis, R.E. Bahu, The sticky issues of drying, *Drying Technology* 10 (1992) 817–837.
- [196] Copley Scientific Ltd., Inhaler Testing Brochure, 2015, <http://www.copleyscientific.com/downloads/brochures>.

Danksagung

An erster Stelle möchte ich mich bei meinen beiden Betreuern bedanken. Meinem Doktorvater Herrn Prof. Dr. Hartwig Steckel danke ich für die freundliche Aufnahme in den Arbeitskreis und die Begleitung der Anfangszüge meiner Arbeit. Meiner Doktor-mutter Frau Prof. Dr. Regina Scherließ danke ich für ihre Unterstützung während meiner gesamten Promotionszeit. Sie gab mir alle gestalterischen Freiheiten bei der Bearbeitung meines Projekts, stand mir aber auch zu jeder Zeit mit Rat und Tat zur Seite.

Herrn Prof. Dr. Thomas Kunze danke ich für die Übernahme des Zweitgutachtens.

Ein weiterer Dank gilt Frau Prof. Dr. Nora Urbanetz für ihr fortwährendes Interesse an dem Projekt und die wertvollen Diskussionen.

Dr. Michael Kappl, Dr. Regina Fuchs und Uwe Rietzler vom Max-Planck-Institut für Polymerforschung danke ich für ihre Hilfe bei der Durchführung und Auswertung der AFM Messungen. Ihre Expertise ermöglichte das Generieren essentieller Daten für diese Arbeit.

Zinaida Todorova von der Otto-von-Guericke-Universität Magdeburg danke ich für die Silanisierung der Glaskugeln und die Messung der Kontaktwinkel.

Ein weiterer Dank gilt meinen Wahlpflichtfachstudenten Anna-Maria, Lena, Insa und Fabian für ihre motivierte Mitarbeit, bei der durchaus interessante Ergebnisse entstanden sind.

Dirk und Kalle, meinen Rettern in technischen Nöten, danke ich für ihre immer prompte Hilfe bei Problemen aller Art. In diesem Zuge gilt ein herzlicher Dank auch Volkmar und Detlef, die jede Hürde im Bereich Software und Hardware im Nu gelöst haben.

Des Weiteren möchte ich mich ganz besonders bei Rüdi bedanken. Mit deinen immer perfekten Coral-Draw Grafiken sowie mit der Aufnahme der Röntgendiffraktogramme hast du maßgeblich zu dieser Arbeit beigetragen. Deine Anekdoten werden mir fehlen!

Mathias, Mats und Tobi danke ich für die Aufnahme der REM Bilder.

Großer Dank gilt auch dir Annika, dein perfektionistischer Korrektorenblick ist unübertroffen!

Vielen Dank auch an meinen ehemaligen Bürokollegen und „Zweitkorrektor“ Dr. Thorsten Müller. Deine fundierten Kommentare und Hinweise haben diese Arbeit noch ein Stückchen runder gemacht.

Ich danke weiterhin allen alten und neuen Kollegen für die gute Aufnahme in den Arbeitskreis und die schöne Zeit am Institut.

Bedanken möchte ich mich auch bei unseren TA´s. Liebe Hanna, deine tatkräftige HPLC Unterstützung in der Projektarbeit war mir eine große Hilfe. Und Anna, auch wenn wir inzwischen fast 1000 NGI Runs zusammen vollbracht haben, werde ich nie genug von deinem „Goldkehlchen“ bekommen können.

Besonderer Dank gilt meiner Freundin Marie, die immer für mich da ist und mir den Rücken stärkt.

Der wohl größte Dank gilt meinen Eltern für ihre fortwährende Unterstützung in allen Lebenslagen. Ohne euren stetigen Rückhalt hätte ich diese Arbeit nie anfertigen können. Ich weiß, dass ich mich immer auf euch verlassen kann!

Lebenslauf

Persönliche Daten

Nachname	Renner
Vorname	Niklas
Geburtsdatum	30.11.1987
Geburtsort	Freiburg im Breisgau
Staatsangehörigkeit	Deutsch

Schulbildung

1994 bis 1998	Hexental Grundschule, Merzhausen
1998 bis 2007	Friedrich Gymnasium, Freiburg
Juni 2007	Allgemeine Hochschulreife

Studium der Pharmazie

Oktober 2008 bis März 2013	Studium der Pharmazie, Albert-Ludwigs-Universität Freiburg
Mai 2013 bis November 2013	Diplomarbeit, Pharmazeutisches Institut der Albert-Ludwigs-Universität Freiburg
Juni 2014	Approbation als Apotheker

Beruflicher Werdegang

September 2007 bis Mai 2008	Zivildienst im Diakoniekrankenhaus, Freiburg
November 2013 bis April 2014	Pharmazeut im Praktikum, Apotheke am Basler Tor, Freiburg
Seit Juli 2014	Promotion am Pharmazeutischen Institut der Christian-Albrechts-Universität zu Kiel

Erklärung nach § 8 der Promotionsordnung

Hiermit erkläre ich gemäß § 8 der Promotionsordnung der Mathematisch-Naturwissenschaftlichen Fakultät der Christian-Albrechts-Universität zu Kiel, dass ich die vorliegende Arbeit, abgesehen von der Beratung durch meinen Betreuer, selbstständig und ohne fremde Hilfe verfasst habe. Weiterhin habe ich keine anderen als die angegebenen Quellen oder Hilfsmittel benutzt und die den benutzten Werken wörtlich oder inhaltlich entnommenen Stellen als solche kenntlich gemacht. Die vorliegende Arbeit ist unter Einhaltung der Regeln guter wissenschaftlicher Praxis entstanden und wurde bei keiner anderen Universität zur Begutachtung eingereicht.

Niklas Renner

